

2008

# Bioanalytical methods for studies of homocysteine and novel cardiovascular disease indicators

Arther T. Gates

*Louisiana State University and Agricultural and Mechanical College*, [agates1@lsu.edu](mailto:agates1@lsu.edu)

Follow this and additional works at: [https://digitalcommons.lsu.edu/gradschool\\_dissertations](https://digitalcommons.lsu.edu/gradschool_dissertations)



Part of the [Chemistry Commons](#)

---

## Recommended Citation

Gates, Arther T., "Bioanalytical methods for studies of homocysteine and novel cardiovascular disease indicators" (2008). *LSU Doctoral Dissertations*. 1455.

[https://digitalcommons.lsu.edu/gradschool\\_dissertations/1455](https://digitalcommons.lsu.edu/gradschool_dissertations/1455)

This Dissertation is brought to you for free and open access by the Graduate School at LSU Digital Commons. It has been accepted for inclusion in LSU Doctoral Dissertations by an authorized graduate school editor of LSU Digital Commons. For more information, please contact [gradetd@lsu.edu](mailto:gradetd@lsu.edu).

BIOANALYTICAL METHODS FOR STUDIES OF HOMOCYSTEINE AND  
NOVEL CARDIOVASCULAR DISEASE INDICATORS

A Dissertation

Submitted to the Graduate Faculty of the  
Louisiana State University and  
Agricultural and Mechanical College  
In partial fulfillment of the  
Requirements for the degree of  
Doctor of Philosophy

In

The Department of Chemistry

By

Arther T. Gates

B.S., Alcorn State University, Alcorn State, 2000

M.S., University of Nebraska-Lincoln, 2002

December 2008

*To my parents, Arther and Delliah Gates and the entire Gates Family for your  
gracious support over the years.*

## ACKNOWLEDGEMENTS

I am grateful to those who have assisted in the development of my potential. My future is brighter because of you.

**Dr. Isiah M. Warner**, for his mentorship and humanity. You had faith in me when I needed it most. I appreciate your high ethical standard and commitment to investigating important scientific problems. Working in your research group has been a great privilege.

**Dr. James W. Robinson**, for introducing me to cardiovascular disease research. You have been a strong guiding influence in my research.

**Dr. Robert M. Strongin**, for challenging me to become more focused and relentless.

**Dale Treleaven**, for helpful advice and assistance in early NMR studies.

**Doctoral Research Committee Members: Dr. Robert Cook, Dr. Jayne Garno, Dr.**

**Kermit Murray, and Dr. Frank Tsai**, for your time and helpful discussions over the years.

**Post Doctoral Researchers: Dr. Kristin Fletcher, Dr. Mark Lowry, Dr. Sayo Fakayode, and Dr. Bilal El Zahab**, for taking the time to provide guidance and honest feedback.

**Abitha Murugesu**, for helping me establish the foundation for this research and dissertation.

**Monica Sylvain and Gabriela Ganea**, for rigorously proofing my dissertation.

**The Warner Research Group**, for being my family away from home. I value your support and friendship.

**Dr. Jennifer Rood**, for personally assisting me in experiments at the Pennington Biomedical Research Center.

## TABLE OF CONTENTS

DEDICATION.....	ii
ACKNOWLEDGEMENTS.....	iii
LIST OF TABLES.....	vii
LIST OF FIGURES.....	viii
LIST OF SCHEMES.....	xi
LIST OF ABBREVIATIONS.....	xii
ABSTRACT.....	xvi
CHAPTER 1. INTRODUCTION.....	1
1.1 Cardiovascular Disease.....	1
1.1.1 Conventional Risk Factors and Biomarkers.....	3
1.1.2 Homocysteine as a Cardiovascular Disease Biomarker.....	5
1.1.3 <i>N</i> -Homocysteine-Protein.....	9
1.2 Conventional Bioanalytical Methods for Homocysteine Analysis.....	10
1.2.1 Chromatographic Methods.....	11
1.2.2 Electrophoretic Methods.....	12
1.2.3 Immunochemical-Based Assays.....	13
1.3 Direct Visual Detection of Homocysteine.....	15
1.4 Spectrochemical Techniques.....	17
1.4.1 UV-visible Spectroscopy.....	17
1.4.2 Circular Dichroism Spectroscopy.....	18
1.4.3 Fluorescence Spectroscopy.....	19
1.5 Mass Spectrometry.....	20
1.6 Bioaccumulation of Polycyclic Aromatic Hydrocarbons in Atherosclerotic Tissues.....	21
1.7 Scope of Dissertation.....	24
1.8 References.....	25
CHAPTER 2. SPECTROCHEMICAL INVESTIGATION OF PYRIDOXAL TETRAHYDROTHIAZINE FORMATION.....	31
2.1 Introduction.....	31
2.2 Methods.....	32
2.2.1 Materials.....	32
2.2.2 Buffer and Sample Preparation.....	32
2.2.3 Instrumentation.....	33
2.3 Calculations and Data Analysis.....	33
2.4 Results and Discussions.....	34
2.4.1 UV-visible Spectroscopy Studies of Thiazine Formation.....	34

2.4.2	Fluorescence Characterizations.....	35
2.5	Conclusions.....	38
2.6	References.....	39
CHAPTER 3.	CAPILLARY ELECTROPHORETIC SCREENING FOR INHIBITION OF HOMOCYSTEINE THIOLACTONE-INDUCED PROTEIN OLIGOMERIZATION.....	40
3.1	Introduction.....	40
3.2	Methods.....	42
3.2.1	Materials.....	42
3.2.2	Preparation of Protein Reaction Mixtures.....	42
3.2.3	SDS-PAGE Protocol.....	43
3.2.4	Instrumentation.....	44
3.2.5	Data Analysis.....	44
3.3	Results and Discussion.....	45
3.3.1	Characterization of the Protein Reaction Mixture.....	45
3.3.2	Preliminary Evaluation of Protein Separation.....	48
3.3.3	Effect of Protein Denaturation on Separation Performance.....	48
3.3.4	Voltage Optimization.....	50
3.3.5	Short-End Injection Method.....	51
3.3.6	Oligomerization Inhibition Studies.....	53
3.4	Conclusions.....	57
3.5	References.....	57
CHAPTER 4.	GOLD NANOSENSOR FOR COLORIMETRIC DETECTION OF <i>N</i> - HOMOCYSTEINE-PROTEIN.....	60
4.1	Introduction.....	60
4.2	Methods.....	62
4.2.1	Materials.....	62
4.2.2	Synthesis of Gold Nanoparticles.....	63
4.2.3	Preparation of Protein Homocystamide.....	63
4.2.4	Sample Characterizations.....	64
4.2.5	Preparation of Sensor Solutions.....	64
4.2.6	Instrumentation.....	65
4.3	Results and Discussions.....	65
4.3.1	Nanoparticle-Serum Protein Compatibility Study.....	65
4.3.2	Effect of Temperature on Sensing.....	69
4.3.3	Confirmation of Nanoparticle Assembly.....	69
4.3.4	Proposed Clinical Detection Scheme.....	70
4.4	Conclusions.....	74
4.5	References.....	76
CHAPTER 5.	PLASMON RESONANCE BEHAVIOR OF <i>N</i> -HOMOCYSTEINYLATED GOLD NANOBIOCONJUGATES.....	78
5.1	Introduction.....	78
5.2	Methods.....	79
5.2.1	Materials.....	79

5.2.2	Synthesis of Nanobioconjugates.....	79
5.2.3	<i>N</i> -homocysteinylation of Nanobioconjugates.....	80
5.2.4	Instrumentation.....	80
5.3	Results and Discussion.....	81
5.3.1	Characterization of Nanobioconjugates.....	81
5.3.2	Monitoring Modification-Directed Nanobioconjugate Assembly.....	85
5.3.3	Assessing Modification-Induced Protein Conformational Change.....	87
5.3.4	Modification-Induced Changes in Redox Potential of Cyt <i>c</i> Nanobioconjugates.....	90
5.3.5	Effects of Disulfide Reduction on Nanobioconjugate Association.....	91
5.4	Conclusions.....	93
5.5	References.....	93
CHAPTER 6.	IMMUNOAFFINITY EXTRACTION OF POLYCYCLIC AROMATIC HYDROCARBONS FROM ATHEROSCLEROTIC HEART TISSUES.	96
6.1	Introduction.....	96
6.2	Methods.....	97
6.2.1	Materials.....	97
6.2.2	Preparation of Atherosclerotic Tissue Samples.....	97
6.2.3	Immunoaffinity Extraction Protocol.....	98
6.2.4	Column Fabrication.....	98
6.2.5	Extract Preparation.....	99
6.2.6	Instrumentation.....	99
6.3	Results and Discussion.....	100
6.3.1	Gas Chromatography-Mass Spectrometry Analysis of Polycyclic Aromatic Hydrocarbon Standards.....	100
6.3.2	Analysis of Atherosclerotic Plaque Extracts .....	100
6.4	Conclusions.....	102
6.5	References.....	104
CHAPTER 7.	SUMMARY OF RESEARCH AND FUTURE STUDIES.....	106
APPENDIX A	CHARACTERIZATIONS OF PROTEIN AND PYRIDOXAL REACTIONS.....	110
APPENDIX B	GOLD NANOSENSOR CHARACTERIZATIONS AND CALIBRATION DATA.....	113
APPENDIX C	NANOBIOCONJUGATE CHARACTERIZATIONS.....	117
APPENDIX D	LETTERS OF PERMISSION.....	120
VITA.....		123

## LIST OF TABLES

<b>Table</b>		<b>Page</b>
1.1	General reference list of serological CVD biomarkers.....	5
1.2	Blood homocysteine levels in normal and hyperhomocysteinemia patients.....	7
1.3	Vitamin B content values in normal and atherosclerotic heart tissues.....	9
1.4	Comparison of conventional bioanalytical methods .....	14
3.1	Separation performance and reproducibility statistics for short-end CE separations of protein reaction mixture.....	53
6.1	PAHs present in cigarette smoke.....	96
6.2	Structures of PAH metabolites detected in sample 1 (69 year old African American male), molecular masses (MW) and retention times.....	103
6.3	Structures of PAH metabolites detected in sample 2 (70 year old Caucasian male), molecular masses (MW) and retention times.....	104



## LIST OF FIGURES

Figure		Page
1.1	Racial dependency of coronary heart disease, high blood pressure, and stroke.....	1
1.2	Illustration of severe atherosclerosis.....	2
1.3	Schematic of <i>in vivo</i> homocysteine metabolism.....	6
1.4	Chemical structures of selected forms of vitamin B.....	8
1.5	Post-translational protein modification via <i>N</i> -homocysteinylation.....	11
1.6	Diagram of capillary electrophoresis instrument.....	13
1.7	Plasmon resonant GNP biochemical sensing.....	16
1.8	Graphic representation of a UV-visible spectrometer.....	18
1.9	Theoretical protein ellipticity curves for $\alpha$ -helix, $\beta$ -sheet, and random coil components.....	19
1.10	Jablonski diagram.....	20
1.11	Block diagram of generic mass spectrometer.....	21
1.12	Chemical structures for EPA list of priority PAHs.....	22
1.13	PAH antibody immobilized to an IAE stationary phase.....	23
1.14	Diagram of IAE cycle and elution profile.....	24
2.1	Formation of pyridoxal tetrahydrothiazine via aldehyde condensation.....	31
2.2	UV-Vis absorption spectra of solutions containing pyridoxal in presence of increasing concentrations of Hcy.....	35
2.3	Fluorescence spectra of PT formation.....	36
2.4	Stern-Volmer plot showing trend for uncorrected and corrected PT fluorescence emission.....	37
2.5	Benesi-Hildebrand plots for PT formation.....	38

3.1	Representative electrophoretic separations of protein reaction mixtures. a) gel separation showing bands corresponding to I, II, and III c, b) electropherogram of non-denatured protein mixture, c) electropherogram for thermally denatured sample and plot of electrophoretic migration time versus species molecular weight (inset).....	47
3.2	Effect of applied voltage on CE separations of protein reaction mixture components: a) electropherograms acquired at -15, -12, -10, and -8 kV. Separations were performed using a freshly prepared column.....	51
3.3	Electropherogram of thermally denatured protein reaction mixture containing cyt <i>c</i> species I-V separated in less than 70 sec using short-end injection. Separation performed with an applied voltage of 8kV (22 $\mu$ A current) and a 50 $\mu$ m i.d., 32 cm total length, 10 cm effective length capillary column.....	52
3.4	Results for aggregation inhibition study represented as a) percent of total protein peak area determined by integration of best fit data; and b) percent change for respective mixture component peak areas normalized to an experimental control versus pyridoxal-5-phosphate concentration.....	54
3.5	Representative short-end CE electropherogram resulting from the separation of the protein reaction mixture treated with a) 0.25 pyridoxal-5-phosphate and b) 2.5 mM pyridoxal-5-phosphate, respectively. Separation performed using an applied voltage of 8kV (22 $\mu$ A current) and a 50 $\mu$ m i.d., 32 cm total length, 10 cm effective length capillary column.....	55
4.1	Photographs of the gold nanoparticle (GNP) sensor a) in the absence of protein b) in the presence of unmodified HSA (9.2 - 85.2 mg/mL) and c) in the presence of HSA-homocystamide (9.2 - 85.2 mg/mL).....	66
4.2	UV-visible absorption spectra of GNP sensor solutions shown in Figure 1 a) Unmodified HSA and b) <i>N</i> -Hcy-HSA. Extended plasmon bands are only observed for sensor solutions containing HSA-homocystamide. The arrows indicate the change in absorption with increasing HSA or HSA-homocystamide. ....	68
4.3	Transmission electron micrograph images of the GNP sensor a) in the presence of HSA-homocystamide at 33,000 $\times$ magnification (inset shows 100,000 $\times$ magnification of a 4-nanoparticle cluster assembly within the oligomeric protein network), and b) in the presence of unmodified HSA (inset shows 100,000 $\times$ magnification of unassembled GNPs surrounded by unmodified HSA). The arrows indicate the location of the insets in lower magnification images.....	71

4.4	Visible absorption spectra of the GNP sensor in response to human sera. a) in the presence of unmodified human sera and b) in the presence of human serum homocystamide. c) Sensor response at 620 nm in the presence of modified and unmodified sera versus human serum concentration, (2 – 14 mg/mL). The arrow indicates the change in signal at 620 nm with increasing concentrations of human serum homocystamide.....	75
5.1	Visible absorption spectra for unmodified (solid line) and 2.5 mM HTL-modified (dashed line), a) HGNP and b) SGNP nanobioconjugates.....	83
5.2	Visible absorption spectra of CGNP bioconjugates (0.3 mM) modified with increasing concentrations of HTL (0-2.5 mM).....	84
5.3	Time course dynamic light scattering (DLS) plots illustrating nanostructure growth for unmodified and <i>N</i> -homocysteinylation nanobioconjugates, a) HGNPs b) SGNPs, and c) CGNPs .....	86
5.4	TEM images of <i>N</i> -homocysteinylation a) HGNP, b) SGNP, and CGNP nanobioconjugates .....	88
5.5	CD spectra of unmodified (solid line) and modified (dashed line) nanobioconjugates a) HGNPs at 25 °C, b) HGNPs after 10 min incubation at 80 °C, c) SGNPs at 25 °C, d) SGNPs after 10 min incubation at 80 °C, e) CGNPs at 25 °C and f) CGNPs after 10 min incubation at 80°C.....	89
5.6	UV-vis spectra of CGNP nanobioconjugate solution spiked with 0.1 mg/mL cyt <i>c</i> unmodified before (dotted line), immediately after <i>N</i> -homocysteinylation with 2.5 mM HTL (solid line), and 24 hr after modification (dashed line).....	91
5.7	SDS-PAGE separations of serum nanobioconjugate assemblies resulting from modification with 10 and 20 mM HTL) before (lanes a and b, respectively) and after treatment with TCEP (lanes c and d, respectively). Identical separations performed with SGNP bioconjugate assemblies are shown in lanes e-h. The stacking regions of the gels are indicated by rectangles.....	92
6.1	Mass spectra (TICs) of <b>a</b> ) mixture containing 10 ppm PAH standards: 1) fluorene, 2) phenanthrene, 3) anthracene, and 4) pyrene. b) mass spectra for phenanthrene and anthracene with molecular ion 178 at 100% abundance. ....	100
6.2	Representative GC-MS TICs for atherosclerotic plaques extracted using: a) organic extract only and b) the OLS-IAE method.....	101

## LIST OF SCHEMES

Scheme	Page
3.1 Homocysteine thiolactone-induced protein modification. Under physiological pH conditions Hcy thiolactone can preferentially acylate protein lysine residues at $\epsilon$ -amino groups to yield <i>N</i> -Hcy-protein.....	41
4.1 Proposed colorimetric gold nanoparticle sensor for HTL-induced protein modification.....	62
4.2 Proposed method for the detection of <i>N</i> -Hcy-protein in human sera .....	73

## LIST OF ABBREVIATIONS

Abbreviation	Name
ADMA	asymmetric dimethylarginine
AHA	American Heart Association
Apo B	apolipoprotein B
Au-S-R	chemisorption binding
CE	capillary electrophoresis
CETP	cholesteryl ester transfer protein
CHD	coronary heart disease
CLD	chemiluminescence detection
CP-MAS	cross polarization magic angle spinning
CVD	cardiovascular disease
Cys	cysteine
cyt <i>c</i>	cytochrome <i>c</i>
CZE	capillary zone electrophoresis
$D_h$	hydrodynamic diameter
DLS	dynamic light scattering
DNA	deoxyribonucleic acid
DTT	dithiothreitol
ECD	electrochemical detection
EDTA	ethylenediamine tetra-acetic acid
ELISA	enzyme-linked immunosorbent assay
ESI	electrospray ionization
FD	fluorescence detection

FWHH	full width at half-height
GC	gas chromatography
GNP	gold nanoparticle
GPX1	glutathione peroxidase 1
HBC	high blood cholesterol
HBP	high blood pressure
Hcy	homocysteine
Hcyt	total homocysteine
HPLC	high-performance liquid chromatography
HSA	human serum albumin
HsCRP	high sensitivity C-reactive protein
HTL	homocysteine thiolactone
HTPA	homocysteine thiolactone-induced protein aggregation
HTPM	homocysteine thiolactone-induced protein modification
IA	immunoassay
IAE	immunoaffinity extraction
ICP	inductively coupled plasma-mass spectrometry
IEC	ion exchange chromatography
IL-18	interleukin 18
IL-6	interleukin 6
LDL	low-density lipoprotein
LOD	limit of detection
Lp (a)	lipoprotein a

Lp-PLA2	lipoprotein-associated phospholipase A2
MMP-9	matrix metalloproteinase 9
MPO	myeloperoxidase
MS	mass spectrometry
MWCO	molecular weight cut-off
N	theoretical plates
N-Hcy-protein	protein homocystamide
NMR	nuclear magnetic resonance
PAH	polycyclic aromatic hydrocarbon
PBS	phosphate-buffered saline
PD	photometric detection
PDADMAC	poly (diallyldimethylammonium chloride)
PLP	pyridoxal-5-phosphate
PMT	photomultiplier tube
PT	pyridoxal tetrahydrothiazine
Rs	resolution
RSD	relative standard deviation
R-S-S-R	disulfide bonding
SAA	serum amyloid A
sCD40	tumor necrosis factor receptor superfamily
SDS-PAGE	sodium dodecyl sulfate-polyacrylamide gel electrophoresis
sICAM-1	soluble intercellular adhesion molecule-1
TBS	tris-buffered saline

TCEP	tris(2-carboxyethyl)phosphine
TEM	transmission electron microscopy
TIMP-1	tissue inhibitor of metalloproteinase-1
TLC	thin layer chromatography
tRNA	transfer ribonucleic acid
UV	ultra violet
Vis	visible



## ABSTRACT

This dissertation explores the development of analytical methods for studies of CVD biomarkers and related biomolecular indicators. Initially, spectroscopic studies were conducted to investigate the chemical reactivity of homocysteine (Hcy), an independent CVD risk factor and serological biomarker. Consequently, we proposed an alternate theory for *in vivo* Hcy clearance based on spontaneous pyridoxal tetrahydrothiazine (PT) formation from Hcy and pyridoxal. The validity of PT-assisted Hcy clearance was further evaluated by use of capillary electrophoretic methods, which allowed rapid monitoring of protein oligomerization in PT-protein reaction mixtures. The results of these studies suggest that PT formation is a plausible mechanism for Hcy clearance. Moreover, PT formation was shown to protect proteins from post-translational modification by homocysteine thiolactone. This dissertation also addresses the need for rapid and direct detection methods for CVD biomarkers. Accordingly, we introduced the first plasmon resonant GNP sensing scheme for protein homocystamide. The nanosensor provides visual conformation of protein homocystamide (*N*-Hcy-protein) by way of a red-to-blue color change. Further sensor investigations conducted with protein nanobioconjugates revealed that the GNP sensing mechanism is dependent on several complex physiochemical and biomolecular interactions including nanoparticle self-assembly, interparticle disulfide cross-linking, and modification-induced protein conformational changes. This dissertation also continues previous atherosclerotic tissue characterization studies by demonstrating the feasibility of using hybrid organic-immunoaffinity extraction for GC-MS analysis of polycyclic aromatic hydrocarbons in human heart plaque samples. This body of work is significant because it proposes new bioanalytical technologies that could enhance CVD screening and treatment.

# CHAPTER 1

## INTRODUCTION

### 1.1 Cardiovascular Disease

Cardiovascular disease (CVD) continues to be the leading cause of mortality in the U.S. According to the American Heart Association (AHA), CVD affects more than 81 million Americans and accounts for about one in every three deaths in this country.<sup>1</sup> Statistics from the AHA also indicate that high blood pressure (HBP) or hypertension affects approximately 73 million people and is thus the most pervasive form of CVD, followed by heart attack (16 million), stroke (5.8 million), heart failure (5.3 million), and congenital heart defects (1.3 million). Instances of CVD vary significantly among different ethnic groups for reasons that are not well understood.

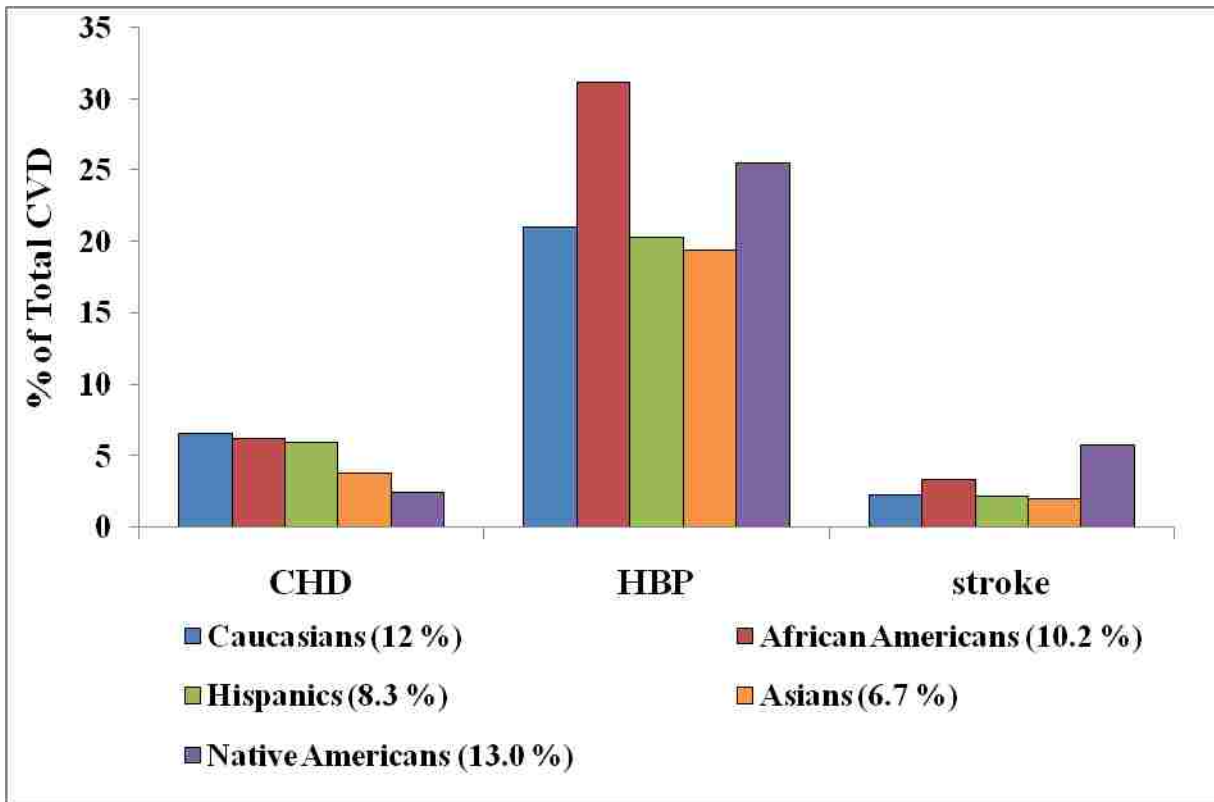


**Figure 1.1** Racial dependency of coronary heart disease, high blood pressure, and stroke.

Figure 1.1 provides a highlight of trends in coronary heart disease (CHD), HBP, and stroke based on ethnicity as reported by the AHA for individuals 18 years of age and older. The values in parenthesis indicate the % of CVD within respective ethnic populations. The y-axis of the bar graph represents the percent of total known CVD instances. African Americans and Native Americans have the highest instances of HBP and stroke, while CHD is slightly more prevalent in the Caucasian population. Atherosclerosis is a common form of CHD that is disproportionately prevalent in the U.S.

The severity of atherosclerosis is often described as Type I, II, or III. Type I, the onset of atherosclerosis, is indicated by mild inflammation of the endothelial cells of the arteries. Type II atherosclerosis is characterized by intimal tissue damage in the arteries and the appearance of fatty plaques. The most severe stage of atherosclerosis is Type III, which is indicated by blood clot (thrombus) formation and deep intimal and medial tissue damage. Figure 1.2 is an illustration of Type III atherosclerosis in which plaques and blood clots have accumulated in the left anterior descending artery of the heart. As a result, there is a critical reduction in arterial blood flow. This severe condition could cause sudden cardiac arrest if left untreated.

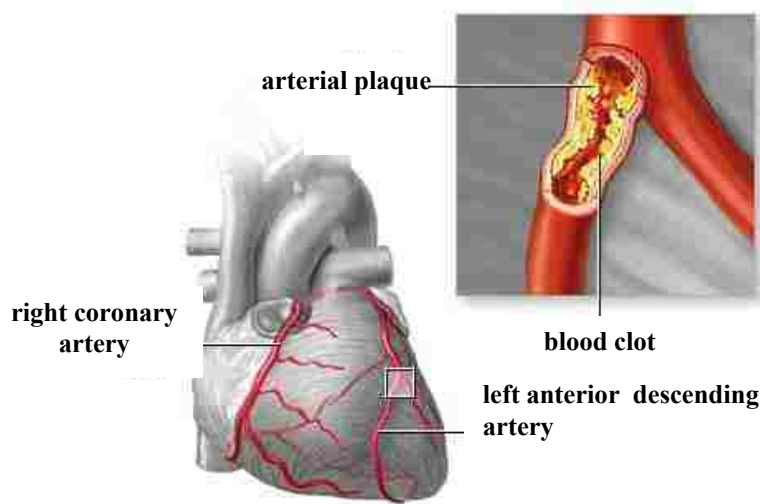


**Figure 1.2** Illustration of severe atherosclerosis.<sup>2</sup>

Most would agree that affordable healthcare is among the most important issues facing our society. Based on the aforementioned data and statistics, the economic burden of CVD-related healthcare services in the U.S. is projected to exceed \$448.5 billion in 2008.<sup>3-5</sup> This estimate will likely increase significantly in the coming years as those born in the “Baby Boomer” generation (1946-1964) reach old age. Fortunately, technology is rapidly evolving to meet the growing demand for diagnostic tools that will allow clinicians to better diagnose and treat CVD.

Our research group and others worldwide are currently developing the next generation of biomedical screening methods for use in high-throughput CVD screening applications. The remainder of this Chapter provides a general review of current bioanalytical screening technologies as well as other topics relevant to CVD including biomarkers, vitamin B, and polycyclic aromatic hydrocarbons (PAHs). The feasibility of using immunoaffinity extraction as a means of enhancing PAH characterizations in human atherosclerotic plaques and tissues is also discussed. This review also addresses recent advances in nanotechnology-based bioanalytical sensors for detection of thiol-containing biomarkers.

### **1.1.1 Conventional Risk Factors and Biomarkers**

The complexity of CVD makes it extremely difficult to identify specific sources of pathogenesis. For this reason, physicians and biomedical researchers are constantly searching for new CVD risk factors and biomarkers for use in clinical diagnosis. Risk factors are either inherent human characteristics or preventable behaviors that correlate with the occurrence of a particular disease. Inherent CVD risk factors cannot be treated and include age, gender, congenital defects, and race. In general, the inherent risk of atherosclerosis increases with age and males tend to be more susceptible to CVD than women. Conversely, preventable risk factors

can be effectively moderated by treatment and or behavior modification.

The most well-known preventable CVD risk factors include tobacco smoking, high blood cholesterol (HBC), HBP, sedentary lifestyle, obesity, diabetes, stress, and alcohol abuse. Smoking is perhaps the most controversial of all preventable CVD risk factors because non-smokers are often inadvertently subjected to second-hand tobacco smoke. For this reason, many municipalities worldwide have moved to protect public health and safety by prohibiting tobacco use in most public places. Analogous public health initiatives are being launched in the U.S. to combat HBC. California was the first state to ban the use of HBC-inducing trans fatty acids in fast food cuisine (2010) and baked goods (2011).<sup>6</sup> Most individuals can moderate their HBC by adopting a low-fat diet. In other cases, the use of cholesterol-lowering medications may be necessary.

Being overweight also increases ones risk of CVD. Excess fat in the abdominal area is thought to be especially detrimental to cardiovascular health.<sup>7</sup> In contrast, maintaining a normal weight and enacting lifestyle changes such as becoming physically active, reducing stress, and avoidance of alcohol abuse are beneficial factors. Diabetes mellitus is also classified as a preventable risk factor. Surprisingly, approximately 75% of diabetics eventually succumb to CVD-related complications.<sup>8</sup> For this reason, it is critical for diabetics to take every available precaution to control their blood glucose levels and weight.

Disease biomarkers are measurable and quantifiable characteristics associated with a pathological process.<sup>9</sup> Based on this definition, some CVD risk factors including HBP and HBC are also classified as biomarkers. Serological CVD biomarkers are found in the blood or serum. Conventional serological CVD biomarkers such as cholesterol, inflammation indicators, and natriuretic peptides have been thoroughly reviewed in the literature and will not be discussed

here.<sup>9-15</sup> Alternatively, a general reference list of current serological biomarkers and associated CVD indicators is provided in Table 1.1. The biomarkers in the general category are considered novel because their pathological functions are not yet well understood. The amino acid homocysteine is of particular interest because there is fervent disagreement within the biomedical community about its significance to CVD (*vide infra*).

**Table 1.1** General reference list of current serological CVD biomarkers. (adapted from ref. 9)

Serological CVD Biomarkers			
cholesterol	inflammation	natriuretic peptides	general
Apo B	HsCRP	ADMA	oxidized LDL
Lp (a)	sICAM-1	MMP-9	GPX1 activity
LDL particle #	IL-6	TIMP-1	nitrotyrosine
CETP	IL-18		homocysteine
Lp-PLA2	SAA		cystatin-C
	MPO		
	sCD40		

### 1.1.2 Homocysteine as a Cardiovascular Disease Biomarker

Homocysteine (Hcy) is a sulfur-containing, nonproteinogenic amino acid that is produced in the body as an intermediate species in protein synthesis. Hcy has two major metabolic fates, conversion to methionine via remethylation pathway and conversion to cysteine (Cys) via transsulfuration pathway.<sup>16</sup> The remethylation pathway is catalyzed by vitamin B<sub>12</sub> and folic acid, while the transsulfuration pathway is catalyzed by vitamin B<sub>6</sub> (Figure 1.3). Individuals with vitamin B deficiencies or congenital metabolic defects are often incapable of maintaining normal Hcy levels. Consequently, intracellular Hcy levels rapidly increase until the cell is forced to

excrete Hcy into the bloodstream, thereby resulting in elevated serum Hcy levels. This condition is known as hyperhomocysteinemia. The scale used for clinical diagnosis of hyperhomocysteinemia is 1) moderate (10-30  $\mu\text{M}$ ), 2) intermediate (30-100  $\mu\text{M}$ ), and 3) severe ( $\geq 100 \mu\text{M}$ ).

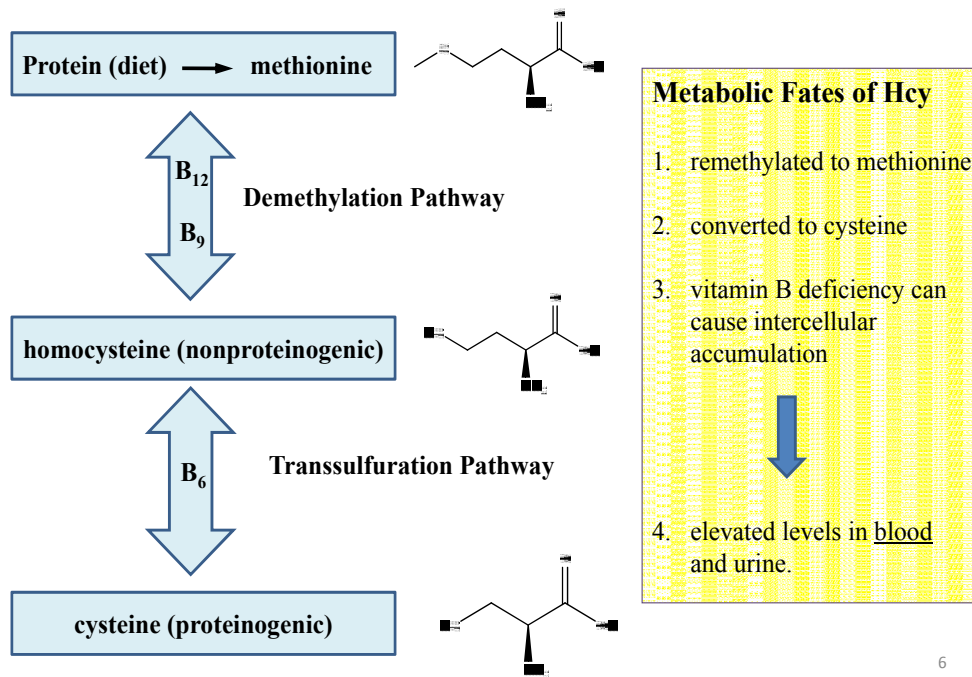


**Figure 1.3** Schematic of *in vivo* homocysteine metabolism.

Hyperhomocysteinemia is believed to directly affect cardiovascular proteins. Excess Hcy may alter the biochemical properties of arterial surfaces, thereby inducing lesions and the onset of atherosclerosis. This theory was initially proposed by Kilmer McCully in 1969 after observing damage to cultured endothelial cells caused by the presence of Hcy.<sup>17</sup> McCully and a team of biomedical researchers subsequently demonstrated that the severity of atherosclerotic lesions and tissue damage in rabbits were directly proportionate to the amount of Hcy injected intravenously.<sup>18</sup> These early observations inspired the direct toxicity model, which identified Hcy as a causative agent in atherosclerosis.<sup>19</sup> Despite its scientific merit, the direct toxicity model was not well received in 1971 because it appeared to contradict the widely accepted

cholesterol-CVD hypothesis, which identified cholesterol as the root cause of heart disease. The ensuing controversy culminated with the loss of McCully's research funding and prestigious faculty positions at the Harvard Medical School and Massachusetts General Hospital in 1979. Nevertheless, McCully continued his research in relative obscurity at the Providence Rhode Island Veterans Hospital. He was finally vindicated in 1997 when a major clinical study concluded that CVD risk increased proportionately with every 10% increase in blood Hcy levels above normal ( $\leq 10 \mu\text{M}$ ).<sup>20</sup>

Today, physicians often consider Hcy along with cholesterol and other risk indicators when diagnosing CVD. Representative blood Hcy concentration values measured in normal individuals and hyperhomocysteinemia patients are listed in Table 1.2. These data suggest that some individuals with hyperhomocysteinemia have Hcy levels that exceed normal levels by more than 10-fold. Hyperhomocysteinemia patients also tend to have higher concentrations of protein-bound Hcy levels. Protein-bound Hcy is not yet classified as a CVD biomarker. *N*-Hcy-protein is presumed to be the most physiologically relevant form of protein-bound Hcy (*vide infra*).

**Table 1.2** Blood homocysteine levels in normal and hyperhomocysteinemia patients.<sup>21</sup>

Hcy levels	Normal subjects	Hyperhomocysteinemia patients
Normal subjects	10.5 ± 4.5	
Hyperhomocysteinemia patients		105 ± 45
Hyperhomocysteinemia patients		105 ± 45
Hyperhomocysteinemia patients		105 ± 45





There is also a wealth of information in the literature pertaining to vitamin B content in atherosclerotic tissues. Representative values for Vitamin B content in autopsied normal and atherosclerotic aortic tissues are shown in Table 1.3. With the exception of folic acid, vitamin B content in normal tissue is considerably higher than in atherosclerotic tissue. Note that vitamin content is expressed as % concentration vitamin B detected in normal pulmonary or vena cava tissues from the same subject. These data reinforce the relationship between vitamin B and CVD.

**Table 1.3** Vitamin B content values in normal and atherosclerotic heart tissues.<sup>30</sup>

<b>Vitamin</b>	<b>normal tissue % content (standard deviation), n = no. of subjects</b>	<b>atherosclerotic tissue % content (standard deviation), n = no. of subjects</b>
<b>Thiamine (B<sub>1</sub>)</b>	107.7 (0.83); n = 32	78.4 (2.42); n = 10
<b>Riboflavin (B<sub>2</sub>)</b>	124.8 (6.43); n = 27	76.7 (6.95); n = 17
<b>Nicotinic acid (B<sub>3</sub>)</b>	120.1 (3.42); n = 11	not reported
<b>Pyridoxal-5-phosphate (B<sub>6</sub>)</b>	122.6 (4.22); n = 45	80.9 (4.02); n = 56
<b>Folic acid (B<sub>9</sub>)</b>	86.8 (2.54); n = 14	84.7 (1.34); n = 6
<b>Cobalamine (B<sub>12</sub>)</b>	191.0 (5.82); n = 14	97.2 (0.10); n = 27

### 1.1.3 N-Homocysteine-Protein

The function of Hcy in the pathogenesis of CVD is poorly understood. However, there is compelling evidence that suggests Hcy thiolactone (HTL), a metabolite of Hcy, may trigger the onset of CVD.<sup>31-33</sup> HTL is a reactive thioester compound synthesized *in vivo* through enzymatic aminoacyl-tRNA synthase pathways at a rate proportional to extracellular Hcy concentration.<sup>34</sup> Hence, HTL production is likely elevated in individuals with hyperhomocysteinemia.<sup>35</sup> Increased *in vivo* production of HTL is known to induce pathogenic effects such as vascular

protein and tissue damage, which may induce early atherosclerotic lesion formation.<sup>36</sup> It has also been shown that HTL readily and preferentially reacts with proteins at the  $\epsilon$ -amino groups of lysine residues under physiological conditions to yield protein homocystamide (*N*-Hcy-protein) species.<sup>21, 37</sup> HTL modification can be detrimental to protein function because it may lead to spontaneous intermolecular disulfide bonding to yield protein oligomers (Figure 1.5).<sup>38</sup> *N*-Hcy-protein also exhibits decreased biological activity, lower solubility, and increased immunogenicity.<sup>39</sup> Moreover, a recent clinical study has revealed a positive correlation between plasma *N*-Hcy-protein levels and instances of major diseased coronary vessels in 254 subjects.<sup>40</sup>

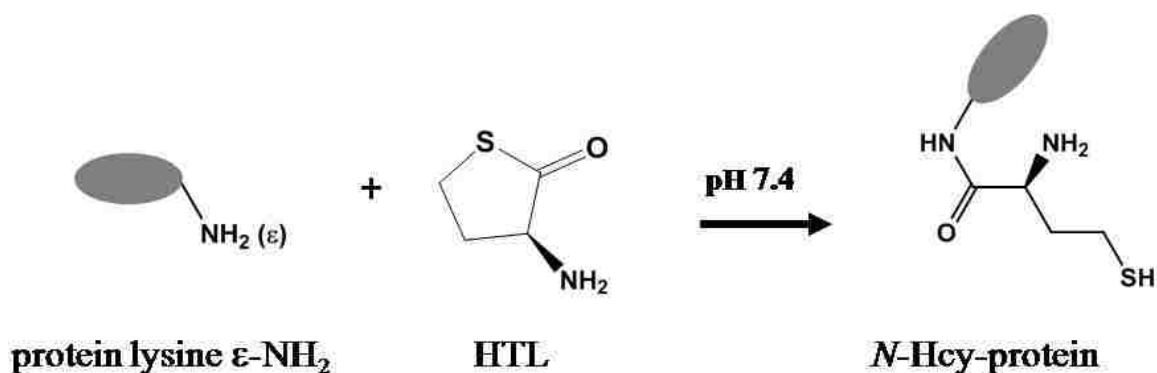


**Figure 1.5** Post-translational protein modification via *N*-homocysteinylation.

## 1.2 Conventional Bioanalytical Methods for Homocysteine Analysis

Given the biomedical significance of Hcy as a CVD biomarker, there is demand for accurate and reliable diagnostics for Hcy. Bioanalytical chemists have responded to this challenge by engineering a variety of methods and techniques. Hcy diagnostic methods are typically classified as either direct or indirect methods. Direct methods of Hcy analysis are usually rapid and require minimal sample preparation. In contrast, indirect methods tend to be time-consuming and laborious due to complicated sample derivatization, separation, and purification steps. One commonality between direct and indirect Hcy diagnostics is the necessity

for sample pretreatment with a disulfide reducing agent in order to liberate oxidized species. The most extensively used aqueous-soluble disulfide reducing agents include 2-mercaptoethanol, dithiothreitol, and 2-carboxyethyl phosphine. The remainder of this chapter provides a brief review of conventional chromatographic, electrophoretic, and immunoaffinity-based methods for analysis of Hcy and related biomolecules. The perceived advantages and disadvantages of each method are also discussed.

### **1.2.1 Chromatographic Methods**

Hcy is found in serum and thus must be separated from a multitude of complex sample components prior to detection. In general, chromatographic methods accomplish analytical separations within a packed column by way of selective partitioning of the analytes between a mobile phase and a stationary phase. The separation can be monitored either on-column or post-column. GC-MS, high-performance liquid chromatography (HPLC), and ion exchange chromatography (IEC) are the most popular indirect methods for Hcy analysis.

The appeal of GC-MS in modern clinical laboratories is waning because biomolecules such as Hcy must undergo tedious chemical derivatization to increase volatility and thermal stability prior to GC separation. HPLC is perhaps the most widely used method of analysis for Hcy because the instrumentation is widely available in clinical laboratories. Reversed phase HPLC systems utilize a polar-aqueous mobile phase and a hydrophobic stationary phase (e. g. C<sub>8</sub> and C<sub>18</sub>), which are more compatible with biomolecules. Furthermore, HPLC is widely applicable to Hcy analyses because it readily accommodates photometric, fluorometric, electrochemical and MS detectors. IEC is primarily used as a sample clean-up technique prior to detection with an amino acid analyzer. IEC discriminates among biomolecules such as proteins, nucleic acids, and amino acids based on electrostatic interactions. Perhaps the most attractive

feature of chromatographic methods is the availability of numerous detection formats. Conversely, the cost associated with operation and maintenance of chromatographic systems can be relatively higher.

### **1.2.2 Electrophoretic Methods**

Capillary electrophoresis (CE) is a high-performance separation technique that has become a viable alternative to chromatographic methods for Hcy analysis. Capillary zone electrophoresis (CZE), the simplest mode of CE, is performed by inducing electroosmotic flow within a micro-bore fused silica capillary filled with an electrolyte solution. The result is near-plug flow, which provides rapid and highly efficient separation of charged analytes based on the principle of electrophoretic mobility. The major advantages of CE over chromatographic methods include shorter analysis times, higher peak efficiencies, and lower sample-reagent consumption. The basic apparatus for CE includes a fused silica capillary, buffer reservoirs, a high voltage power supply, and a detection system. A schematic of a CE instrument is provided in Figure 1.6. Detection options for CE are essentially the same as those listed for LC. However, CE is generally less concentration sensitive than HPLC methods due to the shorter optical path length of the capillary. Protein wall-adsorption is also a potential problem. Recent innovations in CE Hcy analysis are reviewed in the literature and will not be discussed here.<sup>41, 42</sup>

Although CE has become a viable option for protein separations, sodium dodecyl sulfate-polyacrylamide gel electrophoresis (SDS-PAGE) is by far the most commonly used method. SDS is an anionic surfactant that binds with protein molecules such that all species have identical charge-to-mass ratios. The resultant protein-SDS conjugates are subjected to electrophoresis within a molecular sieving gel matrix that facilitates separation based on size. The separation is usually visualized by staining the gel with a protein-specific dye such as coomassie blue. Our

research group and others have used both CE and SDS-PAGE for analysis of *N*-Hcy-protein (*vide infra*).



**Figure 1.6** Diagram of capillary electrophoresis instrument.

### **1.2.3 Immunochemical-Based Assays**

Immunoassays (IAs) exploit the strong and selective affinity interactions of antibodies. The most popular IA format is the enzyme-linked immunosorbent assay (ELISA) method. In its simplest form, ELISA involves the immobilization or bioconjugation of antibodies to a solid support. The conjugated antibody is then incubated in a solution containing the target analyte and allowed to bind. The support is rinsed between sample applications to remove non-specifically bound sample constituents. Detection is usually achieved by introducing specially labeled detection antibodies that produce a colorimetric response upon the addition of an enzyme. Fluorescently labeled antibodies can also be employed to achieve greater analytical sensitivity. ELISA is gradually replacing HPLC as the preferred method for many clinical screening applications because it is relatively inexpensive, less laborious, and more conducive to high-throughput platforms such as 96-well plates. Various ELISA-based Hcy detection methods have been reported, some of which are commercially available as kits.<sup>43-45</sup> The advantages and disadvantages of current bioanalytical technologies for Hcy analysis are summarized in Table 1.4.

**Table 1.4 Comparison of conventional bioanalytical methods. (adapted from ref. 75)**

<b>Method (detection)*</b>	<b>Advantages</b>	<b>Disadvantages</b>
GC-isotopic dilution (MS)	-excellent accuracy and precision -applicable to determination of other amino thiols -superior sensitivity	-MS required -derivatization -complex instrumentation
HPLC (MS-MS)	-no derivatization required -good accuracy and precision achievable using internal standard	- requires expensive MS-MS and deuterated internal standards -complex instrumentation
HPLC (PD)	-high sensitivity (<50 nM) -high precision (1.2 - 2.5 %) -more user friendly than LCMS	-post-column derivatization required for optimum sensitivity
HPLC (FD)	-high sensitivity (not reported) -high precision (1.0 – 4.8 %) -more user friendly than LC-MS	-pre-column derivatization -difficult to automate
HPLC (ECD)	-no derivatization required -comparable analytical performance to other HPLC methods	-susceptible to contamination and electrode fouling
IEC	-serves as a simplistic sample clean-up method -easily automated	-requires post-column derivatization if amino acid analyzer is used
CE (FD)	-shorter analysis time than chromatographic methods -less laborious than HPLC -lower sample and solvent Consumption -easily automated	-CE inherently less sensitive than chromatographic methods -FD usually required to achieve adequate sensitivity
IA (FD, CLD, enzymatic)	-superior selectivity -very user friendly -ELISA kits commercially available -high-throughput (96 well ELISA)	-only L-Hcy can be analyzed -limited dynamic range -higher reagent cost than HPLC or CE -difficult to standardize -antibodies produced in animals

\*MS-MS = tandem mass spectrometry; PD = photometric detection; FD = fluorescence detection; ECD = electrochemical detection; CLD = chemiluminescence detection.

### 1.3 Direct Visual Detection of Homocysteine

One common disadvantage of conventional bioanalytical methods for Hcy analysis is the lack of analytical selectivity for the *N*-Hcy-protein fraction of serum. To date, most methods are only capable of determining total Hcy (Hcyt), which consist of both free and protein-bound Hcy. Researchers have attempted to adapt conventional methods for use in *N*-Hcy-protein detection. However, the resulting procedure is often more costly, complicated, and laborious. For example, some modified HPLC methods require several additional steps including acid hydrolysis, IEC purification, and post-column labeling.<sup>46, 47</sup> Although ELISA shows great promise for *N*-Hcy-protein analysis, method development has been greatly hindered by the lack of commercially available *N*-Hcy-protein antibodies.

Direct visual detection is the latest trend in bioanalytical analysis. Our laboratory has collaborated in the development of several organic dye-based molecular probes for direct visual Hcy sensing. These probes were prepared from inexpensive and commercially available substrates including methyl viologen and fluorine black.<sup>48, 49</sup> Organic molecular probes typically exhibit excellent selectivity for Hcy but are susceptible to non-specific binding to proteins. For this reason, most organic dye-based probes are not useful for direct detection of *N*-Hcy-protein.

Nanotechnology provides a versatile platform for addressing the shortcomings of conventional bioanalytical methods and organic dye-based molecular probes. Direct colorimetric detection of Hcy with GNP sensors is based on the principle of localized plasmon resonance, a phenomenon that occurs when the de Broglie wavelength of colloidal valence electrons is comparable to colloid particle size.<sup>50</sup> Under these conditions, the nanocolloid behaves as a “theoretical quantum box” that contains oscillating electrons. Localized plasmon resonance is produced by the oscillating electrons. The frequency of localized plasmon



resonance is strongly dependent on colloidal composition, particle size, shape, and interparticle distance.<sup>51</sup> GNPs (5 to 20 nm) dispersed in aqueous media generally have plasmon resonance absorption bands in the vicinity of 520 nm.

The utility of colloidal nanoparticles as sensors is based on chemically or biochemically induced self-assembly. Nanoparticle self-assembly decreases interparticle distance, which facilitates plasmon coupling via electron tunneling between particles. The result is diminished plasmon resonance frequency, which causes a proportionate shift in absorption and characteristic transitions in solution color from red to purple-violet.<sup>52</sup> GNPs (5-20 nm) self-assembled in aqueous media usually exhibit plasmon absorption maxima at or beyond 620 nm, depending on the degree of assembly. A diagram of colorimetric sensing with plasmon resonant GNPs is shown in Figure 1.7. In this generic example, 10 nm GNPs are subjected to a specific biochemical stimulus that induces nanoparticle self-assembly and colorimetric response. In practice, it is often necessary to functionalize the GNPs in order to achieve the desired biochemical recognition.

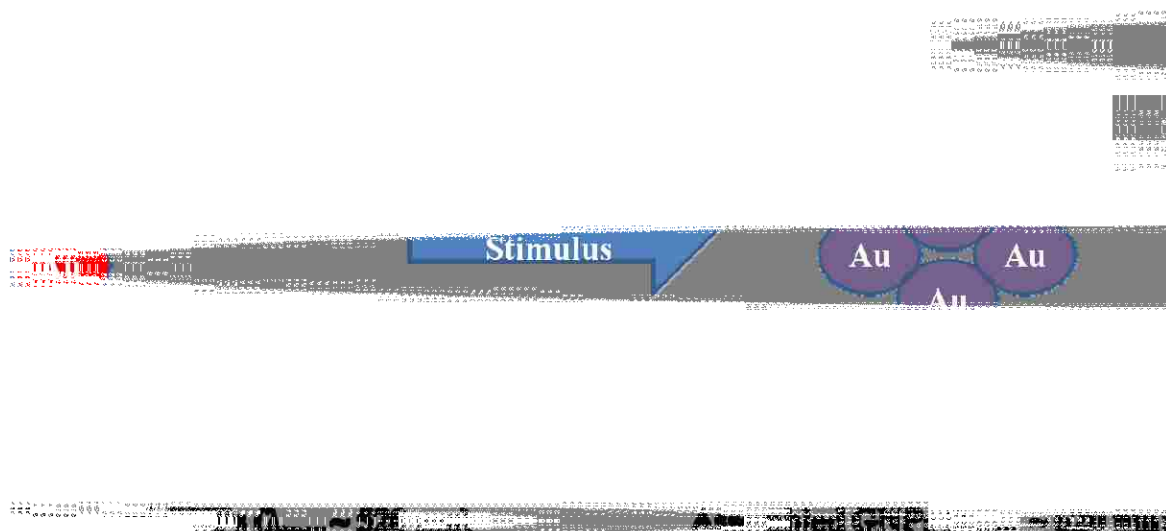


**Figure 1.7.** Plasmon resonant GNP biochemical sensing.

The concept of plasmon resonant biochemical probes originated more than 40 years ago when Bloomfield invented a colloidal gold reagent for plasma protein testing.<sup>53</sup> Recent advancements in plasmon resonant biochemical sensors have been reviewed in the literature.<sup>54</sup> GNPs have shown great promise for sensing a wide range of physiologically relevant molecules including carbohydrates,<sup>55</sup> and DNA.<sup>56, 57</sup> Likewise, GNPs have been used to detect amino thiol biomarkers including Hcy<sup>58</sup>, Cys<sup>59</sup>, and glutathione.<sup>59</sup> The first account of plasmon resonance detection of *N*-Hcy-protein was recently reported by our research group (*vide infra*).<sup>60</sup>

## **1.4 Spectrochemical Techniques**

Spectroscopic methods are an integral part of the research presented in this dissertation. For example, UV-visible (vis) spectroscopy is used for various analytical applications including detection in CE separations and GNP protein sensing. Fluorescence spectroscopy is utilized to assess biomolecular interaction between pyridoxal and Hcy. Additionally, circular dichroism (CD) spectroscopy is employed to probe protein conformational change on the surfaces of gold nanobioconjugates. This section provides a brief introduction to relevant spectrochemical analysis techniques.

### **1.4.1 UV-visible Spectroscopy**

UV-vis absorption spectroscopy is a molecular characterization technique used for analysis of molecules that absorb ultraviolet and visible light (photons). The photon absorption process causes electrons in the analyte molecule to be promoted from the ground energy state to an excited energy state. Spectrochemical information about the molecule is obtained by measuring the magnitude of the electronic transition.<sup>61</sup> A spectrophotometer measures the absorption or transmittance of light by a sample. A graphic representation of a UV-vis spectrometer is shown in Figure 1.8. A light source capable of producing UV and visible

radiation is directed to a diffraction grating, where it is separated into distinct wavelengths. The desired wavelength of light is then projected through an aperture onto the sample cuvet. The transmitted light is usually detected by use of a photomultiplier tube or photodiode-array.

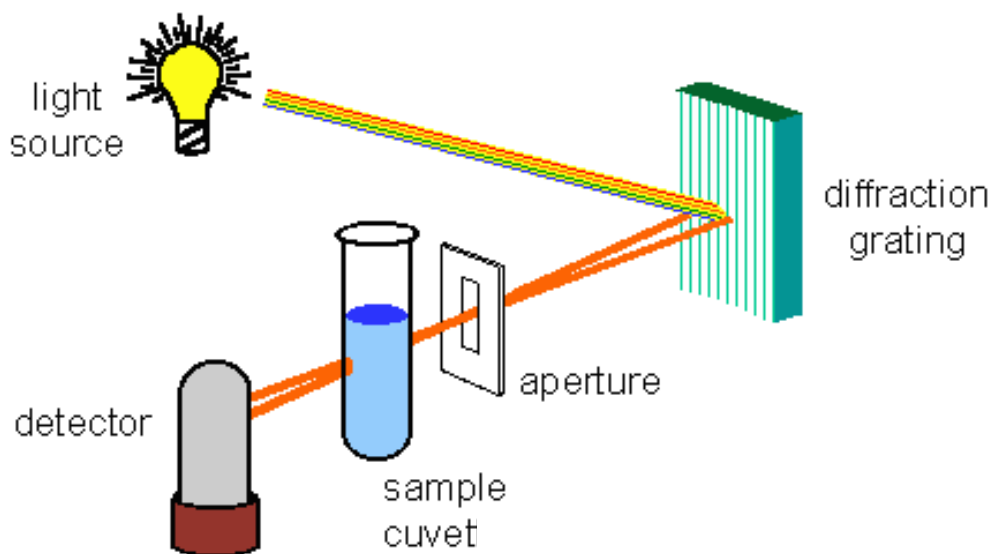


**Figure 1.8** Graphic representation of a UV-visible spectrometer.<sup>62</sup>

The absorption spectrum of a sample is obtained by plotting absorption intensity or absorbance versus excitation wavelength. UV-vis spectroscopy is useful for analytical applications because sample absorbance is proportional to concentration as described by the Beer's law equation;  $A = \epsilon bc$ , where  $A$  is absorbance,  $\epsilon$  is molar absorptivity,  $b$  is the sample pathlength and  $c$  is molar concentration. Based on this relationship, a calibration curve can be generated to determine the concentration of molecules in unknown samples.

### 1.4.2 Circular Dichroism Spectroscopy

Circular dichroism (CD) is a variant of absorption spectroscopy that allows one to detect the chiral signatures of amino acids, RNA, DNA, and other biomolecules. Researchers also use CD to probe protein structural conformations such as  $\alpha$ -helices and  $\beta$ -sheets and random coils (Figure 1.9). Molecular excitation for CD is achieved by use of circularly polarized light, which

is absorbed preferentially on the basis of differences in the chirality of molecular constituents.<sup>63</sup> Hence, the transmitted light becomes elliptically polarized. The term ellipticity ( $\theta$ ) is used to describe the angular bias of CD resulting from a sample.

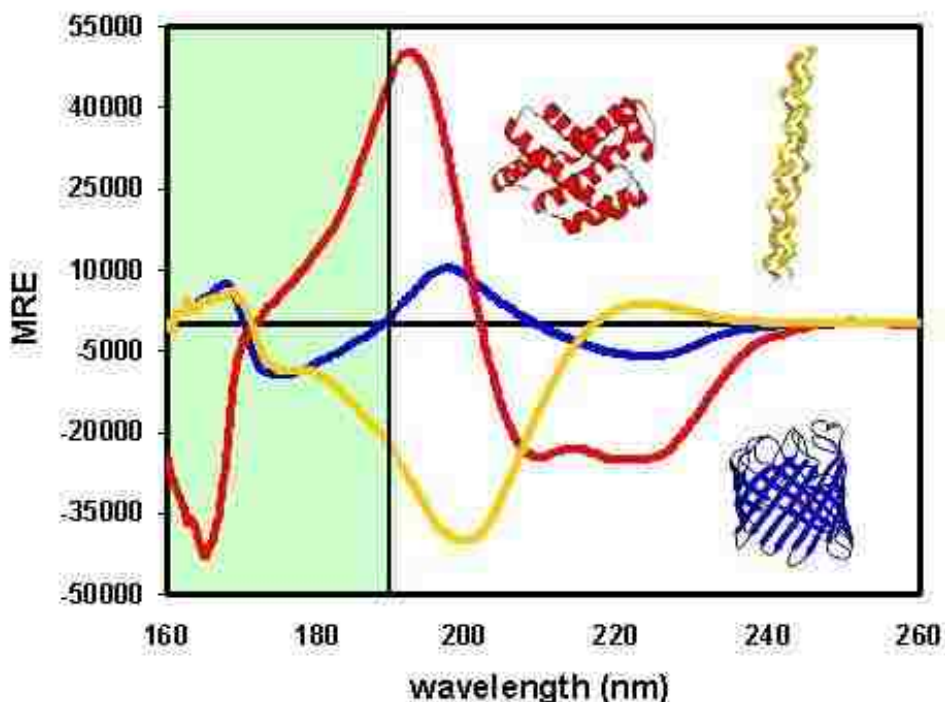


**Figure 1.9** Theoretical protein ellipticity curves for  $\alpha$ -helix (red),  $\beta$ -sheet (blue), and random coil (yellow) components.<sup>64</sup>

### 1.4.3 Fluorescence Spectroscopy

The Jablonski diagram (Figure 1.10) illustrates the processes involved in molecular fluorescence. Initially, excitation via photon absorption promotes the molecule to an excited singlet state ( $S_n$ ). At this point, the molecule encounters both radiative and non-radiative modes of relaxation to the ground state. Non-radiative relaxation modes include collisional quenching, internal conversion, and intersystem crossing. Collisional quenching is energy transfer from one molecule to another by way of collision. Internal conversion is energy loss due to electronic transitions within the same spin state. Intersystem crossing refers to electronic transitions

between spin states of different multiplicities, such as singlet to triplet ( $S_n$  to  $T_n$ ). Fluorescence is a radiative mode of relaxation that occurs when the molecule transitions from the  $S_1$  state to the ground state ( $S_0$ ). The wavelength of fluorescence emission is red-shifted compared to the excitation wavelength.<sup>61</sup> This effect is known as the Stokes shift. Similarly, radiative relaxation can result from phosphorescence, which results from  $T_1$  to  $S_0$  transitions.

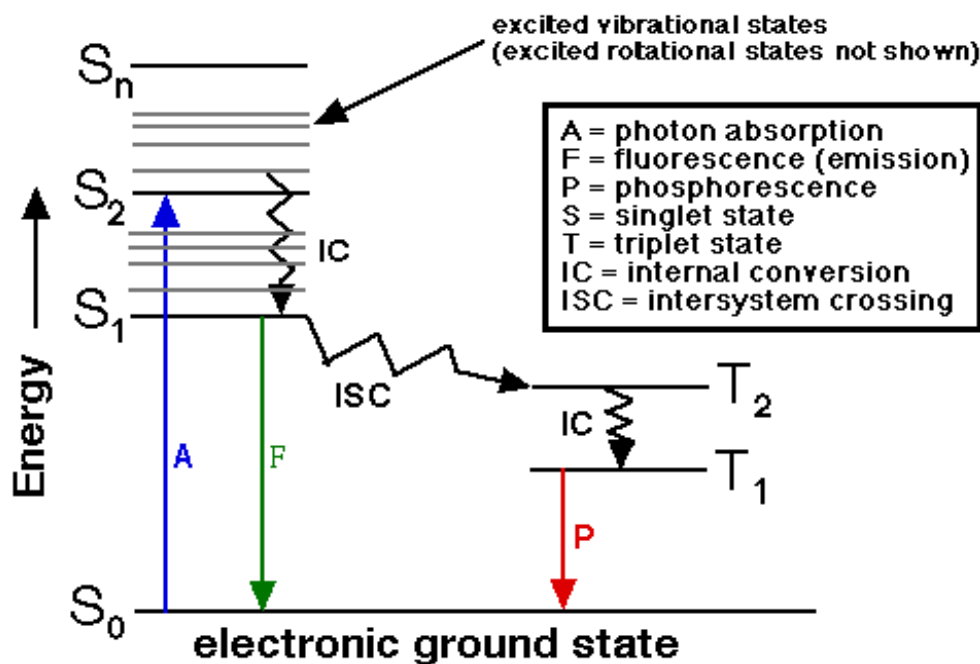


**Figure 1.10** Jablonski diagram.<sup>65</sup>

### 1.5 Mass Spectrometry

Mass spectrometry (MS) is an analytical technique that discriminates charged molecular species based on mass-to-charge ( $m/z$ ) ratio. The basic instrumentation required for MS includes 1) ion source, 2) mass analyzer, 3) detector, and 4) data system (Figure 1.11). The purpose of the ion source is to facilitate ionization of individual analyte molecules. Ionized sample components are then accelerated to the mass analyzer, which separates molecular ions according to  $m/z$  by use of magnetic or electric field sectors. Molecular ion detection is usually accomplished by converting ion current to electrical signal. Upon completion of signal

conversion and data analysis, a mass spectrum is generated by plotting signal intensity versus  $m/z$ .

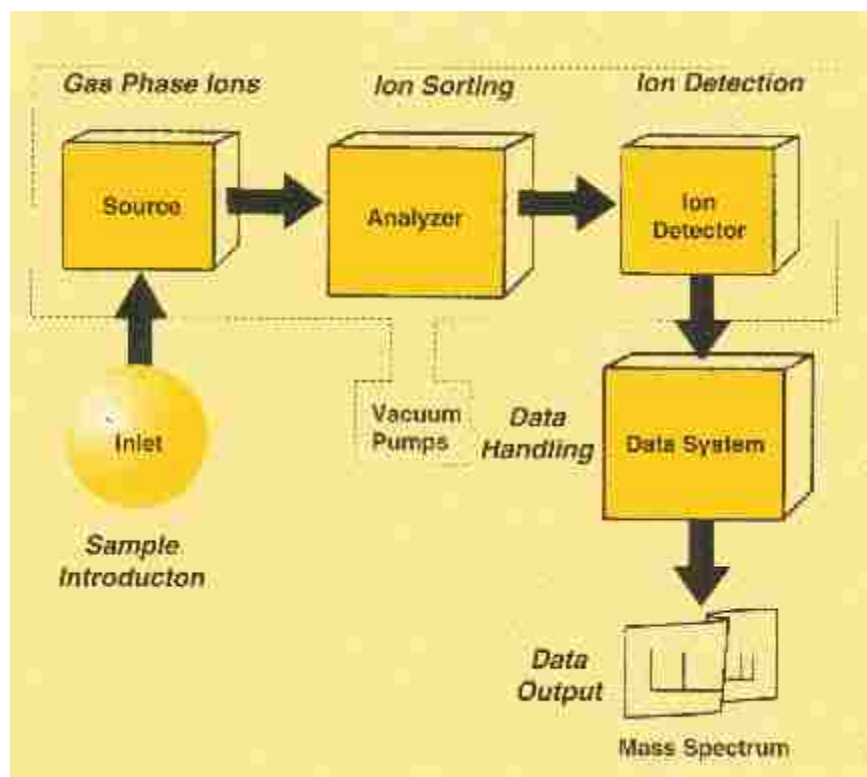


**Figure 1.11** Block diagram of generic mass spectrometer.<sup>66</sup>

### 1.6 Bioaccumulation of Polycyclic Aromatic Hydrocarbons in Atherosclerotic Tissues

Chemical characterizations of cardiovascular tissues and plaques have greatly enhanced knowledge of CVD pathology.<sup>67-73</sup> Our laboratory has contributed to this effort by evaluating calcium-hydroxyapatite,<sup>74-77</sup> and cholesterol<sup>78</sup> content in atherosclerotic plaques and tissues. These studies have afforded a better understanding of the physiochemical differences between native and bypass atherosclerotic plaques. PAH content in cardiovascular tissues is also of interest to biomedical researchers because of the potential for bioaccumulation. PAHs are a class of toxic, hydrophobic, and potentially carcinogenic environmental pollutants created as byproducts of combustion. The solubility and toxicity of PAHs increase upon enzymatic conversion to more polar metabolites which are more soluble in physiological media. Figure

1.12 gives the structures for 16 PAHs currently monitored and regulated by the United States Environmental Protection Agency. Significant levels of PAHs have been detected in the air,<sup>79, 80</sup> water sources,<sup>81, 82</sup> food products,<sup>83, 84</sup> and soil.<sup>85, 86</sup> However, very little is known about the PAH content in atherosclerotic tissues. This is partially due to the lack of selective methods for extracting PAHs from atherosclerotic plaques and tissues. For this reason, new strategies for obtaining higher analyte selectivity are explored in this dissertation.

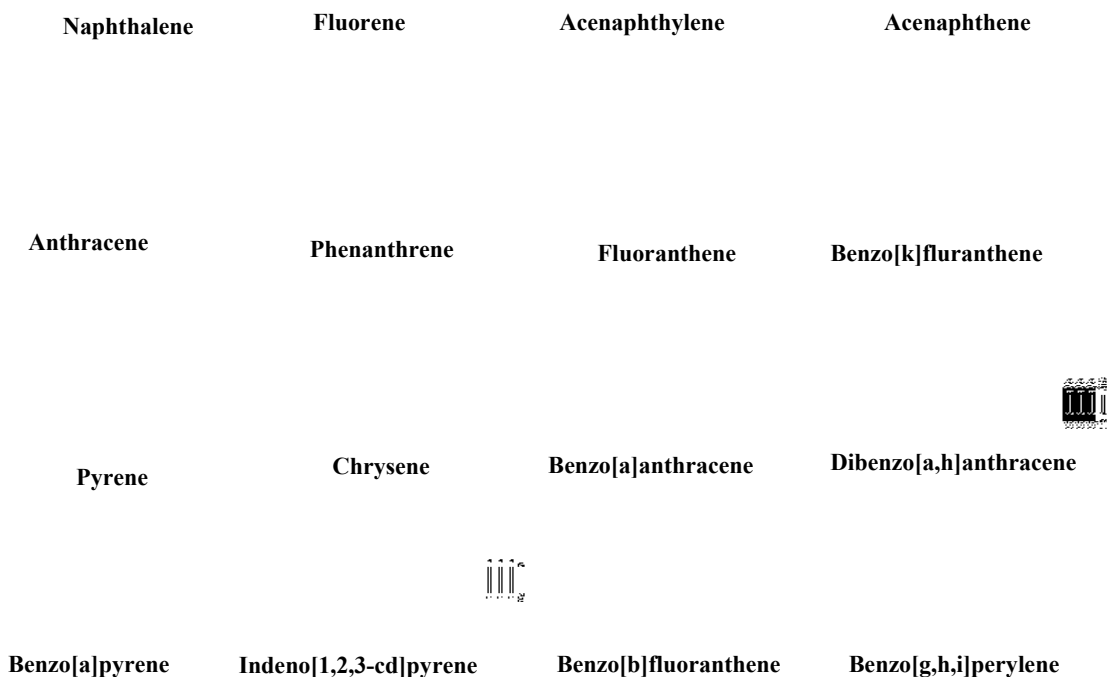


**Figure 1.12** Chemical structures for EPA list of priority PAHs.

Immunoaffinity-based methods could help address the need for greater selectivity in the analysis of PAHs in atherosclerotic plaques and tissues. Immunoaffinity extraction (IAE) is a technique that uses immobilized antibodies to bind a specific molecular target, thereby simultaneously extracting and concentrating the target analyte. The primary advantage of IAE is

its compatibility with complex biological sample matrices. Figure 1.13 shows a graphic representation of a PAH antibody. The  $F_c$  or constant region of the antibody is covalently immobilized to an IAE stationary phase. PAH binding occurs at the  $F_{ab}$  or binding region of the antibody, also known as the “binding pocket”.

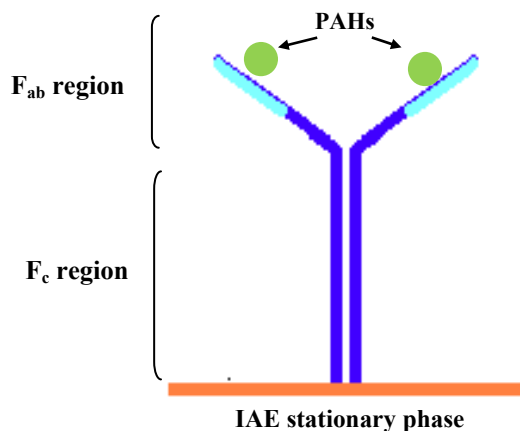


**Figure 1.13** PAH antibody immobilized to an IAE stationary phase.

A process diagram of the IAE cycle for PAH analysis is shown in Figure 1.14. In the first step, the mobile phase is maintained at physiological pH to facilitate binding of PAH molecules (green dots) to the immobilized antibodies as the sample is passed through the column. Non-PAH sample components (red squares and blue dots) do not bind and are thus not retained on the column. Non-specifically bound sample components are washed off the column in the second step. In the third step, the mobile phase conditions are changed, usually by lowering pH, to disrupt the antibody binding and elute the PAH molecules from the column. If desired, the PAH molecules can be detected for quantification during the elution step prior to fraction collection. The column is regenerated in the final step by reestablishing the initial mobile phase conditions. Under ideal conditions, the IAE cycle can be repeated hundreds of times. We have proposed a hybrid organic solvent-IAE method for PAH analysis in



atherosclerotic plaque. The feasibility of this method is discussed in Chapter 6 of this dissertation.

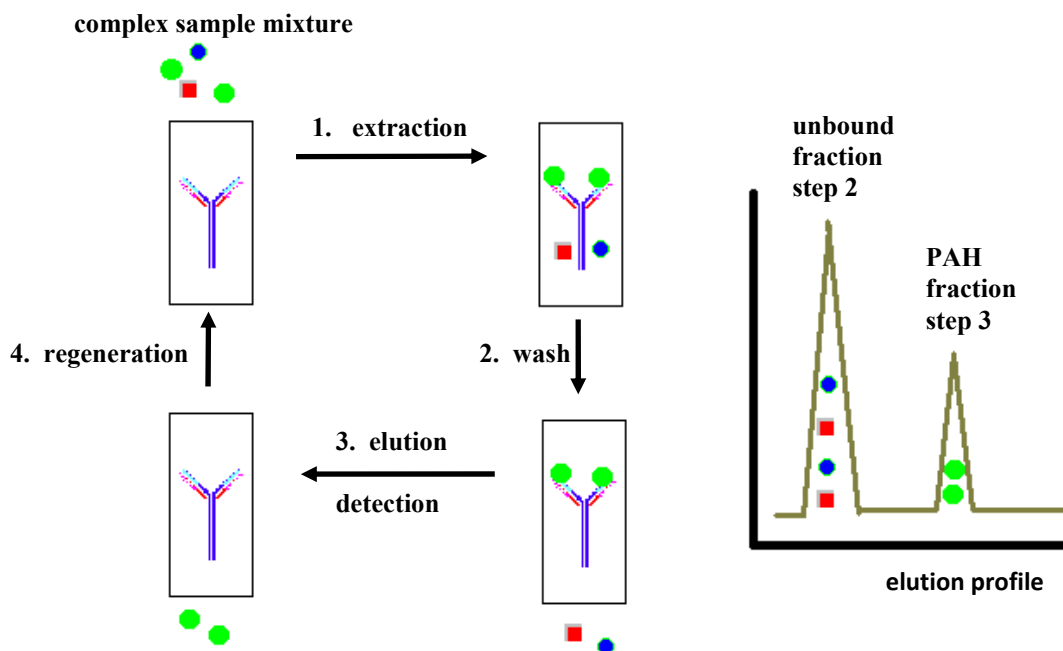


**Figure1.14** Diagram of IAE cycle and elution profile.

## 1.7 Scope of Dissertation

The Warner Research Group has worked diligently over the past decade to elucidate the chemical processes involved in CVD. Along the way, we have pioneered the use of sophisticated analytical techniques such as cross polarization magic angle spinning (CP-MAS) NMR<sup>76</sup> and inductively coupled plasma-mass spectrometry (ICP-MS)<sup>75, 77</sup> in elemental characterizations of atherosclerotic plaques. The findings from these earlier studies have afforded a better understanding of atherosclerosis. This dissertation continues this fundamental CVD research and describes the implementation of several new research directives related to the study of Hcy and related CVD indicators. The first chapter is a general review of topics relevant to the research presented in this dissertation. Chapter 2 describes the exploration of molecular interactions related to *in vitro* pyridoxal tetrahydrothiazine formation in order to establish an

empirical basis for nonenzymatic Hcy clearance in the body. This topic is further evaluated in Chapter 3, which is a report on the use of CE to monitor inhibition of *N*-homocysteinylation-induced protein oligomerization by pyridoxal. In addition, spectroscopic data pertaining to *in situ* pyridoxal tetrahydrothiazine formation in the presence of *N*-Hcy-protein is presented and discussed. Chapter 4 provides an account of our efforts to develop a plasmon resonant sensor for plasma *N*-Hcy-Protein detection in serum. GNP self-assembly behavior is examined in the presence of both unmodified and *N*-Hcy-protein by use of UV-vis spectroscopy and transmission electron microscopy. More in-depth investigations of the underlying physiochemical processes involved in plasmon resonance Hcy sensing are presented in Chapter 5. Three different types of gold nanobioconjugates are prepared by coating colloidal gold with albumin, cytochrome *c*, or serum, respectively. Plasmon resonance absorption, nanobioconjugate assembly, and protein conformational changes are monitored. The mechanism of gold nanobioconjugate association is also evaluated. Chapter 6 is a discussion of the feasibility of using a hybrid organic-immunoaffinity extraction method to enhance GC-MS analyses of PAHs in atherosclerotic heart plaque samples. The performance of the hybrid method is subsequently compared to a conventional organic extraction method. Chapter 7, the final installment of this dissertation, provides a comprehensive research synopsis as well as recommendations for future research.

## 1.8 References

- (1) Rosamond, W.; Flegal, K.; Furie, K.; Go, A.; Greenlund, K.; Hasse, N.; Hailpern, S. M.; Ho, M.; Howard, V.; Kissela, B.; Kittner, S.; Lloyd-Jones, D.; McDermott, M.; Meigs, J.; Moy, C.; Nichol, G.; O'Donnell, C.; Roger, V.; Sorlie, P.; Steinberger, J.; Thom, T.; Wilson, M.; Hong, Y. *Circulation* 2008, *117*, e25-e147.
- (2) <http://www.nlm.nih.gov/MEDLINEPLUS/ency/imagepages/18050.htm> (accessed November 13, 2008)
- (3) Russo, C. A.; Andrews, R. M. In *HCUP Statistical Brief No. 26*; Agency for Healthcare Research and Quality: Rockville, MD, 2006.

- (4) Elixhauser, A.; Jiang, H. J. In *HCUP Statistical Brief No. 5*; Agency for Healthcare Research and Quality: Rockville, MD, 2006.
- (5) In *2006 Statistical Supplement*; Centers for Medicare and Medicaid Services: Baltimore, MD, 2006.
- (6) Black, J. In *Washington Post*: Washington, DC, 2008, pp A02.
- (7) Rosito, G. A.; Massaro, J. M.; Hoffman, U.; Ruberg, F. L.; Mahabadi, A. A.; Vasan, R. S.; O'Donnell, C. J.; Fox, C. S. *Circulation* 2008, *117*, 605-613.
- (8) website; American Heart Association, 2008; Vol. 2008.
- (9) Pearson, T. A.; Mensah, G. A.; Alexander, R. W.; Anderson, J. L.; Cannon, R. O. I.; Criqui, M.; Fadl, Y. Y.; Fortmann, S. P.; Hong, Y.; Meyers, G. L.; Rifai, N.; Smith, S. C. J.; Taubert K; Tracy, R. P.; Vinicor, R. *Circulation* 2003, *107*.
- (10) Ridker, P. M.; Brown, N. J.; Vaughan, D. E.; Harrison, D. G.; Mehta, J. L. *Circulation* 2004, *109*, IV-6.
- (11) Danesh, J.; Collins, R.; Peto, R. *Circulation* 2000, *102*, 1082-1085.
- (12) Danesh, J.; Wheeler, J. G.; Hirschfield, G. M.; Pepys, M. B.; Eda, S.; Eiriksdottir, G.; Gudnason, V.; Rumley, A.; Lowe, G. D. O. *N. Engl. J. Med.* 2004, *350*, 1387-1397.
- (13) Malik, I.; Danesh, J.; Whincup, P.; Bhatia, V.; Papacosta, O.; Walker, M.; Lennon, L.; Thomason, A.; Haskard, D. *Lancet* 2001, *358*, 971-976.
- (14) Daniels, L. B.; Maisel, A. S. *Journal of the American College of Cardiology* 2007, *50*, 2357-2368.
- (15) Lee, C. Y. W.; Burnett, J. C. *Heart Failure Reviews* 2007, *12*, 131-142.
- (16) Medina, M. A.; Urdiales, J. L.; Amores-Sanchez, M. I. *Eur. J. Biochem.* 2001, *268*, 3871-3882.
- (17) McCully, K. S. *Amer. J. Path.* 1969, *56*, 111-128.
- (18) McCully, K. S. *J. Sci. Expl.* 2001, *15*, 5-20.
- (19) McCully, K. S. *Nature* 1971, *231*, 391.
- (20) Verhoef, P.; Kok, F. J.; Kruyssen, D. A.; Schouten, E. G.; Wittenman, J. C.; Grobbee, D. E.; Ueland, P. M.; Refsum, H. *Arterioscler. Thromb. Vasc. Biol.* 1997, *5*, 989-995.

- (21) Jakubowski, H. *J. Nutr.* 2000, *130*, 377S-381S.
- (22) Nygard, O.; Vollset, S. E.; Refsum, H. *JAMA* 1995, *274*, 1526-1533.
- (23) Brattstrom, L.; Lindgren, A.; Israelsson, B. *J. Intern. Med.* 1994, *236*, 633-641.
- (24) Selhub, J.; Jacques, P. F.; P.W.F., W. *JAMA* 1994, *270*, 2693-2698.
- (25) Andersson, A.; Brattstrom L.; Israelsson, B. *Euro. J. Clin. Investi.* 1992, *22*, 79-87.
- (26) Naureth, H. J.; Joosten, E.; Riezler, R. *Lancet* 1995, *346*, 85-89.
- (27) Glueck, C. J.; Shaw, P.; Lang, J. E.; Tracy, T.; Smith, L.; Wang, Y. *Amer. J. Cardio.* 1995, *75*, 132-136.
- (28) Lentz, S. R., and Haynes, W.G. *Cleveland Clinic Journal of Medicine* 2004, *71*, 729-734.
- (29) Jakubowski, H. *Chem. Eur. J.* 2006, *12*, 8039-8043.
- (30) Kirk, J. E. *Monographs of Atherosclerosis*; S. Karger: New York, 1973.
- (31) Mercie, P.; Garnier, O.; Lascoste, L. *Apoptosis* 2000, *5*, 403-411.
- (32) Jakubowski, H.; Ambrosius, W. T.; Pratt, J. H. *FEBS Lett.* 2001, *491*, 35-39.
- (33) Jakubowski, H. *Biomed. Pharmacother.* 2001, *55*, 443-447.
- (34) Jakubowski, H. *Biochemistry* 1997, *36*, 11077-11085.
- (35) Jakubowski, H. *J. Nutr.* 2006, *136*, 1741S-1749S.
- (36) Austin, R. C.; Lentz, S. R.; Werstuck, G. H. *Cell. Death Differ.* 2004, *11*, S56-S64.
- (37) Jakubowski, H. *FASEB J.* 1999, *13*, 2277-2283.
- (38) Hop, E. C. A.; Bakhtiar, R. *Rapid Commun. Mass Spectrom.* 2002, *16*, 1049-1053.
- (39) Rosenberg, A. *AAPSJ* 2006, *8*, E501-E507.
- (40) Yang, X.; Gao, Y.; Zhou, J. *Clin. Chim. Acta* 2006, *364*, 230-234.
- (41) Bayle, C.; Causse, E.; Couderc, F. *Electrophoresis* 2004, *25*, 1457-1472.
- (42) Poinot, V.; Bayle, C.; Couderc, F. *Electrophoresis* 2003, *24*, 4047-4062.
- (43) Shipchandler, M. T.; Moore, E. G. *Clin. Chem.* 1995, *41*, 991-994.

- (44) Nexø, E.; Engbaek, F.; Ueland, P. M.; Westby, C.; O'Gorman, P.; Johnston, C.; Kase, B. F.; Guttormsen, A. B.; Alfheim, I.; McPartlin, J.; Smith, D.; Møller, J.; Rasmussen, K.; Clarke, R.; Scott, J. M.; Refsum, H. *Clinical Chemistry* 2000, *46*, 1150-1156.
- (45) Tan, Y. Y.; Hoffman, R. M. *Nature Protocols* 2008, *3*, 1388-1394.
- (46) Jakubowski, H. *Anal. Biochem.* 2008, *380*, 257-261.
- (47) Uji, Y.; Motomiya, Y.; Hanyu, N.; Ukaji, F.; Okabe, H. *Clin. Chem.* 2002, *48*, 941-944.
- (48) Rusin, O.; St Luce, N. N.; Agbaria, R. A.; Escobedo, J. O.; Jiang, S.; Warner, I. M.; Dawan, F. B.; Lian, K.; Strongin, R. M. *Journal of the American Chemical Society* 2004, *126*, 438-439.
- (49) Wang, W. H.; Rusin, O.; Xu, X. Y.; Kim, K. K.; Escobedo, J. O.; Fakayode, S. O.; Fletcher, K. A.; Lowry, M.; Schowalter, C. M.; Lawrence, C. M.; Fronczek, F. R.; Warner, I. M.; Strongin, R. M. *Journal of the American Chemical Society* 2005, *127*, 15949-15958.
- (50) Alivisatos, A. P. *Science* 1996, *271*, 933-937.
- (51) Brust, M.; Kiely, C. J. *Colloids Surf. A* 2002, *202*, 175-186.
- (52) Grant, C. D.; Schwartzberg, A. M.; Norman, T. J.; Zhang, J. Z. *JACS* 2002, *125*, 549-553.
- (53) Bloomfield, N. *Am. J. Clin. Pathol.* 1964, *41*, 15-21.
- (54) Liao, H. W.; Nehl, C. L.; Hafner, J. H. *Nanomedicine* 2006, *1*, 201-208.
- (55) Reynolds, A. J.; Haines, A. H.; Russell, D. A. *Langmuir* 2007, *22*, 1156-1163.
- (56) Liu, J. W.; Lu, Y. *J. Fluoresc.* 2004, *14*, 343-354.
- (57) Storhoff, J. J.; Mirkin, C. A. *Chem. Rev.* 1999, *99*, 1849-1862.
- (58) Lim, I. S.; Ip, W.; Crew, E.; Njoki, P. N.; Mott, D.; Zhong, C.; Pan, Y.; Zhou, S. *Langmuir* 2007, *23*, 826-833.
- (59) Zhang, F. X.; Han, L.; Israel, L. B.; Daras, J. G.; Maye, M. M.; Ly, N. K. *Analyst* 2002, *127*, 462-465.
- (60) Gates, A. T.; Fakayode, S. O.; Lowry, M.; Ganea, G. M.; Murugesu, A.; Robinson, J. W.; Strongin, R. M.; Warner, I. M. *Langmuir* 2008, *24*, 4107-4113.
- (61) Ingle, J. D.; Crouch, S. R. In *Spectrochemical Analysis*; Lafferty, K. M., Ed.; Prentice

- Hall: Upper Saddle River, New Jersey, 1988, pp 13-29.
- (62) [www.chemicool.com/img1/graphics/spectrometer1.gif](http://www.chemicool.com/img1/graphics/spectrometer1.gif) (accessed November 13, 2008)
- (63) Ingle, J. D.; Crouch, S. R. In *Spectrochemical Analysis*; Lafferty, K. M., Ed.; Prentice Hall: Upper Saddle River, New Jersey, 1988, pp 380.
- (64) [www.britishbiophysics.org.uk/what-is/cd/cd.html](http://www.britishbiophysics.org.uk/what-is/cd/cd.html) (accessed November 13, 2008)
- (65) <http://www.shsu.edu/~chemistry/chemiluminescence/JABLONSKI.html> (accessed November 13, 2008)
- (66) <http://www.asms.org/whatisms/images/fig1.gif> (accessed November 13, 2008).
- (67) Rapp, J. H.; Lespine, A.; Hamilton, R. L.; Colyvas, N.; Chaumeton, A. H.; Tweediehardman, J.; Kotite, L.; Kunitake, S. T.; Havel, R. J.; Kane, J. P. *Arterio. & Thromb.* 1994, *14*, 1767-1774.
- (68) Suarna, C.; Dean, R. T.; SouthwellKeeley, P. T.; Moore, D. E.; Stocker, R. *Free Rad. Res.* 1997, *27*, 397-408.
- (69) Romer, T. J.; Brennan, J. F.; Fitzmaurice, M.; Feldstein, M. L.; Deinum, G.; Myles, J. L.; Kramer, J. R.; Lees, R. S.; Feld, M. S. *Circulation* 1998, *97*, 878-885.
- (70) van de Poll, S. W. E.; Schut, T. C. B.; van den Laarse, A.; Puppels, G. J. *J. Ram. Spec.* 2002, *33*, 544-551.
- (71) Frank, H. *Am. Heart J.* 2001, *141*, S45-S48.
- (72) Haka, A. S.; Fitzmaurice, M.; Feld, M. S. *Modern Path.* 2003, *16*, 54A-54A.
- (73) Morrisett, J.; Vick, W.; Sharma, R.; Lawrie, G.; Reardon, M.; Ezell, E.; Schwartz, J.; Hunter, G.; Gorenstein, D. *Mag. Res. Imag.* 2003, *21*, 465-474.
- (74) Thiam, S.; Tracy, R. E.; Robinson, J. W.; Warner, I. M. *J. Environ. Sci.H* 2004, *39*, 1497-1503.
- (75) Murungi, J. I.; Thiam, S.; Tracy, R. E.; Robinson, J. W.; Warner, I. M. *Journal of Environmental Science and Health Part a-Toxic/Hazardous Substances & Environmental Engineering* 2004, *39*, 1487-1496.
- (76) Thiam, S., Cook, R., Tracy, R.E., Treleaven, D., Robinson, J.W. and Warner, I.M. *Journal of Applied Spectroscopy* 2004, *71 (N1)*, 79-85.
- (77) Thiam, S.; Tracy, R. E.; Robinson, J. W.; Warner, I. M. *Journal of Environmental Science and Health Part a-Toxic/Hazardous Substances & Environmental Engineering*

- 2004, 39, 1497-1503.
- (78) Thiam, S.; Shamsi, S. A.; Henry, C. W.; Robinson, J. W.; Warner, I. M. *Anal. Chem.* 2000, 72, 2541-2546.
- (79) Zhou, H. C.; Jin, B. S.; Zhong, Z. P.; Huang, Y. J.; Xiao, R.; Li, D. J. *J. Environ. Sci.-China* 2005, 17, 141-145.
- (80) Bylina, B. G.; Rakwic, B.; Pastuszka, J. S. *Pol. J. Environ. Stu.* 2005, 14, 117-123.
- (81) Shi, Z.; Tao, S.; Pan, B.; Fan, W.; He, X. C.; Zuo, Q.; Wu, S. P.; Li, B. G.; Cao, J.; Liu, W. X.; Xu, F. L.; Wang, X. J.; Shen, W. R.; Wong, P. K. *Environ. Pol.* 2005, 134, 97-111.
- (82) Devier, M. H.; Augagneur, S.; Budzinski, H.; Le Menach, K.; Mora, P.; Narbonne, J. F.; Garrigues, P. *J Environ. Monit.* 2005, 7, 224-240.
- (83) Ramesh, A.; Walker, S. A.; Hood, D. B.; Guillen, M. D.; Schneider, K.; Weyand, E. H. *Intern. J. Tox.* 2004, 23, 301-333.
- (84) Guillen, M. D.; Sopelana, P. *J Food Prot.* 2004, 67, 1904-1913.
- (85) Lors, C.; Mossmann, J. R. *Pol. Arom. Comp.* 2005, 25, 67-85.
- (86) Skrbic, B.; Cvejanov, J.; Durisic-Mladenovic, N. D. *J. Environ. Sci. H.* 2005, 40, 29-42.

## CHAPTER 2

### SPECTROCHEMICAL INVESTIGATION OF PYRIDOXAL TETRAHYDROTHIAZINE FORMATION

#### 2.1 Introduction

Vitamin B<sub>6</sub> (pyridoxal) is an important bioactive aldehyde cofactor that helps mediate various enzymatic processes associated with Hcy metabolism and protein synthesis.<sup>1, 2</sup> Alternatively, pyridoxal can undergo facile nonenzymatic reactions with both Hcy and HTL under physiological conditions to form a stable and biologically inert pyridoxal tetrahydrothiazine (PT) complex (Figure 2.1).<sup>3</sup> The PT reaction is initiated by S<sub>N</sub>1 nucleophilic substitution between the pyridoxal aldehyde group and the primary amine on either Hcy or HTL. The reaction is subsequently completed by way of thiolate nucleophilic attack at the newly created aldehyde carboimide, which gives a six-member thiazine ring.<sup>3, 4</sup>

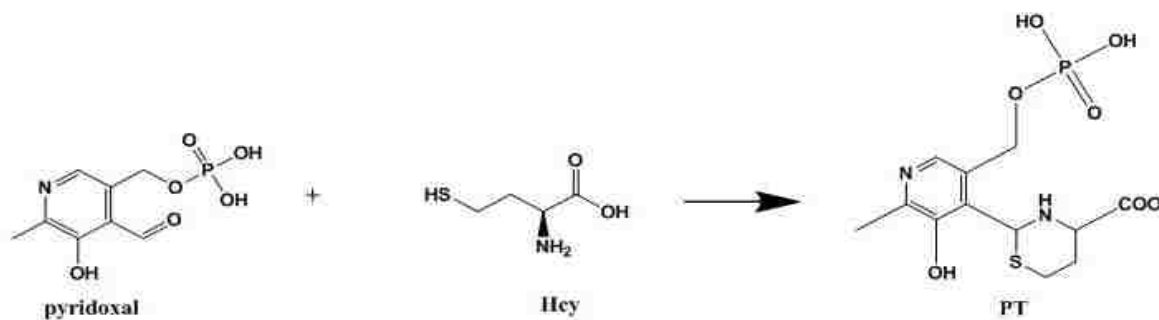


**Figure 2.1** Formation of pyridoxal tetrahydrothiazine via aldehyde condensation.

Since the thiazine reaction occurs spontaneously under physiological pH conditions, we hypothesize that PT formation could serve as an auxiliary mechanism for *in vivo* Hcy clearance, thereby lower blood Hcy levels and CVD risk. This premise is referred to as the PT-Hcy sequestration and clearance hypothesis. Such a scenario has implications for inhibiting protein homocysteinylolation in individuals who are unable to clear Hcy due to congenital metabolic



defects. The premise was initially evaluated by monitoring the spectrochemical behavior of pyridoxal-5-phosphate in the presence of Hcy. The primary goal of this study is to gain a better understanding of the fundamental molecular interactions involved in PT production.

## **2.2 Methods**

### **2.2.1 Materials**

Pyridoxal-5-phosphate, D,L-Hcy, and HTL were obtained from Sigma-Aldrich, Inc. (St. Louis, MO) at the highest available purity. Ultra-grade tris-base and tris-hydrochloride were obtained from Invitrogen Life Technologies (Carlsbad, CA) and Amersco (Solon, OH), respectively. Ultra-pure water (18 M $\Omega$  resistance) was obtained from a PURELAB Ultra Genetic (Wycombe, UK) water purification system. All other reagents used in this work were of analytical purity or greater.

### **2.2.2 Buffer and Sample Preparation**

Tris-buffered saline (TBS), pH 7.4, 50 mM, was prepared according to a standard laboratory recipe; 6.35 g tris-hydrochloride, 1.18 g tris-base, and 8.77 g sodium chloride dissolved in 1 L of water. The pH of the buffer was subsequently adjusted to 7.4 with either concentrated sodium hydroxide or hydrochloric acid. The TBS buffer was degassed by sonication for 20 min prior to use. Pyridoxal stock solutions were prepared by dissolving the HCl salt in TBS. Hcy stock solutions were prepared fresh daily to avoid oxidation. Pyridoxal and Hcy stock solutions were mixed directly in the cuvet to obtain the desired molar ratio. Reaction mixtures were incubated for 1h at 37°C. Cuvets were rinsed sequentially with methanol, water, and the sample prior to each measurement.

### 2.2.3 Instrumentation

Steady-state fluorescence excitation and emission spectra were acquired in triplicate at room temperature using a Spex Fluorolog-3 spectrofluorimeter (model FL#-22TAU3; Jobin Yvon, Edison, NJ) equipped with a 450-W xenon lamp and R928P photomultiplier tube (PMT) emission detector. Raw fluorescence signal was normalized to the reference PMT signal to account for lamp intensity fluctuations. Fluorescence spectra were blank subtracted and corrected for inner-filter effects when necessary. Absorption spectra were collected using a UV-Vis-NIR spectrophotometer (model UV-3101PC) manufactured by Shimadzu (Columbia, MD). Both fluorescence and UV absorption measurements were acquired in 10 mm<sup>2</sup> quartz cuvetts.

### 2.3 Calculations and Data Analysis

Primary and secondary inner-filter corrections for fluorescence spectra were performed when necessary using equation 1;<sup>5</sup>

$$F_{corr} = F_{obs} 10^{\left[ \frac{OD_{ex} + OD_{em}}{2} \right]}; \quad (1)$$

where  $F_{corr}$  is corrected fluorescence intensity,  $F_{obs}$  is observed fluorescence intensity,  $OD_{ex}$  and  $OD_{em}$  are the optical densities for the excitation and emission wavelengths respectively.

Molecular interaction between Hcy and pyridoxal was assessed using the Benesi-Hildebrand method<sup>6, 7</sup>. The Benesi-Hildebrand method can be used to obtain binding kinetics information from fluorescence data. For example, equation 2 describes 1:1 stoichiometry for a thiazine complex.



Thus, the association constant for equation 2 is represented by equation 3;

$$K_{\text{thiazine complex}} = \frac{[\text{thiazine complex}]_n}{[\text{pyridoxal}][\text{Hcy}]^n}; \quad (3)$$

where [thiazine complex], [pyridoxal], and [Hcy] are the equilibrium concentrations of the product and reactants, respectively. The stoichiometry of the system is denoted by n, which is continuously varied in the experiment such that the [pyridoxal] remains constant and [Hcy]  $\gg$  [pyridoxal]. The relationship between fluorescence intensity and [Hcy] is given by equation 4;

$$\frac{1}{F - F_0} = \frac{1}{K(F_\infty - F_0)[\text{Hcy}]_0^n} + \frac{1}{F_\infty - F_0}; \quad (4)$$

where F is the fluorescence intensity of pyridoxal in the presence of Hcy,  $F_0$  is the fluorescence intensity of pyridoxal in the absence of Hcy,  $F_\infty$  is the fluorescence intensity observed for pyridoxal associated with Hcy,  $[\text{Hcy}]_0$  is the initial concentration of Hcy and K is the association constant for the system. K is empirically determined by obtaining the slope of the line resulting

from plotting  $\frac{1}{F - F_0}$  versus  $\frac{1}{[\text{Hcy}]_0^n}$ . The stoichiometry of the system is empirically

determined by substituting different values for (n) into the equation of the line. For instance, n-values of 1, 2, and 3, represent stoichiometries of 1:1, 1:2, and 1:3, respectively. The best linear fit ( $R^2$ ) is obtained when the correct stoichiometric value is chosen.

## 2.4 Results and Discussion

### 2.4.1 UV-visible Spectroscopy Studies of Thiazine Formation

The spectrochemical behavior of pyridoxal was evaluated in the presence of Hcy under physiological pH conditions using UV-vis spectroscopy (Figure 2.2). Pyridoxal exhibits two

broad and intense absorption bands at ~277 and 414 nm. The addition of Hcy to the pyridoxal solution caused these peaks to diminish while a new absorption band emerged at 330 nm to indicate PT formation. The arrows in the figure indicate the change in UV-vis absorption due to PT in solutions containing 1:0, 1:0.5, 1:1, 1:2, 1:5, and 1:10 [pyridoxal]:[Hcy]<sup>n</sup>, respectively. The reaction was found to be stable and irreversible under the conditions used in this study.

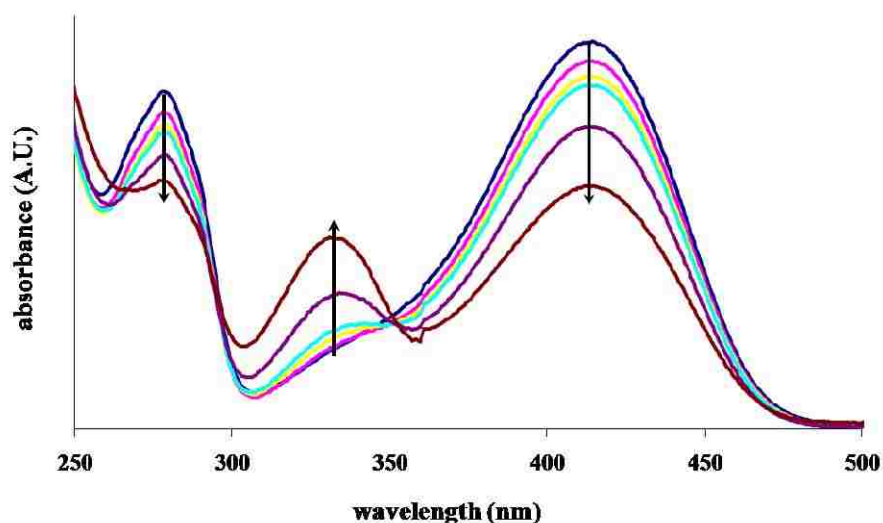


**Figure 2.2** UV-Vis absorption spectra of solutions containing pyridoxal in presence of increasing concentrations of Hcy.

#### 2.4.2 Fluorescence Characterizations

Hcy-dependent enhancements in pyridoxal fluorescence intensity were initially monitored at 414 nm while scanning excitation wavelength. The resultant spectra indicate that pyridoxal fluorescence is proportional to PT absorption, which was previously monitored at 330 nm (Figure 2.3a). Normalized excitation spectra are shown in Figure 2.3b to illustrate the magnitude of the shift (~10 nm) caused by increased PT production. Corresponding emission spectra were acquired by excitation at 330 nm (Figure 2.3c). The emission spectra illustrate fluorescence enhancements at 400 nm, which are consistent with PT formation.

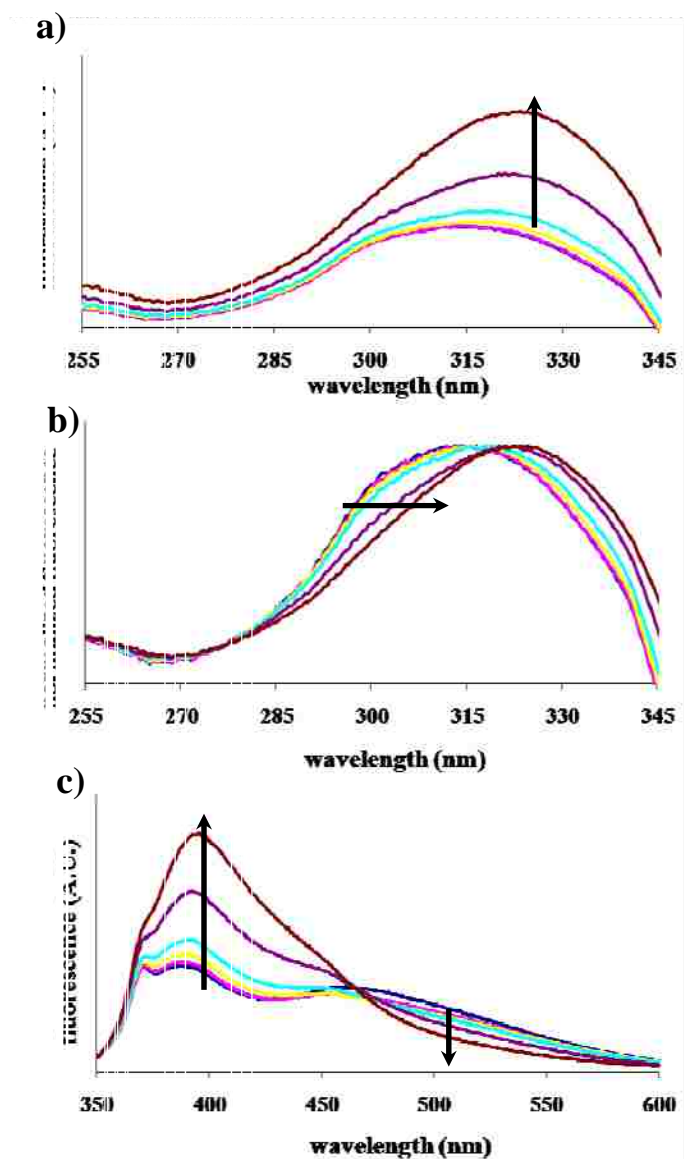


**Figure 2.3** Fluorescence spectra of PT formation.

The Stern-Volmer equation was applied to both the uncorrected and inner-filter corrected emission data in order to assess fluorescence quenching as a function of Hcy concentration.

Figure 2.4 is a plot of  $F_0/F-1$  versus [Hcy], where  $F_0$  is the fluorescence intensity of pyridoxal in the absence of Hcy, and  $F$  is the observed fluorescence intensity for pyridoxal in the presence of increasing concentrations of Hcy. The correlation coefficients obtained for uncorrected and corrected Stern-Volmer plots were 0.941 and 0.950, respectively. However, it is readily apparent

that both data sets are non-linear, which may indicate non-Stern-Volmer behavior. The most likely reason for these inconclusive results is that the experimental conditions used in this study do not yield 1:1 association, which is a precondition for use of the Stern-Volmer relationship.

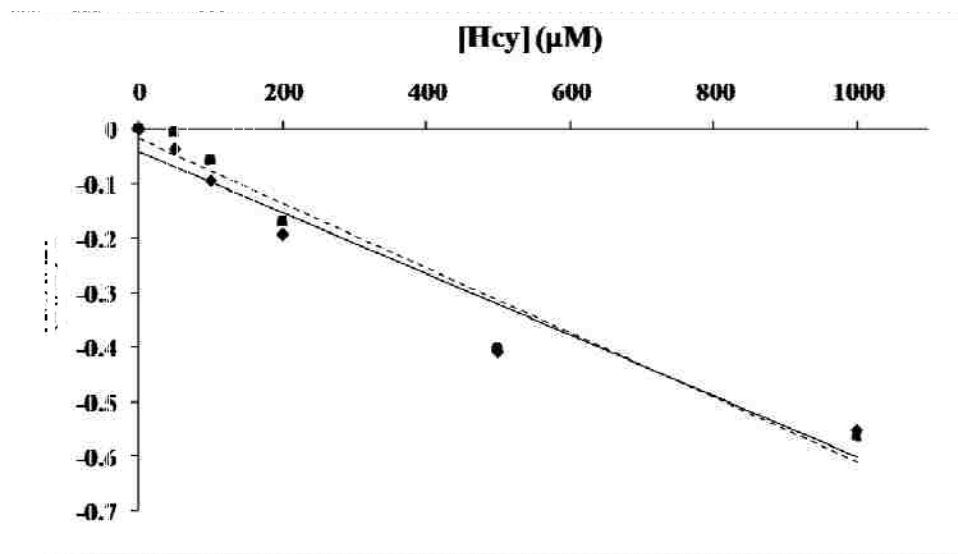


**Figure 2.4** Stern-Volmer plot showing trend for uncorrected (solid line) and corrected (dotted line) PT fluorescence emission.

Next, the Benesi-Hildebrand treatment was applied to the PT system to estimate binding stoichiometry. In this exercise,  $\frac{1}{F - F_0}$  was plotted versus  $\frac{1}{[Hcy]_0^n}$ ; where n represents the stoichiometry of the system. Benesi-Hildebrand plots for the PT system are shown in Figure 2.5. The coefficient of correlation obtained for n = 1, 2, and 3 were 0.994, 0.998, and 0.987, respectively. The stoichiometric value, n = 2, gave the best fit and suggests 1:2 stoichiometry for the PT system. This may help explain the previously observed deviation from the Stern-Volmer behavior. As previously discussed, PT formation is usually the result of 1:1 association, which is not supported by the Benesi-Hildebrand data. One possible explanation for this discrepancy is that pyridoxal-5-phosphate, not pyridoxal, was used in these studies. Consequently, a second Hcy molecule could associate with the phosphate group ( $PO_4^-$ ) due to electrostatic interactions,

resulting in 1:2 stoichiometry. This scenario becomes especially probable when pyridoxal-5-phosphate is in the presence of excess Hcy.

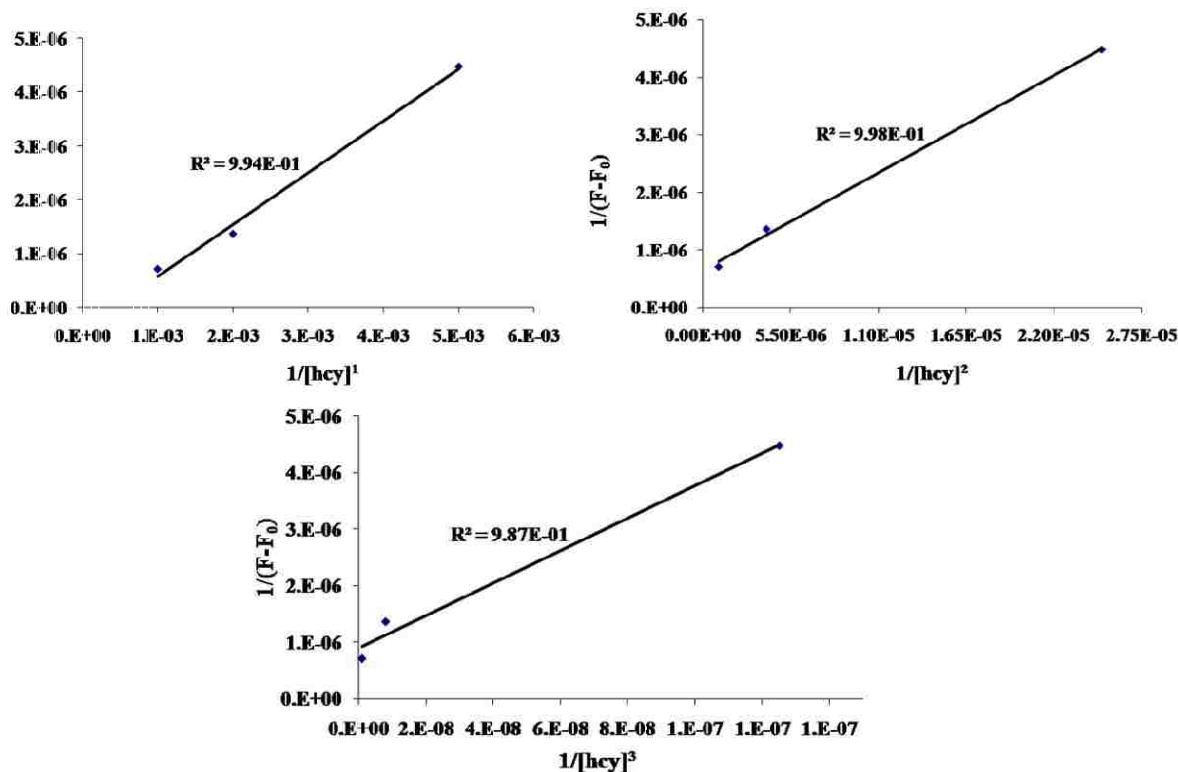


**Figure 2.5** Benesi-Hildebrand plots for PT formation.

It is also important to consider the biochemical fates of pyridoxal and pyridoxal-5-phosphate. Pyridoxal-5-phosphate version is the preferred ingredient in vitamin supplements for practical reasons including ease of synthesis-extraction and long shelf-life. However, the body possesses mechanisms for converting between the two forms of pyridoxal based on biological need. Thus, it is likely that pyridoxal and the phosphate-5-phosphate coexist *in vivo*.

## 2.5 Conclusions

In summary, we have confirmed that pyridoxal-5-phosphate readily interacts with Hcy and HTL under physiological pH and temperature conditions. Initial attempts to characterized the molecular interactions involved in PT formation using the Stern-Volmer yielded inclusive results. Hence, the Benesi-Hildebrand treatment was applied to system to assess the

stoichiometry of the PT reaction. Benesi-Hildebrand analysis indicated the possibility of 1:2 stoichiometry, which appeared to contradict the 1:1 mechanisms reported in the literature. The discrepancy in stoichiometry was attributed to differences in the chemical forms of pyridoxal used in the experiment. Indeed non-phosphorylated pyridoxal undergoes 1:1 association with Hcy. However, pyridoxal-5-phosphate was used in this study. It was also found that pyridoxal-5-phosphate may bind two molecules of Hcy simultaneously, via Schiff base linkage and via electrostatic binding at the phosphate group. This preliminary report provides empirical support for the PT-Hcy sequestration and clearance hypothesis, but further study is needed to determine if PT formation can occur in the presence of proteins and other biomolecules. In light of this goal, the TBS buffer system will be replaced with phosphate buffered saline, which is considered by most to be more biologically relevant. Phosphate is also the preferred buffer for protein experiments.

## 2.6 References

- (1) Toney, M. D. *Arch. Biochem. Biophys.* 2005, *433*, 279-287.
- (2) Liu, W. S.; Toney, M. D. *J. Biochem.* 2004, *43*, 4998-5010.
- (3) Jakubowski, H. *Chem. Eur. J.* 2006, *12*, 8039-8043.
- (4) Medici, A.; Pedrini, P.; Venturoli, C.; Dondoni, A. *J. Org. Chem.* 1981, *46*, 2790-2793.
- (5) Lakowicz, J. R. *Principles of Fluorescence Spectroscopy*, 2nd Ed. ed.; Plenum Press: New York, 1999.
- (6) Lopez, E. A.; Bosque-Sendra, J. M.; Rodriguez, L. C.; Garcia Campana, A. M.; Aaron, J. *J. Anal Bioanal. Chem* 2003, *375*, 414-423.
- (7) Benesi, H. A. H., J.H. *JACS* 1949, *71*, 2703-2707.



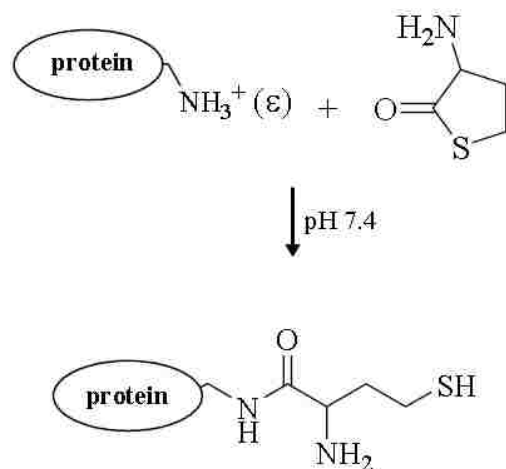
## CHAPTER 3

### CAPILLARY ELECTROPHORETIC SCREENING FOR INHIBITION OF HOMOCYSTEINE THIOLACTONE- INDUCED PROTEIN OLIGOMERIZATION

#### 3.1 Introduction

The material presented in this chapter is reproduced in part with permission from *Analytical Chemistry*, 2007, volume 79, pages 8249 -8256; Gates, A. T.; Lowry, M.; Fletcher, K. A.; Merugesu, A.; Rusin, O.; Robinson, J. W.; Strongin, R. M.; Warner, I. M.; Rapid Electrophoretic Screening of Homocysteine Thiolactone-Induced Protein Oligomerization Using Cationic Polyelectrolyte-Coated Capillaries, which was copyrighted in 2007 by the American Chemical Society.

Increased *in vivo* HTL production is believed to initiate vascular damage and the formation of early atherosclerotic lesions.<sup>1, 2</sup> The proposed mechanism for post-translational protein modification by HTL involves the site-specific acylation of  $\epsilon$ -amino groups on lysine residues to yield a thiolated species known as *N*-Hcy-protein (Scheme 3.1).<sup>3, 4</sup> If left uninhibited, individual *N*-Hcy-protein molecules in proximity to each other may undergo spontaneous intermolecular disulfide bonding to yield aggregate species.<sup>3, 5</sup> HTL-induced protein aggregation (HTPA) may bring about several unfavorable physiological effects. In particular, aggregated proteins often exhibit decreased biological activity, decreased solubility,<sup>3</sup> and increased immunogenicity.<sup>6</sup> As one would expect, the extent of physiological dysfunction caused by protein aggregation varies among the many different types of proteins. Empirical evidence of HTPA has been reported for LDL,<sup>7</sup> cyt *c*, and human serum protein<sup>3</sup> under physiological conditions. Moreover, a recent clinical study reported the discovery of higher than normal levels of Hcy thiolactone-modified proteins in individuals with coronary heart disease.<sup>8</sup>



**Scheme 3.1** Homocysteine thiolactone-induced protein modification. Under physiological pH conditions Hcy thiolactone can preferentially acylate protein lysine residues at  $\epsilon$ -amino groups to yield *N*-Hcy-protein

Given the potential clinical significance of HTPA as an indicator of cardiovascular and neurovascular diseases, the development of rapid primary screening methods for HTPA is of importance. SDS-PAGE is perhaps the most widely used technique for a variety of routine protein screening applications. Although SDS-PAGE is often very effective for the separation of most protein aggregates, lengthy analysis times and tedious staining procedures are a hindrance to its use in most high throughput clinical screening applications. In addition, SDS-PAGE is generally considered to be semi-quantitative, limiting its utility in quantitative applications. In contrast, capillary electrophoresis (CE) equipped with UV detection is quantitative and generally provides sufficient sensitivity without the necessity for dye-staining or radioisotope labeling as is often the case for SDS-PAGE.

With CE instrumentation becoming more common place in laboratories, capillary electrophoretic separation can be practical alternative to conventional SDS-PAGE for clinical and pharmaceutical-type protein separations.<sup>9-11</sup> Further, reports in the literature of CE-based protein separation techniques have steadily increased over the past decade.<sup>12-15</sup> This trend is due

in part to the ongoing development of polyelectrolyte coatings, which provide can provide an effective remedy for protein-wall adsorption.<sup>16</sup> Our laboratory has established the usefulness of various micellar coatings as stationary phases for capillary electrophoretic chromatography.<sup>17-22</sup> Our more recent studies have employed amino acid-functionalized molecular micellar stationary phases for open tubular-capillary electrochromatography. These coatings allow for facile column fabrication and exceptional separation performance for both chiral and achiral analytes.<sup>18-22</sup>

Herein, we report the development of a rapid capillary electrophoretic method for the quantitative assessment of HTPA. Capillaries coated with poly (diallyldimethylammonium chloride) (PDADMAC) were used to minimize protein-wall adsorption. Hcy thiolactone and cyt *c* were reacted *in vitro* to induce protein aggregation. The resultant mixture containing monomeric and aggregate species was separated using CE equipped with UV detection. We also demonstrate a short-end injection method for *in vitro* pre-clinical HTPA inhibition screening.

## **3.2 Methods**

### **3.2.1 Materials**

Bovine cyt *c*, L-HTL, pyridoxal-5-phosphate hydrogen chloride, streptomycin sulfate, SDS-PAGE protein molecular weight markers, PDADMAC 20% w/v water solution ( $M_w$  200,000-350,000), tris (hydroxymethyl) aminomethane (TRIS), and all other reagents used for preparing reaction and background electrolytes were obtained from Sigma-Aldrich (St. Louis, MO) at the highest purity available and used without further purification. Ultra pure water (18.2 M $\Omega$ ) was obtained by use of an Elga model PURELAB Ultra™ water filtration system.

### **3.2.2 Preparation of Protein Reaction Mixtures**

Protein reaction mixtures were prepared by dissolving Hcy thiolactone (2.5 mM) and cyt

*c* (10 mg/mL) in pH 7.4, 100 mM sodium phosphate, 0.2 mM ethylenediaminetetraacetic acid (EDTA) buffer, according to procedures previously reported by Jakubowski.<sup>3</sup> It was found that 12 h (at 25 °C) was the approximate minimum time required for appreciable aggregate formation to occur in the protein reaction mixture without protein precipitation. Accordingly, samples used for CE studies were reacted at 25 °C while mixing for 12 h to obtain the protein aggregate mixture. The modification reaction was quenched by removing the protein from the reaction mixture using a Millipore (Bedford, MA) Amicon Ultra, 10,000 kDa molecular weight cut-off (MWCO) filter device centrifuged at 3600 rpm for 20 min or until completion. The protein retentate was rinsed with 2 mL of the reaction buffer to remove nonspecifically bound material. Protein and filtrates were stored at -20 °C for no more than one week. Unless otherwise indicated, the protein retentates were reconstituted in either the background electrolyte (50 mM pH 8.5 tris buffer). All protein and buffer solutions were passed through a 0.45 µm nylon syringe filter prior to separation by CE. Protein reaction mixtures for HTPA inhibition studies were prepared and treated in the same manner as described above, except the appropriate quantity of pyridoxal-5-phosphate stock solution was simultaneously added with the HTL and protein solution to obtain the desired component concentrations.

### **3.2.3 SDS-PAGE Protocol**

SDS-PAGE experiments were conducted using a Mini-Protean 3™ gel electrophoresis unit with 1000 V power supply. Polyacrylamide gels (4-20%) were purchased from Bio-Rad (Hercules, CA). The sample buffer was prepared by combining 0.2 mL of 0.5% (w/v) bromophenol blue, 2.0 mL of 10% (w/v) SDS, 2.5 mL of glycerol, 1.25 mL of pH 6.8, 0.5 M TRIS hydrochloride, and 3.55 mL bioscience grade water to obtain a total volume of 9.5 mL. Protein samples were diluted to 0.1 µg/mL with sample buffer and thermally denatured under

non-reducing conditions at 95 °C for 5 min prior to SDS-PAGE analyses. The stock running buffer was prepared by dissolving 15.15 g tris-base, 72 g glycine, and 10.0 g SDS in bioscience grade water to obtain a final volume of 1L and working pH of 6.8. The stock run buffer was diluted 10-fold to obtain the final running buffer. SDS-PAGE separations were run at 200 V for 30 min at room temperature followed by staining for 1 h with SimplyBlue SafeStain Coomassie G-250, obtained from Invitrogen (Carlsbad, CA). The gels were destained water for at least 12 h to obtain optimum band contrast. A Kodak Gel Logic 100 digital imaging system purchased from Eastman Kodak Company (Rochester, NY) was used for gel imaging.

### **3.2.4 Instrumentation**

A Beckman Coulter (Fullerton, CA) P/ACE MDQ capillary electrophoresis system equipped with a photodiode array detector was used for separations. Fused-silica capillaries (50  $\mu\text{m}$  i.d.) were purchased from Polymicro Technologies (Phoenix, AZ) and cut to 32 cm total length, having an effective length of 22 cm. Capillaries were modified with 20 mg/mL PDADMAC dissolved in pH 8.5, 50 mM tris buffer. A capillary coating was deposited over a 12 h period using alternating rinse cycles of PDADMAC solution at high pressure (20 psi) for 5 min and low pressure (0.5 psi) for 120 min as previously described elsewhere.<sup>23</sup> After coating, capillaries were rinsed with the background electrolyte at 5 psi for 40 min to remove excess PDADMAC. Electrokinetic injections and separations were performed under reversed polarity conditions at  $25 \pm 1$  °C. The capillary was rinsed with the background electrolyte for 2 min at 5.0 psi prior to each run. Separations were simultaneously monitored from 200 to 320 nm using a photodiode array detector.

### **3.2.5 Data Analysis**

Data acquired at 200 nm were exported to a spreadsheet and fit to Gaussian peaks.

Migration time, peak width, and peak area determinations for CE separations were computed based on the best fit data.

Resolution ( $R_s$ ), full width at half-height (FWHH), and number of theoretical plates (N) were calculated using the following equations:

$$R_s = \frac{(t_{r,2} - t_{r,1})}{\frac{1}{2}(w_1 + w_2)}, \quad (1)$$

$$\text{FWHH} = w_{\frac{1}{2}} = 2.35\sigma, \quad (2)$$

$$N = 554 \left( \frac{t_r}{w_{\frac{1}{2}}} \right)^2, \quad (3)$$

where  $t_{r,1}$  and  $t_{r,2}$  are the migration times for the earlier and later eluting peaks, respectively;  $w$  is peak width at baseline for each peak,  $w_{\frac{1}{2}}$  is FWHH, and  $\sigma$  is the standard deviation of the Gaussian peaks.

Short-end injection is a technique used in CE to obtain shorter analysis times by circumventing instrumental limitations on minimum capillary length.<sup>24-26</sup> Short-end injections and separations were performed by applying voltage in reversed polarity with reference to the outlet in order to obtain EOF towards the detection window, resulting in an effective capillary length of 10 cm with no change in total capillary length (32 cm). Short-end electrokinetic injections were performed from the outlet-end of the capillary using 5 kV for 7 sec.

### 3.3 Results and Discussion

#### 3.3.1 Characterization of the Protein Reaction Mixture

As previously discussed, HTPA is initiated by acylation of protein lysine residues by HTL. Consequently, the degree of reactivity of Hcy thiolactone toward a given protein is largely

dependent on lysine content. Cyt *c* is a ubiquitous, basic metalloprotein found associated with the mitochondria of most cells. Bovine cyt *c* was selected as the model protein for demonstrating the proposed method because it is relatively small in size (MW 12,327 kDa), highly soluble, and has a relatively high lysine content (20% w/w),<sup>27</sup> making it susceptible to modification by HTL and the subsequent aggregation of *N*-Hcy-protein species.

HTL-induced cyt *c* aggregation was previously demonstrated by Jakubowski using SDS-PAGE with radioisotope imaging.<sup>3</sup> Similarly, SDS-PAGE analysis was used initially to confirm aggregation in the protein reaction mixtures prior to proceeding to CE analyses. As expected, monomer and aggregate bands were visible in gel images after dye staining with coomassie blue (Figure 3.1a). The three relatively broad bands were identified as monomeric (I), dimeric (II), and trimeric (III) cyt *c* species as determined by comparison with SDS-PAGE protein molecular weight markers. Treatment of the same protein reaction mixture with 5 mM dithiothreitol (DTT), a disulfide reducing agent, eliminated aggregate bands (data not shown). Additional characterization of the protein reaction mixture using MALDI TOF-MS (Figure A.1 in Appendix A) also detected monomer and aggregate species in the protein reaction mixture having signal intensities comparable with those observed with SDS-PAGE and are consistent with covalently bonded cyt *c* aggregation due to intermolecular disulfide formation.

Protein-wall adsorption can be especially problematic for capillary zone electrophoresis separations of proteins. The surface of bare fused silica capillaries is not usually conducive to separation of proteins because of electrostatic attraction between the anionic deprotonated silanol groups and the positively charged protein residues. Therefore, it is often necessary to modify the silica surface with an appropriate coating to reduce protein adsorption. The cationic polyelectrolyte PDADMAC was selected for separation of the protein reaction mixture

containing cyt *c* (pI~10), which is also cationic under the experimental condition used in this study.

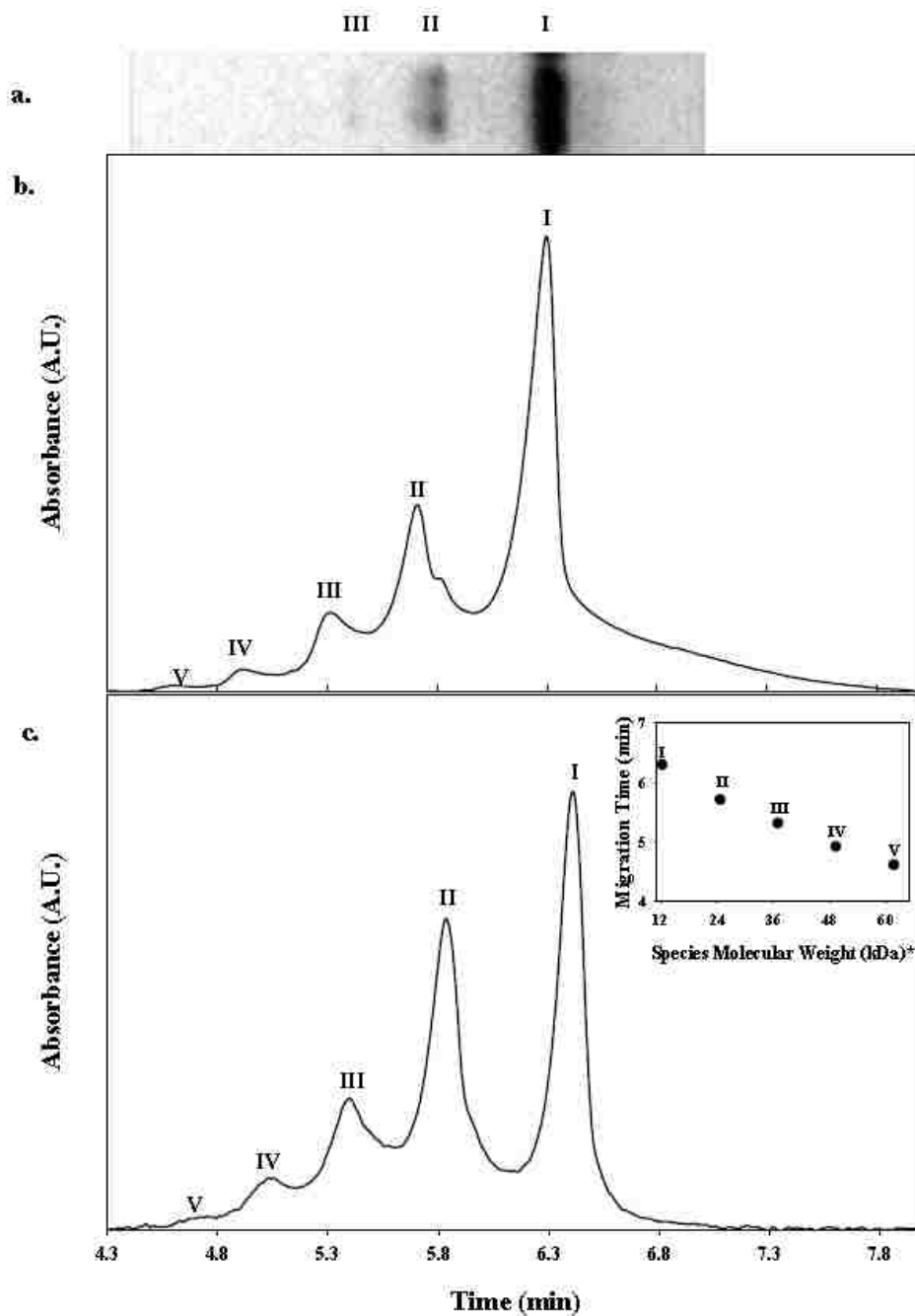


**Figure 3.1** Representative electrophoretic separations of protein reaction mixtures. a) gel separation showing bands corresponding to I, II, and III c, b) electropherogram of non-denatured protein mixture, c) electropherogram for thermally denatured sample and plot of electrophoretic migration time versus species molecular weight (inset).



### **3.3.2 Preliminary Evaluation of Protein Separation**

The separation of proteins using PDADMAC-modified capillaries can be greatly affected by polymer molecular weight and column coating conditions. In that regard, it has been shown that capillary coating procedures that use a combination of high ionic strength and high molecular weight PDADMAC provide enhanced surface coverage and charge inversion.<sup>23</sup> In addition, it has been proposed that larger molecular weight PDADMAC polymers may facilitate the formation of “loop and tail” structures on the capillary surface, with which protein analytes may interact.<sup>23</sup> For that reason, PDADMAC having a molecular weight range of 200-350 kDa was chosen as the wall coating in this work.

Figure 3.1b is a typical electropherogram resulting from the separation of native protein reaction mixtures using PDADMAC coated capillaries. The increased sensitivity provided by UV detection allowed for the detection of two additional peaks attributed to tetrameric (IV) and pentameric (V) species that were not visible in the SDS-PAGE image shown in Figure 3.1a. The analysis time for the separation shown in Figure 3.1b was less than 8 min, including the rather significant tailing of the monomer peak. The migration order was determined to be tetramer (IV), trimer (III), dimer (II) and monomer (I), respectively. We note that migration time for modified protein species was inversely related to molecular weight as is expected for the reversed polarity conditions used in these studies.

### **3.3.3 Effect of Protein Denaturation on Separation Performance**

Separations performed with non-denatured samples tended to result in peak tailing and poor peak shape. The prominent asymmetric features observed for the monomer and dimer peaks in native protein reaction mixtures are primarily attributed to protein conformation effects. Protein conformation effects are caused by the various shapes which proteins may assume under

native conditions due to their secondary and tertiary structure. Oligomeric protein species, such as those produced by HTPA, may also exhibit some degree of quaternary structure. Collectively, these factors may contribute to undesirable electrophoretic separation performance including band broadening and poor peak shape. Consequently, it is sometimes necessary to treat protein samples with denaturing agents prior to electrophoretic separation to minimize conformation effects. For example, protein denaturation for SDS-PAGE is typically achieved by boiling the protein mixtures in a high ionic strength buffer that contains the anionic surfactant SDS and reducing agents such as dithiothreitol or 2-mercaptoethanol. This approach is not compatible with basic proteins or the cationic polyelectrolyte coating used in this study. Hence, SDS was omitted from sample pretreatment to preserve the cationic character of *cyt c*. Disulfide reducing agents were also excluded from sample preparation to avoid the unintentional cleavage of intermolecular disulfide bonded aggregates. Instead, samples were thermally denatured under non-reducing conditions in the background electrolyte by heating at 90 °C for 5 min prior to analysis. Figure 3.1c illustrates the substantial improvement in peak symmetry observed for thermally denatured protein samples. It is also noted that tailing of the monomer peak is significantly reduced. There was also marked improvement in the irregular peak shape previously observed for the dimer peak under native conditions. Additionally, thermal denaturation allowed for better detection of a minor pentameric component. The analysis time for the denatured sample was less than 7 min. These results suggest that thermal denaturation alone is sufficient pretreatment for this study.

The inset in Figure 3.1c shows a plot of protein molecular weight versus migration time generated from the average of five consecutive runs of thermally denatured samples containing species I-V. Note that the x-axis was generated based on integer multiples of the molecular

weight for monomeric bovine cyt *c* as reported by the manufacturer. Migration times determined from best fit data exhibited good precision, having standard deviations less than 0.5% for all detected species.

The analysis of protein samples denatured with organic solvents including methanol, ethanol, acetonitrile, and acetone was also evaluated. In general, the use of volatile organic solvents greatly complicated sample preparation and CE analyses. Relatively high organic solvent content, around 1:1 buffer/organic solvent, was usually required to achieve results comparable to thermally denatured samples. However, the addition of organic solvent to the samples often caused appreciable protein precipitation, which often resulted in erratic baselines and poor separation reproducibility (data not shown). In addition, protein precipitation also caused frequent column blockages resulting in a reduction in column lifetime. For these reasons, organic solvents were also excluded from sample preparation procedures.

### **3.3.4 Voltage Optimization**

The effect of applied voltage on migration time and peak efficiency was investigated for the separation of protein reaction mixture components using 21 cm effective length columns. Figure 3.2 illustrates the effect of a range of applied voltages on the separation of cyt *c* aggregates using a freshly prepared capillary. As expected, the shortest analysis time (2.33 min) was obtained at -15 kV. However, voltages higher than -15 kV often resulted in unstable current and poor reproducibility. In addition, separation efficiency improved with increasing voltage as indicated by a roughly 2-fold improvement in peak width observed from -8 to -15 kV (data not shown). Resolution also improved significantly with increasing voltage. Resolution ( $R_s$ ) between the monomer and dimer peaks at -8 kV and -15 kV were 1.04 and 1.20, respectively. Evaluation of these data suggests that peak efficiency was limited primarily by longitudinal band

broadening under the conditions used for these studies.

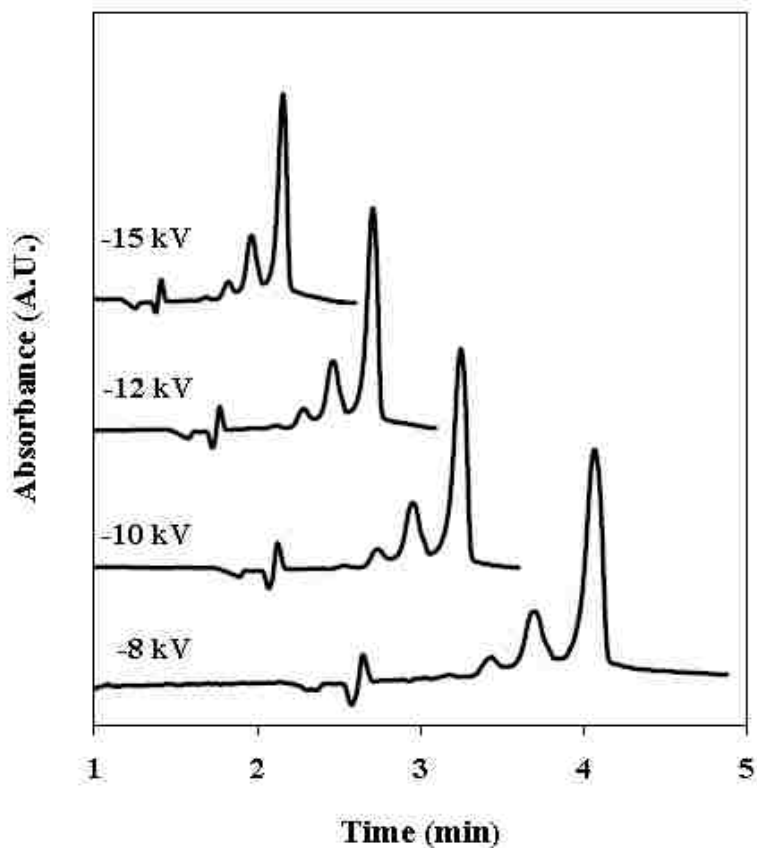


**Figure 3.2** Effect of applied voltage on CE separations of protein reaction mixture components: a) electropherograms acquired at -15, -12, -10, and -8 kV. Separations were performed using a freshly prepared column.

### 3.3.5 Short-End Injection Method

Initial studies for this work were conducted using capillaries with a total length of 32 cm (21 cm effective capillary length). In order to obtain more rapid separations, the effective length of the capillary was decreased to 10 cm by injecting and separating from the outlet-end of the capillary. Figure 3.3 shows a typical short-end electropherogram where separation of the protein reaction mixture containing species I-V was achieved in less than 70 sec. Although there was minor deterioration in peak shape observed for the tetrameric and pentameric species, overall short-end separation performance was acceptable.

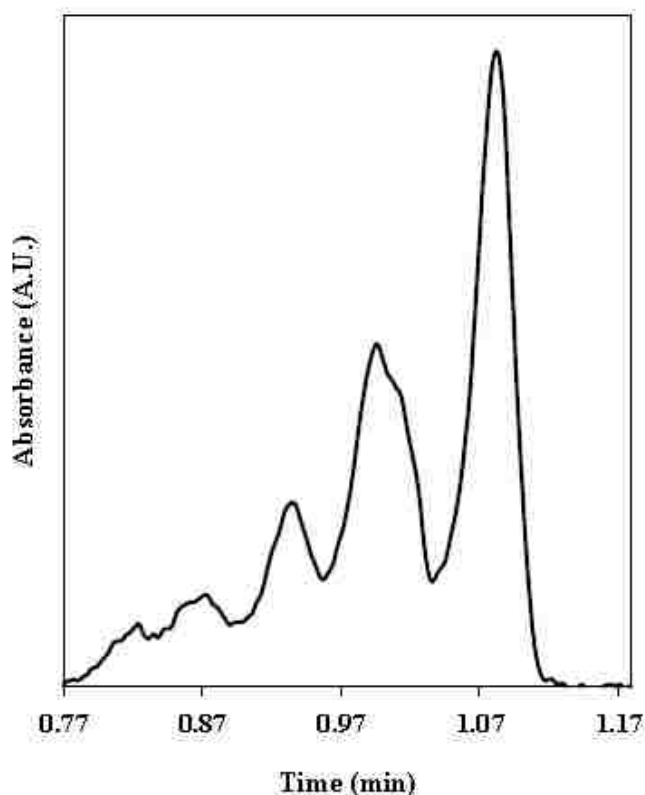


**Figure 3.3** Electropherogram of thermally denatured protein reaction mixture containing cyt *c* species I-V separated in less than 70 sec using short-end injection. Separation performed with an applied voltage of 8kV (22  $\mu$ A current) and a 50  $\mu$ m i.d., 32 cm total length, 10 cm effective length capillary column.

In order to assess the stability of the short-end injection method, reproducibility and electrophoretic efficiency were evaluated for 5 successive runs without regenerating the PDADMAC coating. Various column performance values are provided in Table 3.1. Run-to-run reproducibility for migration times was generally excellent, having RSD values  $< 0.5\%$  for all monomer, dimer, and trimer peaks. Good precision was observed for peak area values, indicating reproducible injection volumes and near ideal electrophoretic behavior with respect to minimized analyte-wall adsorption. The relatively high number of theoretical plates ( $N$ ), in some instances approaching one million, indicate exceptional column efficiency for separating monomer and aggregate species. In addition, satisfactory column-to-column reproducibility was

also achieved as indicated by RSD values < 1% (n = 10) for migration times obtained from 5 consecutive runs performed with two different PDADMAC coated capillaries. Overall, short-end injection provided satisfactory separation performance for the analysis of the protein reaction mixture in significantly less time than normal injection conditions.

**Table 3.1.** Separation performance and reproducibility statistics for short-end CE separations of protein reaction mixture.\*

<b>Protein Mixture Component</b>	<b>Migration Time, min</b>	<b>Peak Area</b>	<b>Number of Theoretical Plates (N) × 10<sup>5</sup></b>
Monomer (I)	1.92 (0.28)	220.54 (3.90)	8.55 (3.24)
Dimer (II)	1.75 (0.42)	63.76 (4.38)	5.75 (5.93)
Trimer (III)	1.62 (0.48)	15.08 (5.77)	7.70 (6.73)

\*Migration time, peak area, and number of theoretical plates (N) values calculated for successive runs (n=5) without regeneration of the poly (diallyldimethylammonium chloride) (PDADMAC) coating. Percent relative standard deviation (%RSD) values are given in parentheses. Separations performed using 8 kV applied voltage.

### 3.3.6 Oligomerization Inhibition Studies

Pyridoxal-5-phosphate (PLP) is the aldehyde-functionalized cofactor derivative of vitamin B<sub>6</sub>. The antiatherogenic properties of PLP for lowering plasma Hcy levels and risk of cardiovascular disease are documented in the medical literature.<sup>28, 29</sup> However, very little is known about the effect of PLP on HTPA. Recently reported mechanistic studies suggest the possibility of pyridoxal tetrahydrothiazine formation via condensation of Hcy thiolactone with PLP as a means of neutralizing Hcy thiolactone *in vivo*.<sup>30</sup> Similarly, we propose that in situ pyridoxal tetrahydrothiazine formation could possibly disrupt Hcy thiolactone-induced protein modification *in vitro*, thereby inhibiting HTPA. To further investigate this hypothesis, the previously optimized short-end CE method was applied to the evaluation of HTPA inhibition.

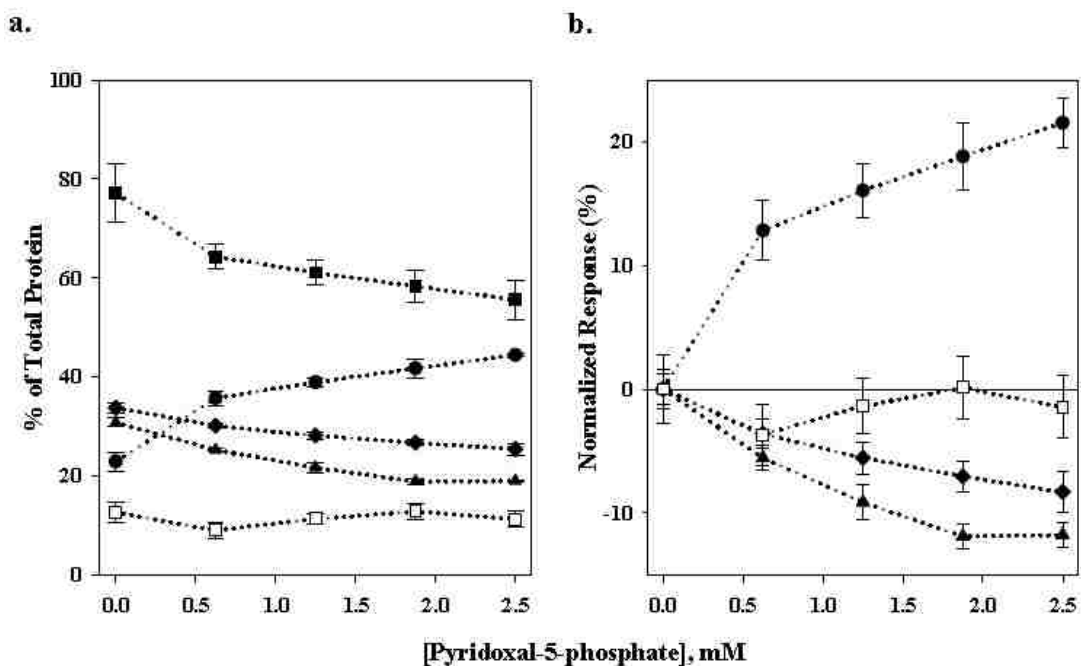


**Figure 3.4** Results for aggregation inhibition study represented as a) percent of total protein peak area determined by integration of best fit data; and b) percent change for respective mixture component peak areas normalized to an experimental control versus pyridoxal-5-phosphate concentration.

Representative results for protein reaction mixtures in the presence of PLP are summarized in Figure 3.4. Mixture components are denoted as monomeric, I (●); dimeric, II (▲); trimeric, III (▲); and tetrameric, IV (□); respectively. The total of aggregates (■) is obtained by taking the sum of the respective contributions of mixture components II-IV. The experimental control sample (0 mM PLP) was found to contain *cyt c* species I-IV, in which aggregates (II-IV) represented  $77.12 \pm 1.72\%$  of total *cyt c* (Figure 3.4a). All aggregate species decreased with increasing concentrations of PLP to a minimum value of  $55.58 \pm 1.42\%$  observed at 2.5 mM PLP (Figure 3.4b). At the same time, there was a complementary increase in the monomeric species with increasing concentrations of PLP. The trimer species exhibited the greatest change of total protein ( $-11.79 \pm 0.94\%$ ) followed by the dimer ( $-8.32 \pm 1.60\%$ ). The changes observed for the minor tetrameric component with respect to the experimental control

were within experimental error. Figures 3.5a and 3.5b show representative electropherograms acquired for protein reaction mixtures treated with 0.25 and 2.5 mM PLP after 24 h. Note the overall reduction in aggregate species for the sample treated with 2.5 mM PLP. Comparable inhibition trends were also visible in SDS-PAGE slab gels (Figure A.2 in Appendix A). Collectively, these results suggest that *in vitro* HTPA is effectively inhibited by PLP.

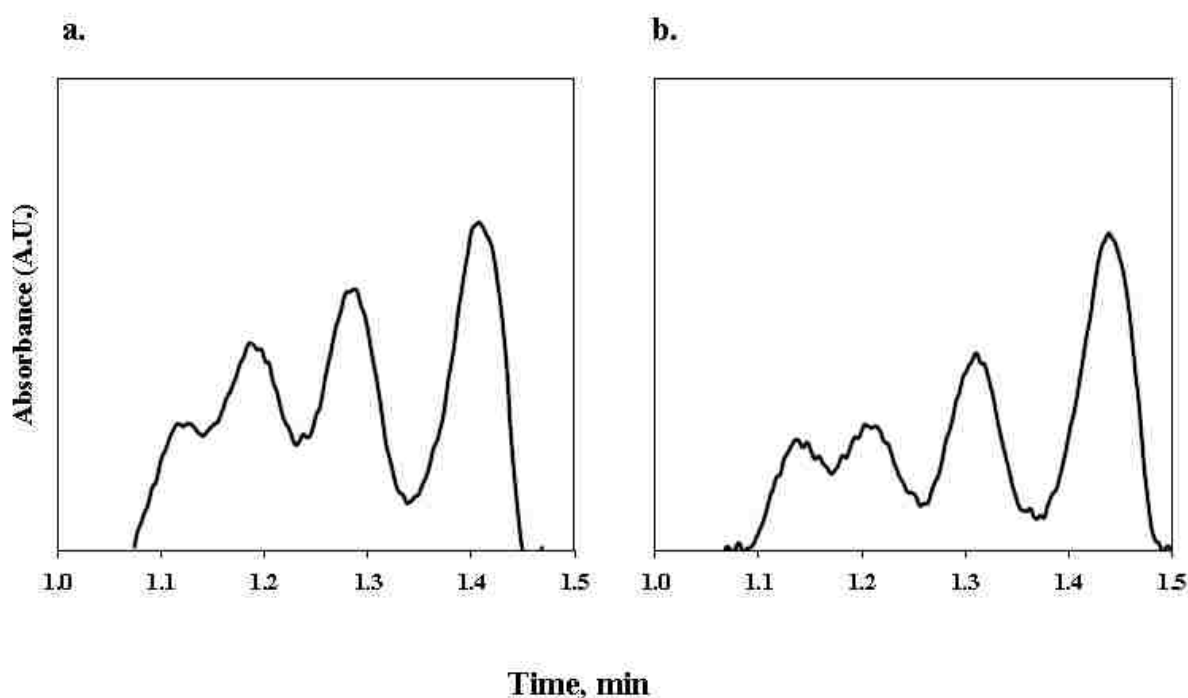


**Figure 3.5** Representative short-end CE electropherogram resulting from the separation of the protein reaction mixture treated with a) 0.25 mM pyridoxal-5-phosphate and b) 2.5 mM pyridoxal-5-phosphate, respectively. Separation performed using an applied voltage of 8kV (22  $\mu$ A current) and a 50  $\mu$ m i.d., 32 cm total length, 10 cm effective length capillary column.

Analysis times for PLP-treated samples separated under optimized conditions were typically around 1.5 minutes, approximately twice as long as those obtained for untreated samples. It is probable that PLP, which is anionic under experimental conditions, binds non-specifically with the protein resulting in decreased cationic character and increased electrostatic interaction between the protein and the PDADMAC coating. Despite efforts to thoroughly rinse



the protein prior to analysis, some PLP remained associated with the protein as was indicated by the characteristic reddish-orange color of the reaction solutions. Nevertheless, more than adequate resolution was obtained to achieve a quantitative analysis.

In situ pyridoxal tetrahydrothiazine formation was initially proposed as the mechanism for HTPA inhibition of PLP. Therefore, efforts were made to determine if pyridoxal tetrahydrothiazine could be detected in the protein reaction mixtures. Protein reaction mixtures (500  $\mu$ L) containing 10 mg/mL cyt *c*, 2.5 mM Hcy thiolactone, and the desired quantity of PLP were prepared as previously described and allowed to react for 12 h. For comparison, a set of control reaction mixtures containing identical amounts of PLP and Hcy thiolactone (without protein) was also prepared. The reaction mixtures were passed through a 10 kDa MWCO centrifugation filter to remove the protein. Reaction mixture filtrates and control samples were diluted 10-fold and analyzed using UV-Vis spectroscopy. Individual reaction components, PLP and pyridoxal tetrahydrothiazine, were monitored at 390 nm and 330 nm<sup>30</sup>, respectively.

Tetrahydrothiazine formation in the control reactions increased linearly with PLP concentration (Figure A.3a in Appendix A). In situ tetrahydrothiazine formation in protein filtrates also increased in response to increasing PLP concentration until a maximum was reached at 1.88 and 2.5 mM (Figure A.3b in Appendix A). The maximum absorption for the tetrahydrothiazine product for protein samples was approximately 2-fold less than the maximum observed for the control reaction. This reduction in product absorption for filtrate samples is likely the result of non-specific binding of PLP and/or pyridoxal tetrahydrothiazine to the protein. The presence of cyt *c*-bound PLP was indicated by a subtle color change in the retentate from red to reddish-orange. In situ tetrahydrothiazine production was also limited to a lesser extent by *N*-Hcy-protein formation. Overall, this result suggests that in situ tetrahydrothiazine

formation inhibits HTPA *in vitro*.

### 3.4 Conclusions

We have shown that CE with UV detection provides a practical alternative to semi-quantitative SDS-PAGE for monitoring homocysteine thiolactone-induced protein aggregation. Capillaries coated with PDADMAC provided good column stability and reproducibility. Under optimized conditions, short-end injection typically allowed the separation of thermally denatured protein reaction mixtures in less than 70 sec.

In this study we have also demonstrated rapid primary HTPA inhibition screening with analysis around 1.5 min, which is a considerable improvement over the hour timeframe typically required to perform a comparable SDS-PAGE analysis. We have shown that PLP effectively inhibits HTPA *in vitro*. This inhibitory effect is attributed to *in situ* formation of pyridoxal tetrahydrothiazine, which was detected in the protein samples treated with PLP. This preliminary finding is congruent with mechanistic studies previously reported by Jakubowski that proposed pyridoxal tetrahydrothiazine formation as a possible mode of neutralizing Hcy thiolactone in the body. However, further study is needed to determine if inhibition of HTPA by PLP is a physiologically relevant phenomenon. Future work may include the evaluation of various other polyelectrolyte coatings and an expanded field of aggregate inhibitor compounds.

### 3.5 References

- (1) Mercie, P.; Garnier, O.; Lascoste, L. *Apoptosis* 2000, 5, 403-411.
- (2) Austin, R. C.; Lentz, S. R.; Werstuck, G. H. *Cell. Death Differ.* 2004, 11, S56-S64.
- (3) Jakubowski, H. *FASEB J.* 1999, 13, 2277-2283.
- (4) Jakubowski, H. *J. Nutr.* 2000, 130, 377S-381S.
- (5) Hop, E. C. A.; Bakhtiar, R. *Rapid Commun. Mass Spectrom.* 2002, 16, 1049-1053.

- (6) Rosenberg, A. *AAPSJ* 2006, 8, E501-E507.
- (7) Naruszewicz, M.; Mirkiewicz, E.; Olszewski, A. J.; McCully, K. S. *Nutr. Metab. Cardiovas.* 1994, 4, 70-77.
- (8) Yang, X.; Gao, Y.; Zhou, J. *Clin. Chim. Acta* 2006, 364, 230-234.
- (9) Jabeen, R.; Payne, D.; Wiktorowcz, J.; Mohammad, A.; Petersen, J. *Electrophoresis* 2006, 27, 2413-2438.
- (10) Shihabi, Z. K. *J. Liq. Chromatogr. Related Technol.* 2000, 23, 79-95.
- (11) Jenkins, M. A.; Guerin, M. D. *J. Chromatogr. B* 1996, 682, 23-34.
- (12) Dolnik, V. *Electrophoresis* 2006, 27, 126-141.
- (13) Hutterer, K.; Dolnik, V. *Electrophoresis* 2003, 24, 3998-4012.
- (14) Dolnik, V.; Hutterer, K. M. *Electrophoresis* 2001, 22, 4163-4178.
- (15) Dolnik, V. *Electrophoresis* 1997, 18, 2353-2361.
- (16) Gonzalez, N.; Elvira, C.; San Roman, J.; Cifuentes, A. *J. Chromatogr. A* 2003, 1012, 95-101.
- (17) Harrell, C. W.; Dey, J.; Shamsi, S. A.; Foley, J. P.; Warner, I. M. *Electrophoresis* 1998, 19, 712-718.
- (18) Zhu, X. F.; Kamande, M. W.; Thiam, S.; Kapnissi, C. P.; Mwongela, S. M.; Warner, I. M. *Electrophoresis* 2004, 25, 562-568.
- (19) Kapnissi, C. P.; Valle, B. C.; Warner, I. M. *Anal. Chem.* 2003, 75, 6097-6104.
- (20) Kamande, M. W.; Zhu, X. F.; Kapnissi-Christodoulou, C.; Warner, I. M. *Anal. Chem.* 2004, 76, 6681-6692.
- (21) Kamande, M. W.; Kapnissi, C. P.; Zhu, X. F.; Akbay, C.; Warner, I. M. *Electrophoresis* 2003, 24, 945-951.
- (22) Kamande, M. W.; Fletcher, K. A.; Lowry, M.; Warner, I. M. *J. Sep. Sci.* 2005, 28, 710-718.
- (23) Wang, Y.; Dubin, P. L. *Anal. Chem.* 1999, 71, 3463-3468.
- (24) Cahours, X.; Viron, C.; Morin, P.; Renimel, I.; Andre, P.; Lafosse, M. *Anal. Chim. Acta* 2001, 441, 15-21.
- (25) Souverain, S.; Geiser, L.; Rudaz, S.; Veuthey, J. L. *J. Pharm. Biomed. Anal.* 2006, 40,

235-241.

- (26) Fan, L. Y.; Cheng, Y. Q.; Li, Y. Q.; Chen, H. L.; Chen, X. G.; Hu, Z. D. *Electrophoresis* 2005, 26, 4345-4354.
- (27) Nakashima, T.; Higa, H.; Matsubara, H.; Benson, A.; Yasunobu, K. *J. Bio. Chem.* 1966, 241, 1166-1177.
- (28) Endo, N.; Nishiyama, K.; Otsuka, A.; Kanouchi, H.; Taga, M.; Oka, T. *Br. J. Nutr.* 2006, 95, 1088-1093.
- (29) Verhoef, P.; Kok, F. J.; Kruyssen, D. A.; Schouten, E. G.; Wittenman, J. C.; Grobbee, D. E.; Ueland, P. M.; Refsum, H. *Arterioscler. Thromb. Vasc. Biol.* 1997, 5, 989-995.
- (30) Jakubowski, H. *Chemistry* 2006, 12, 8039-8043.

## CHAPTER 4

### GOLD NANOSENSOR FOR COLORIMETRIC DETECTION OF *N*-HCY-PROTEIN

#### 4.1 Introduction

The material presented in this chapter is reproduced in part with permission from *Langmuir*, 2008, volume 24, pages 4107-4113; Gates, A. T.; Fakayode, S. O.; Lowry, M.; Ganea, G. M.; Murugesu, A.; Robinson, J. W.; Strongin, R. M.; Warner, I. M.; Gold nanoparticle sensor for homocysteine thiolactone-induced protein modification, which was copyrighted in 2008 by the American Chemical Society.

The emergence of HTL-induced protein modification (HTPM) as a CVD indicator has created a need for new detection methods for *N*-Hcy-protein. Our laboratory has contributed to the development of several organic dye-based colorimetric and fluorimetric sensors for the detection of various amino thiol disease biomarkers, including Cys and Hcy.<sup>1-4</sup> Several of these sensors show promise for amino thiol detection in human blood plasma. We have also reported the use of redox indicators for electrochemical detection of glutathione, another important amino thiol biomarker.<sup>5</sup> Our recent work has focused on exploring new detection schemes and strategies for investigating the physiochemical properties of *N*-Hcy-protein. For example, we reported the development a rapid capillary electrophoresis (CE) method for separating mixtures containing oligomeric *N*-Hcy-protein derived from *in vitro* modified cytochrome *c*. This CE method was successfully applied to monitoring the inhibition of HTL-induced protein oligomerization via *in situ* pyridoxal tetrahydrothiazine formation.<sup>6</sup>

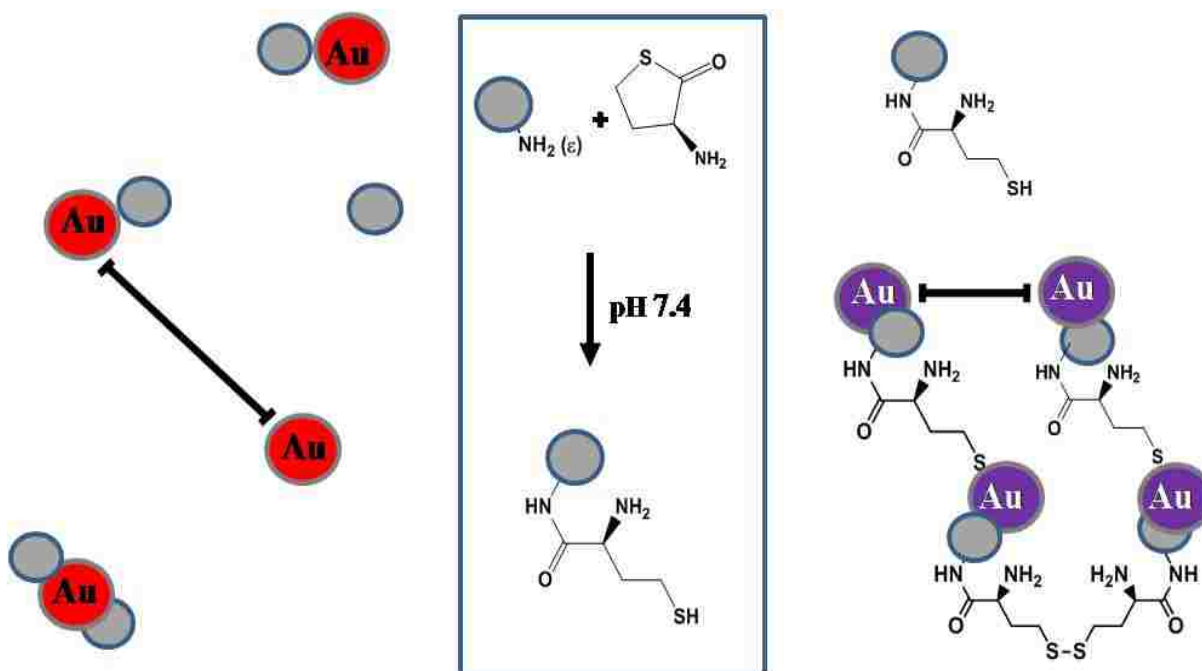
Separations techniques such as TLC<sup>7</sup> and HPLC<sup>8</sup> have also been employed to quantify *N*-Hcy-protein, but few specific detection schemes have been reported. Enzyme linked immunosorbent assays (ELISAs) are perhaps the most commonly used affinity technique for *N*-

Hcy-protein determination.<sup>9, 10</sup> ELISAs are a highly sensitive and versatile format that can be configured to generate either a colorimetric or fluorimetric response. Another advantage of ELISA is the wide commercial availability of 96-well plate kits, which provide a user-friendly interface that is amenable to high throughput applications. Unfortunately, the development of ELISA kits for *N*-Hcy-protein has been hampered by the lack of commercially available antibodies.

Plasmon resonant sensors provide an elegant option for *N*-Hcy-protein detection. In particular, GNP-based plasmon resonant biochemical sensors exploit biomolecular interaction in order to stimulate nanoparticle self-assembly. It is often necessary to functionalize the nanoparticles with affinity ligands in order to achieve the desired specificity.<sup>11-13</sup> However, thiol detection applications do not necessarily require the use of functionalized nanoparticles because gold is intrinsically thiol reactive. For instance, citrate-capped GNPs have been successfully employed as colorimetric sensors for various amino thiols including Hcy<sup>14</sup>, cysteine<sup>15</sup>, and glutathione.<sup>15</sup> Amino thiols tend to readily adsorb onto the surface of colloidal gold via chemisorption interactions. Plasmon resonance thiol sensing has been shown to occur via noncovalent electrostatic-type interactions between the amino and carboxylic acid groups.<sup>14, 15</sup>

Herein, we report the use of citrate-capped colloidal GNPs as a sensor for HTPM. Scheme 4.1 illustrates the proposed mechanism for the colorimetric GNP sensor. In the presence of unmodified protein, the nanoparticles interact in a nonspecific manner with individual protein molecules but remain randomly dispersed throughout the protein solution. As a result, the sensor solution retains the characteristic red color of dispersed colloidal GNPs. In contrast, the nanoparticles bind with the HTL-modified proteins via chemisorption-type binding (Au-S-R), thereby facilitating nanoparticle assembly via cross-linking. Nanoparticle assembly is further stabilized by intermolecular disulfide bonding (R-S-S-R) between *N*-Hcy-protein species. The

scale bars are shown to emphasize the relative difference in interparticle distances for dispersed and assembled GNPs, respectively. UV-Vis absorption spectroscopy and transmission electron microscopy (TEM) were employed to investigate the assembly behavior of colloidal gold nanoparticles in response to *N*-Hcy-protein. To the best of our knowledge, direct colorimetric detection of serum *N*-Hcy-protein using GNPs has not been previously reported.



**Scheme 4.1** Proposed colorimetric GNP sensor for HTL-induced protein modification.

## 4.2 Methods

### 4.2.1 Materials

*L*-Hcy thiolactone hydrogen chloride, hydrogen tetrachloroaurate trihydrate, trisodium citrate, EDTA, and all other reagents used for the preparation of buffer and serum protein solutions were obtained from Sigma-Aldrich (St. Louis, MO) at the highest purity available and used as received. Ultra pure water (18.2 M $\Omega$ ) was obtained from an Elga model PURELAB Ultra water filtration system.

#### **4.2.2 Synthesis of Gold Nanoparticles**

Citrate-capped GNPs ca.13 nm diameter were synthesized using the well-known Turkevich-Frens method.<sup>16, 17</sup> Briefly, a solution of hydrogen tetrachloroaurate trihydrate was prepared in water and heated to reflux while stirring, followed immediately by the addition of a 40 molar excess of freshly prepared trisodium citrate-water solution, which initiated the reduction of the hydrogen tetrachloroaurate trihydrate. The aurate-citrate solution was allowed to reflux for approximately 25 min or until completion of the redox reaction as indicated by a change in solution color from faint yellow to dark red. The excess citrate in solution creates a negatively charged surface on the GNPs, thereby minimizing nonspecific GNP aggregation post-synthesis.<sup>17</sup> The resultant GNP solution was allowed to cool to room temperature prior to storage in an amber glass bottle. Aurate (1.0 mM) was reduced in 40mM citrate resulting in a GNP stock solution of 1.0 mM, assuming complete reduction of the gold. GNP solutions were purified using a 0.1  $\mu\text{m}$  polytetrafluoroethylene syringe filter devices. Nanoparticle size was confirmed using dynamic light scattering (DLS) and transmission electron microscopy (TEM).

#### **4.2.3 Preparation of Protein Homocystamide**

The *N*-Hcy-protein stock solutions used in this study were prepared using procedures similar to those previously reported by Jakubowski.<sup>18</sup> Briefly, essentially fatty acid free human serum albumin purchased from Sigma-Aldrich (St. Louis, MO) was dissolved in pH 7.4, 100 mM, sodium phosphate buffer containing 0.2 mM EDTA and incubated at 25 °C in the presence of 4.6 mM HTL for 4 h at room temperature. The post-translational modification reaction was quenched by filtering the protein reaction solution through a 10 kDa molecular weight cut-off centrifugal membrane device (Millipore, Billerica, MA) to remove any unreacted HTL as well as other low molecular weight byproducts such as Hcy. The protein retentate was rinsed twice with



1 mL buffer aliquots to remove nonspecifically bound HTL or Hcy. The rinsed modified protein was promptly reconstituted with buffer to obtain the *N*-Hcy-protein stock solution.

#### **4.2.4 Sample Characterization**

Electrospray ionization- time of flight-mass spectrometry (ESI-TOF-MS) was used to verify the post-translational modification of HSA by HTL. The mass spectrometry data indicates that the *in vitro* modification reaction protocol used in this study is efficient and typically yields a extensively modified HSA solution. The majority of the resultant HSA species typically contained  $\sim 1 - 4$  Hcy per protein molecule post-modification. A substantial signal corresponding to dimeric HSA was also detected due to modification-induce oligomerization. Based on these findings, the concentrations of the HSA and serum homocystamide solutions are reported in units of mg/mL or  $\mu\text{g/mL}$ , assuming complete modification. Mass spectra (Figure B.1) and additional discussion are provided in Appendix B.

Unless otherwise noted, *N*-Hcy-protein standard solutions were prepared by diluting the stock solution with phosphate buffer. Excess biological materials were heat sterilized prior to disposal in an approved biohazard waste container. All appropriate safety apparels such as protective gloves, clothing, and eyewear were worn while handling the potentially biohazardous human serum protein material.

#### **4.2.5 Preparation of Sensor Solutions**

*N*-Hcy-protein solutions were immediately treated with the GNP sensor in order to minimize the loss of colorimetric response due to spontaneous intermolecular disulfide bonding between modified proteins and other miscellaneous auto-oxidation processes. The *N*-Hcy-protein solutions used in this study were not treated with a disulfide reducing agent. Unless otherwise indicated, a 100  $\mu\text{L}$  aliquot of the *N*-Hcy-protein or control solution was treated with 200  $\mu\text{L}$  of 1.0 mM GNP stock solution at room temperature. Changes in the visible absorption

due to the GNPs and the nanoparticle-modified protein complex were monitored immediately at 520 nm and 620 nm, respectively. The UV absorption associated with the protein was monitored between 220-280 nm. Protein-sensor solutions were typically diluted 2-fold prior to measuring UV-visible absorption.

#### **4.2.6 Instrumentation**

Absorption measurements were acquired using a Shimadzu, model UV-3101PC UV-Vis-NIR, spectrophotometer with either quartz (UV-visible) or disposable polystyrene (visible only) reduced volume cells. DLS measurements were performed using a Malvern Zetasizer Nano ZS (Worcestershire, UK). TEM images were acquired with a JEOL model 100CX transmission electron microscope using an acceleration voltage of 80kV. TEM specimens were prepared by adsorbing a thin layer of the sensor-protein solution onto carbon-coated grids followed by air-drying. The sample grids were treated with 2% uranyl acetate staining reagent prior to TEM imaging.

### **4.3 Results and Discussion**

#### **4.3.1 Nanoparticle-Serum Protein Compatibility Study**

A preliminary assessment of the proposed GNP sensor was performed using the model protein human serum albumin (HSA). HSA was chosen for these studies because it is a major protein constituent in human serum, accounting for approximately half of the total serum protein. In addition, it is known that highly stable albumin-GNP conjugates are readily obtained via adsorption interactions under physiological pH and ionic strength conditions.<sup>19-21</sup> However, it was necessary to evaluate the behavior of the proposed HSA-GNP system under the conditions used for these studies.

Figure 4.1 is an image of cuvettes containing equivalent concentrations of the GNP sensor (~ 0.3 mM) in the presence of either HSA or HSA-homocystamide (0-85.2 mg/mL)

dissolved in phosphate buffer (100 mM at pH 7.4). The protein concentration range used for this study encompasses the expected physiological concentration range for HSA in human plasma, ~34 - 54 mg/mL.<sup>22</sup> As expected, the GNPs were only sparingly soluble in the phosphate buffer in the absence of HSA. The resultant metallic-grey colored suspension shown in Figure 4.1a is slightly opaque due to scattering from salt-induced aggregation and precipitation of the GNPs. This behavior is attributed to the citrate-capped GNPs becoming destabilized by the relatively high ionic strength of the phosphate buffer.<sup>23</sup>

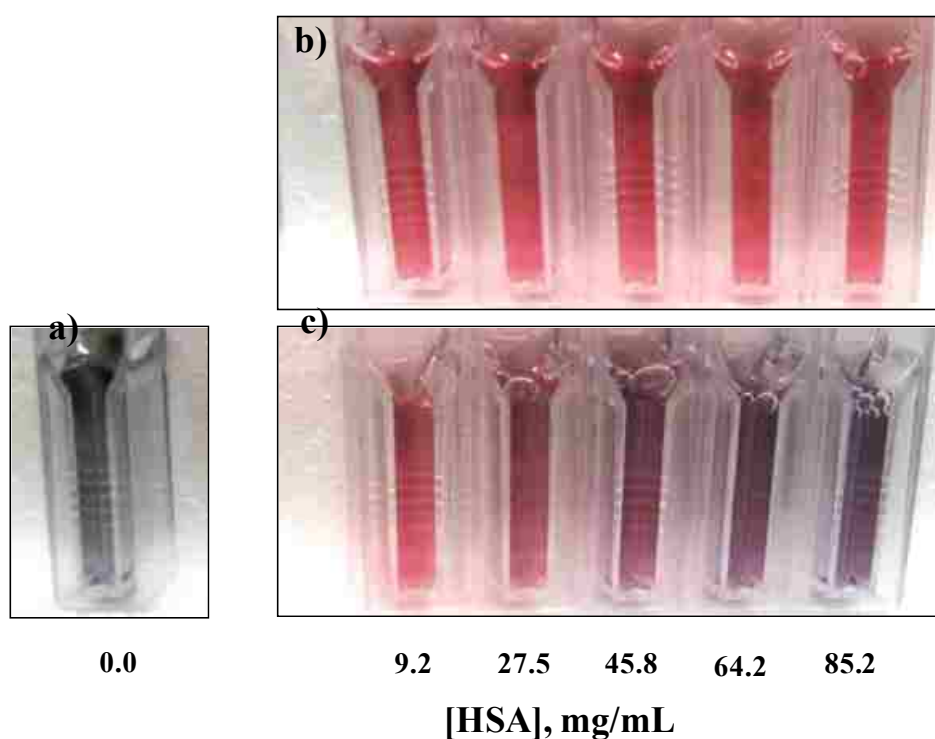


**Figure 4.1** Photographs of the gold nanoparticle (GNP) sensor a) in the absence of protein b) in the presence of unmodified HSA (9.2 - 85.2 mg/mL) and c) in the presence of HSA-homocystamide (9.2 - 85.2 mg/mL).

Cuvettes containing unmodified HSA (9.2 - 85.2 mg/mL) are shown in Figure 4.1b. All samples were prepared in 100 mM phosphate, 0.2 mM EDTA buffer. Each cuvette contains 0.3 mM GNP. The nanoparticles remain stable and dispersed in the presence of unmodified HSA, as indicated by the reddish-pink color of the sensor solutions. Notably, there is no discernible

change in the color of the sensor solutions in response to increasing concentrations of unmodified HSA, which suggests that nonspecific nanoparticle assembly does not occur in the presence of unmodified HSA. Furthermore, the UV-vis absorption spectra shown in Figure 4.2a are similar to those previously reported for bovine serum albumin-GNP conjugates dissolved in 10 mM phosphate at pH 7.0.<sup>19</sup>

The GNP sensor produced a significant colorimetric signal in response to increasing concentrations of *N*-Hcy-protein, which is clearly visible in Figure 4.1c. The sensor solutions transition from reddish-pink to a deep purple-violet color, which is easily distinguishable from the highly scattering metallic grey-colored suspension produced in the absence of protein due to salt-induced nanoparticle aggregation.

The corresponding UV-visible absorption spectra for sensor-protein solutions collected approximately 20 min after treatment with the GNPs (Figures 4.1b-c) are provided in Figure 4.2. The absorption spectra shown in Figure 4.2a indicate the absorption maximum ( $\lambda_{\text{max}}$ ) for the GNP sensor in the presence of unmodified HSA is ~520 nm, which is comparable to absorption of dispersed gold nanoparticles in water. No significant change in the visible absorption spectra was observed in response to increasing concentrations of unmodified HSA over the concentration range investigated in this study. Conversely, the absorption spectra of the sensor in the presence of an equivalent concentration range of HSA-homocystamide have red-shifted extended plasmon bands (Figure 4.2b). A proportional increase in UV absorption at the protein absorption bands ~220 - 280 nm was also observed in response to increasing concentrations of both unmodified HSA and HSA-homocystamide in the sensor solutions. A representative plot of the colorimetric response of the GNP sensor detected at 620 nm in the presence of HSA-homocystamide is provided in Appendix B (Figure B.2). The colorimetric response was found to be linear ( $r^2 = 0.9849$ ) over a range of HSA concentrations (2.8 - 28 mg/mL). The limit of

detection (LOD) and calibration sensitivity for the method were 2.3 mg/mL and  $2.7 \text{ AU} \cdot (\mu\text{g/mL})^{-1}$ , respectively. Collectively, these results suggest that the colorimetric signal produced by the GNP sensor is due to HTL modification-directed nanoparticles assembly and not to salt-induced nanoparticle aggregation. Moreover, the stability of the GNP sensor in the HSA-phosphate buffer solutions suggests that the GNP sensor will be stable in the presence of human sera (*vide infra*).

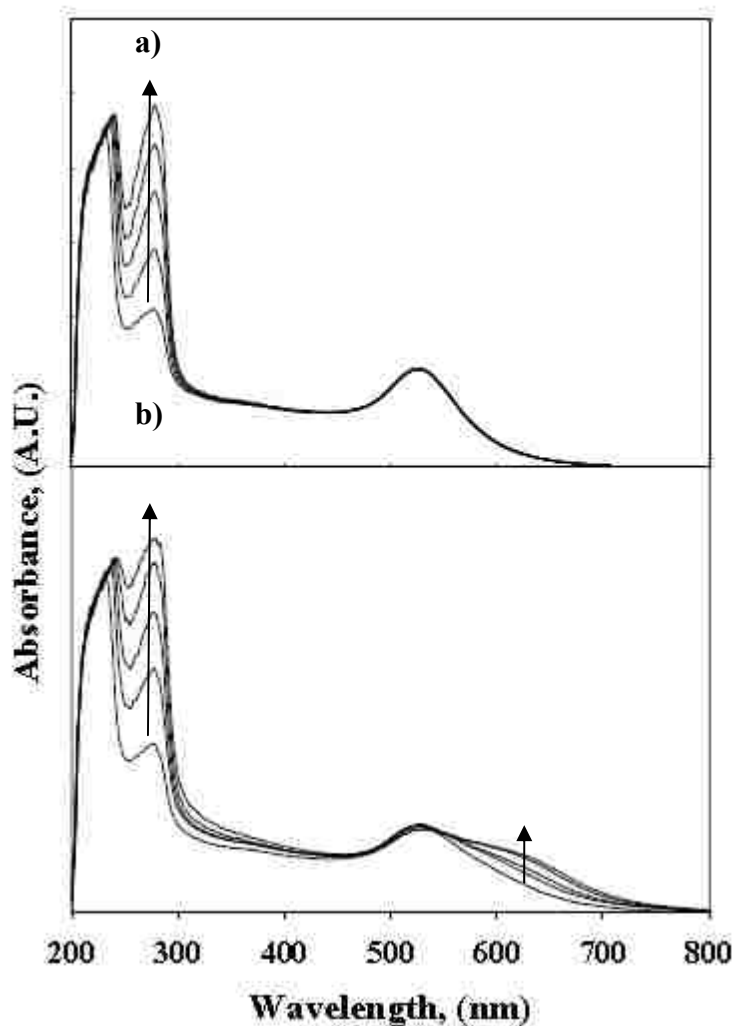


**Figure 4.2** UV-visible absorption spectra of GNP sensor solutions shown in Figure 1. a) Unmodified HSA and b) *N*-Hcy-HSA. Extended plasmon bands are only observed for sensor solutions containing HSA-homocystamide. The arrows indicate the change in absorption with increasing HSA or HSA-homocystamide.

### 4.3.2 Effect of Temperature on Sensing

Many GNP sensors reported in the literature are designed such that nanoparticle assembly is achieved via reversible noncovalent interactions.<sup>24-26</sup> Consequently, nanoparticle assembly is often loosely associated and environment-dependent. For example, Mirkin et al. demonstrated temperature-dependent reversible nanoparticle assembly over a decade ago using DNA-functionalized GNPs.<sup>27</sup> This system exploits noncovalent DNA hybridization interactions to produce a colorimetric signal that could be effectively “switched on and off” by cycling the solution temperature between 0 and 80 °C, the latter of which is well above the dissociation temperature of the DNA-nanoparticle complex. Additionally, a temperature and pH-sensitive Hcy GNP sensor was recently developed by Lim et al.<sup>14</sup> This GNP sensor utilizes reversible zwitterionic-type interactions to generate a colorimetric response.

A distinguishing characteristic of the proposed GNP sensor for *N*-Hcy-protein is that it was designed to exhibit essentially irreversible binding behavior via thiol binding interactions. In principle, a tightly bound nanoparticle-protein assembly would allow for highly stable and long-lived colorimetric detection. Consequently, it was found that sensor solutions containing HSA-homocystamide incubated in an 80 °C water bath for 20 min exhibited remarkable stability as indicated by a persistent colorimetric signal. Only a very slight increase in colorimetric signal was observed after exposing the sensor solutions to 80 °C for ~10 min. This result is likely caused by additional GNP binding sites being exposed due to thermal denaturation of the modified protein.

### 4.3.3 Confirmation of Nanoparticle Assembly

Transmission electron microscopy (TEM) was used to image the GNP sensor in the presence of HSA and HSA homocystamide. As expected, the purple-colored GNP sensor- *N*-Hcy-protein solutions contained oligomeric HSA, which appears as a dark sponge-like film in

the TEM image ( $33,000 \times$  magnification) shown in Figure 4.3a. The GNPs appear as clearly defined black dots in the TEM images. Further examination of Figure 4.3a reveals an assortment of nanoparticle clusters within the oligomeric protein network. The multiplicity of shapes and sizes of the nanoparticle assemblies in the sensor specimen is consistent with the broad extended plasmon bands observed at 620 nm (Figure 4.2b).<sup>28, 29</sup> The inset of Figure 4.3a ( $100,000 \times$  magnification) shows an example of modification-directed nanoparticle assembly, a 4-nanoparticle cluster within the oligomeric protein network. Other regions within the oligomeric protein network containing GNP clusters are highlighted in Figure B.3 in Appendix B. These data suggest that both modification-induced protein oligomerization and modification-directed nanoparticle assembly occur concomitantly in the GNP sensor solutions containing *N*-Hcy-protein.

In contrast, neither nanoparticle assembly nor protein oligomerization is observed in a specimen prepared from the red-colored GNP sensor solution containing unmodified HSA (Figure 4.3b). The unmodified protein appears as dark semitransparent spots in the TEM images. Closer examination of the sensor specimens containing unmodified HSA reveals that the spherical GNPs are randomly dispersed throughout the specimen, within individual protein spots. The inset of Figure 4.3b shows GNPs in the presence of unmodified HSA at  $100,000 \times$  magnification. Nanoparticle assembly is not induced by unmodified HSA, presumably due to the lack of *N*-Hcy-protein binding sites. The absence of significant nanoparticle assembly in the unmodified protein sample is consistent with the absorption spectra shown in Figure 4.2a and is consistent with the expected results for this detection scheme.

#### **4.3.4 Proposed Clinical Detection Scheme**

Biochemical sensor design requires careful consideration of the intended sample matrix. Blood and urine samples have been traditionally collected from patients for use in generic

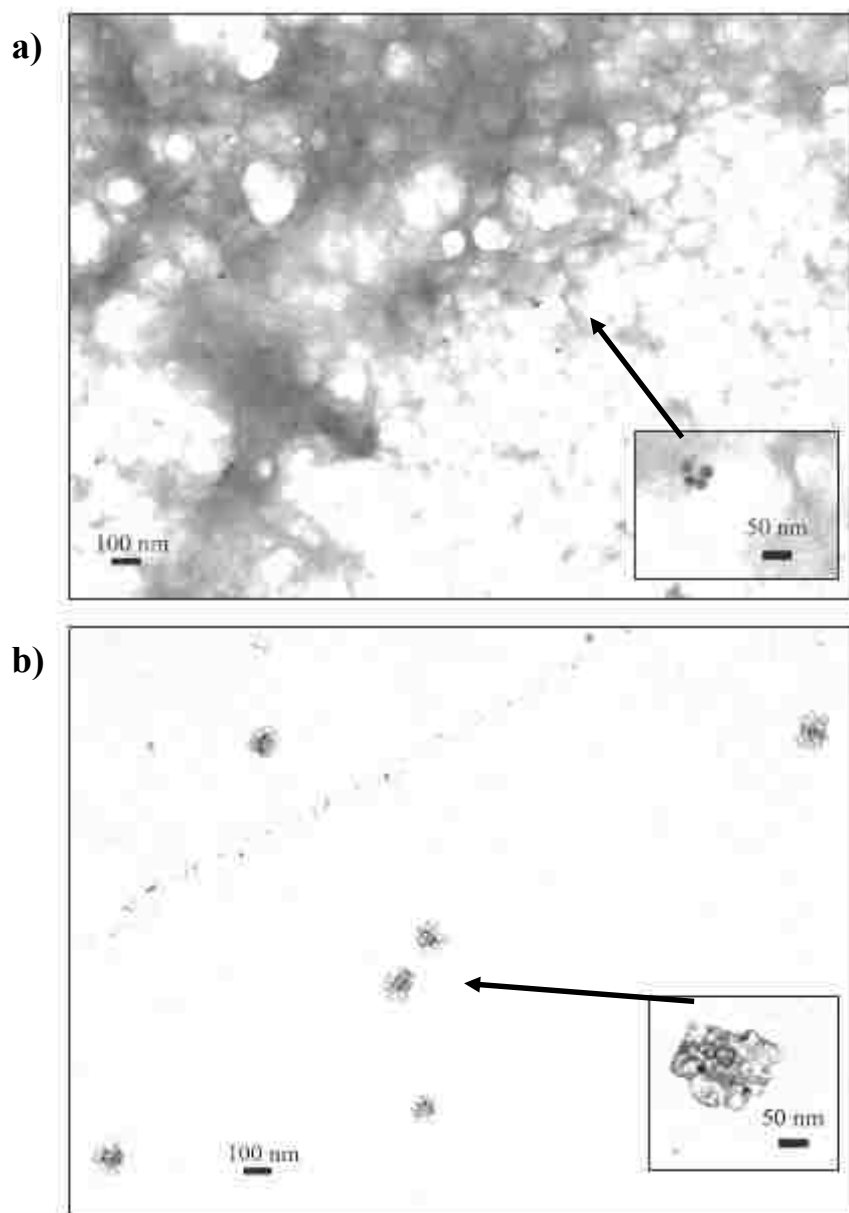


**Figure 4.3** Transmission electron micrograph images of the GNP sensor a) in the presence of HSA-homocystamide at 33,000  $\times$  magnification (inset shows 100,000  $\times$  magnification of a 4-nanoparticle cluster assembly within the oligomeric protein network), and b) in the presence of unmodified HSA (inset shows 100,000  $\times$  magnification of unassembled GNPs surrounded by unmodified HSA). The arrows indicate the location of the insets in lower magnification images.

clinical diagnostics. Urine analysis is a versatile medical screening procedure that has used historically for the *in vitro* detection of a number of physiologically relevant analytes including illicit drugs, steroids, and numerous other analytes. The detection of HTL in urinary excretions

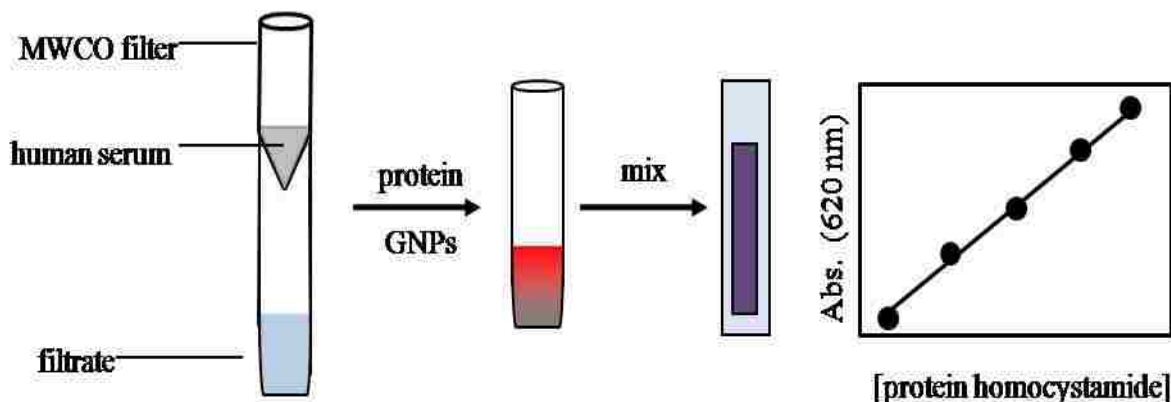


has been reported.<sup>30</sup> However, the existence of substantial amounts of *N*-Hcy-protein in urinary excretions is not expected because of the relatively low protein content of urine. In contrast, human serum is a more ideal sample medium for the protein sensor because it is relatively protein-rich and thus more likely to contain detectable levels of *N*-Hcy-protein. Another potential advantage of working with human serum is that it is already routinely screened for other cardiovascular disease risk factors such as cholesterol.

Unlike the purified HSA used in the previous studies, human serum is a complex medium that consists of an assortment of proteins and small molecules, including carbohydrates, drugs, hormones, etc, which may exist as free or protein-bound species. Human serum also contains various thiol-containing species that could interfere with the GNP sensor. For example, cysteine (Cys)<sup>29</sup>, glutathione<sup>29</sup>, and Hcy<sup>14</sup> are typically found at micromolar concentrations in human sera. Fortunately, these low molecular weight species can be easily removed from sera by use of a molecular cutoff filter device prior to treatment with the GNP sensor.

Frozen whole human sera collected and pooled from healthy adult donors were purchased from Sigma-Aldrich (St. Louis, MO) for use in this component of our study. The sera solutions were faintly yellow in color and slightly turbid due to sparingly soluble components. The protein content of the sera was determined by a gravimetric assay of lyophilized 1 mL aliquots after washing with deionized water. The average protein concentration of the aliquots was  $52.4 \pm 6.7$  mg/mL ( $n = 4$ ). Sera were typically diluted with phosphate buffer to obtain ~65 % (v/v) serum solution in order to decrease the viscosity and turbidity. The diluted serum was post-translationally modified with HTL *in vitro* as previously described. Scheme 4.2 depicts the proposed scheme for detecting serum *N*-Hcy-protein using the GNP sensor. First, the protein modification mixture is purified by use of centrifugal 10 kDa MWCO filters. Next, the modified *N*-Hcy-protein retained by the MWCO filter is promptly reconstituted with phosphate buffer in

order to obtain a stock solution. The resultant *N*-Hcy-protein is then immediately treated with the GNP sensor. Finally, the resultant GNP- *N*-Hcy-protein solution is diluted and transferred to a cuvette for monitoring of the colorimetric response.



**Scheme 4.2** Proposed method for the detection of *N*-Hcy-protein in human sera.

Representative absorption plots of the sensor under various experimental conditions are shown in Figure 4.4. Similar to the HSA model studies, unmodified sera were found to be reasonably stable and did not produce appreciable shifts in the plasmon resonance band over the sera concentration range investigated in this study (Figure 4.4a). Consistent with the HSA model studies, the sensor also produces extended plasmon resonance bands in the presence of serum *N*-Hcy-protein (Figure 4.4b). Figure 4.4c is a comparison plot of sensor signal versus serum protein concentration. It is apparent that the colorimetric signal detected at 620 nm increases in response to increasing concentrations of serum *N*-Hcy-protein, but remains relatively constant in the presence of equivalent concentrations of unmodified sera. Notably, the sensor response deviates from linearity at modified serum concentrations lower than ~5 mg/mL, giving a background signal of ~0.12 AU. This effect is partially attributed to the GNPs being sparingly soluble in the phosphate buffer at low protein concentrations, which produces increased sample

turbidity and light scattering. The colorimetric response in the range of 6.0 - 14 mg/mL modified serum protein provides excellent linearity ( $r^2 = 0.9994$ ) and a calibration sensitivity of  $13.6 \text{ AU} \cdot (\mu\text{g/mL})^{-1}$ . The calculated LOD of the serum method is 5.2 mg/mL.

Human plasma can contain from 0.1 – 13  $\mu\text{M}$  *N*-Hcy-protein, which is comparable to the mg/mL protein concentration range.<sup>31</sup> Accordingly, a solution containing 2.3 mg/mL sera homocystamide and 0.7 mM GNP was allowed to react as previously described. The resultant solution containing the HSA-homocystamide-GNP complex was serially diluted with ultra pure water in order to evaluate the dilutional stability of the *N*-Hcy-protein-GNP assembly at concentrations well below the physiologically relevant range. The resultant curve exhibited excellent linearity ( $r^2 = 0.9899$ ), which is expected for a tightly bound colorimetric complex (Figure B4 in the Appendix B). The sensor also provided an exceptional calibration sensitivity,  $0.30 \text{ AU} \cdot (\text{ng/mL})^{-1}$ . These data further support the hypothesis of modification-directed nanoparticle assembly via chemisorption and intermolecular disulfide bonding interactions.

Overall, the proposed GNP sensor exhibited exceptional performance for the detection of the *in vitro* modified serum protein species used in these studies. This is largely because freshly prepared *N*-Hcy-protein was promptly treated with the sensor, thereby minimizing the effects of auto-oxidation in the protein reaction mixture. However, essentially all of the *N*-Hcy-protein produced *in vivo* exist in an oxidized state and would thus be unavailable for binding with the sensor. Therefore, the issue of disulfide bound *N*-Hcy-protein species must be addressed prior to applying this method to screening clinical samples.

#### **4.4 Conclusions**

We have demonstrated a straightforward colorimetric method for the detection of serum *N*-Hcy-protein, an emergent cardiovascular disease biomarker. GNP assembly was observed

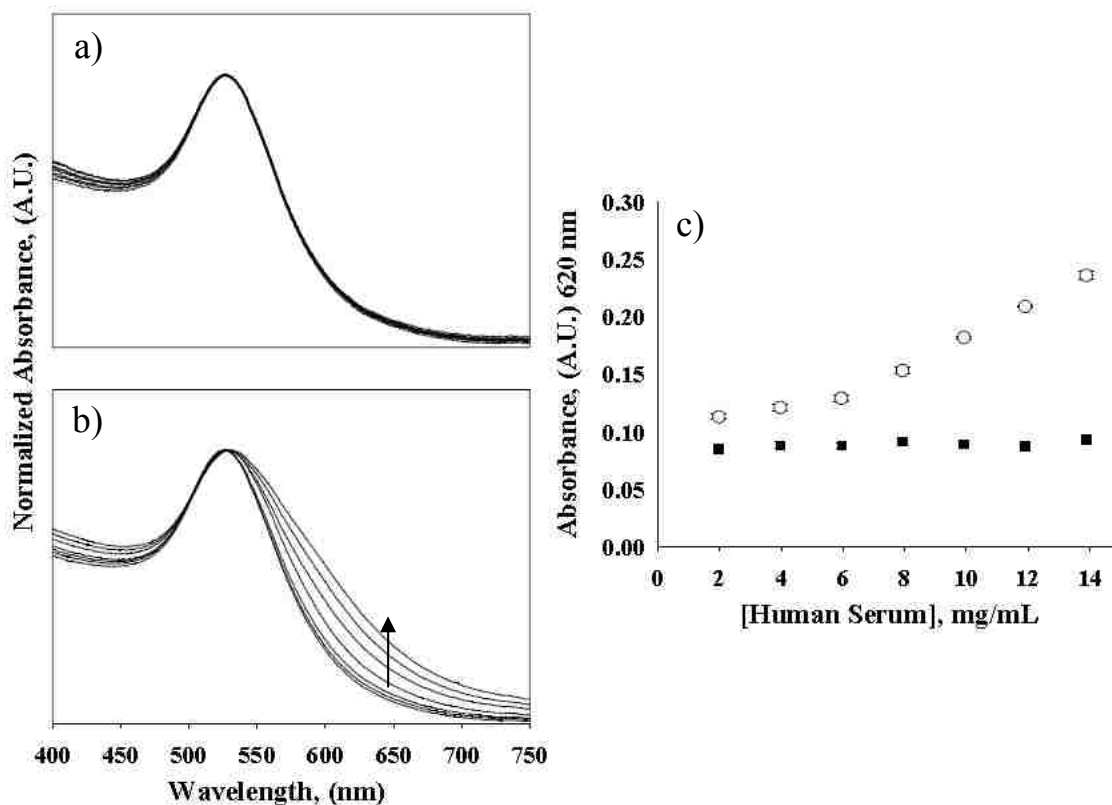


**Figure 4.4** Visible absorption spectra of the GNP sensor in response to human sera. a) in the presence of unmodified human sera and b) in the presence of human serum homocystamide. c) Sensor response at 620 nm in the presence of modified (○) and unmodified (■) sera versus human serum concentration, (2 – 14 mg/mL). The arrow indicates the change in signal at 620 nm with increasing concentrations of human serum homocystamide.

only in the presence of serum *N*-Hcy-protein. TEM images of the GNP sensor in the presence of unmodified and HTL-modified serum protein are consistent with the absorption data. The TEM images are also indicate modification-directed nanoparticle assembly as well as modification-induced protein oligomerization. The nanoparticle- *N*-Hcy-protein complex exhibited excellent stability and irreversible binding behavior under the condition used in this study. Studies are underway to adapt this model GNP biochemical sensor for use in clinical sera samples. Based on our studies to date, we believe that the approach reported here will lead to the development of a GNP sensing scheme that could aid in the rapid detection and diagnosis of cardiovascular disease.

## 4.5 References

- (1) Wang, W. H.; Rusin, O.; Xiangyang, X.; Kwang, K.; Escobedo, J. O.; Fakayode, S. O.; Fletcher, K. A.; Lowry, M.; Schowalter, C. M.; Lawrence, C. M.; Fronczeck, F.; Warner, I. M.; Strongin, R. M. *JACS* 2005, *127*, 15949-15958.
- (2) Rusin, O.; St Luce, N. N.; Agbaria, R. A.; Escobedo, J. O.; Jiang, S.; Warner, I. M.; Dawan, F. B.; Lian, K.; Strongin, R. M. *JACS* 2004, *126*, 438-439.
- (3) Escobedo, J. O.; Wang, W.; Strongin, R. M. *Nat. Protocols* 2006, *1*, 2759-2762.
- (4) Wang, W. H.; Escobedo, J. O.; Lawrence, C. M.; Strongin, R. M. *J. Am. Chem. Soc.* 2004, *126*, 3400-3401.
- (5) Pacsial-Ong, E. J.; McCarley, R. L.; Wang, W.; Strongin, R. M. *Anal. Chem.* 2006, *78*, 7577-7581.
- (6) Gates, A. T.; Lowry, M.; Fletcher, K. A.; Merugesu, A.; Rusin, O.; Robinson, J. W.; Strongin, R. M.; Warner, I. M. *In press Anal. Chem.* 2007.
- (7) Jakubowski, H.; Zhang, L.; Bardeguet, A.; Aviv, A. *Circ. Res.* 2000, *87*, 45-51.
- (8) Uji, Y.; Motmiya, Y.; Hanyu, N.; Ukaji, F.; Okabe, H. *Clin. Chem.* 2002, *48*, 941-944.
- (9) Ferguson, E.; Parthasarathy, S.; Joseph, J.; Kalyanaraman, B. *J. Lipid Res.* 1998, *39*, 925-933.
- (10) Yang, X.; Gao, Y.; Zhou, J. *Clin. Chim. Acta* 2006, *364*, 230-234.
- (11) Liu, J. W.; Lu, Y. *Anal. Chem.* 2004, *76*, 1627-1632.
- (12) Liu, J. W.; Lu, Y. *J. Fluoresc.* 2004, *14*, 343-354.
- (13) Schofield, C. L.; Field, R. A.; Russell, D. A. *Anal. Chem.* 2007, *79*, 1356-1361.
- (14) Lim, I. S.; Ip, W.; Crew, E.; Njoki, P. N.; Mott, D.; Zhong, C.; Pan, Y.; Zhou, S. *Langmuir* 2007, *23*, 826-833.
- (15) Zhang, F. X.; Han, L.; Israel, L. B.; Daras, J. G.; Maye, M. M.; Ly, N. K. *Analyst* 2002, *127*, 462-465.
- (16) Kimling, J.; Maier, M.; Okenve, B.; Kotaidis, V.; Ballot, H.; Plech, A. *J. Phys. Chem. B* 2006, *110*, 15700-15707.
- (17) Frens, G. *Nat. Phys. Sci.* 1973, *241*, 20-22.
- (18) Jakubowski, H. *FASEB J.* 1999, *13*, 2277-2283.

- (19) Shang, L.; Wang, Y.; Jiang, J.; Dong, S. *Langmuir* 2007, *23*, 2714-2721.
- (20) Brewer, S. H.; Glomm, W. R.; Johnson, M. C.; Knag, M. K.; S., F. *Langmuir* 2005, *21*, 9303-9307.
- (21) Liu, S.; Yang, Z.; Liu, Z.; Kong, L. *Anal. Biochem.* 2006, *353*, 108-116.
- (22) Walter, H.; Schobel, B. *Hum. Genet.* 1975, *30*.
- (23) Wilcoxon, J. P.; Martin, J. E. *Phys. Rev. A* 1989, *39*, 2675-2688.
- (24) Naka, K.; Itoh, H.; Chujo, Y. *Langmuir* 2003, *19*, 5496-5501.
- (25) Guo, Y.; Yudan, X.; Li, J.; Yang, W. *J. Phys. Chem. C* 2007, *111*, 9172-9176.
- (26) Li, M.; Mann, S. *J. Mater. Chem.* 2004, *14*, 2260-2263.
- (27) Mirkin, C. A.; Letsinger, R. L.; Mucic, R. C.; Storhoff, J. J. *Nature* 1996, *382*, 607-609.
- (28) Schwartzberg, A. M.; Grant, C. D.; Wilcott, A.; Talley, C. E.; Huser, T. R.; Bogomolni, R.; Zhang, J. Z. *J. Phys. Chem. B* 2004, *108*, 19191-19197.
- (29) Sudeep, P. K.; Joseph, S. T. S.; Thomas, K. G. *JACS* 2005, *127*, 6516-6517.
- (30) Chwatko, G.; Jakubowski, H. *Clin. Chem.* 2005, *51*, 408-415.
- (31) Jakubowski, H. *CMLS* 2004, *61*, 470-487.

## CHAPTER 5

### SPECTROCHEMICAL STUDIES OF *N*-HOMOCYSTEINYLATED GOLD NANOBIOCONJUGATES

#### 5.1 Introduction

The biomedical significance of homocysteine (Hcy) as a cardiovascular disease (CVD) biomarker has only recently emerged.<sup>1, 2</sup> The relationship between Hcy and CVD was further strengthened by clinical data that suggest lowering blood Hcy levels reduces risk of acute myocardial infarction.<sup>3</sup> The most commonly used techniques for Hcy analysis are HPLC, CE, and IA methods.<sup>4</sup> Functionalized chromophores and fluorophores have also been used to achieve more rapid and direct detection.<sup>5-8</sup> These conventional methods measure total blood Hcy (Hcyt), but are often incapable of discriminating the *N*-Hcy-protein fraction. *N*-Hcy-protein is the product of a unique type of post-translational protein modification that involves site specific acylation of proteins at  $\epsilon$ -NH<sub>2</sub> groups on lysine residues by homocysteine thiolactone (HTL), the highly reactive thioester metabolite of Hcy.<sup>9</sup> Like Hcy, elevated plasma levels of *N*-Hcy-protein correlate with increased risk of CVD.<sup>10</sup>

Plasmon resonant gold nanosensors provide a versatile platform for biomedical analyses.<sup>11</sup> GNPs have proven to be especially well-suited for the detection of aminothiols biomarkers such as Hcy, Cys, and glutathione.<sup>12-14</sup> The first plasmon resonance detection scheme for *N*-Hcy-protein was described in Chapter 4. It was found that GNPs undergo irreversible self-assembly in the presence of *N*-Hcy-protein to yield a rapid and direct colorimetric response. The resultant nanoparticle assemblies exhibited excellent thermal and dilutional stability. These interesting findings warranted further examination of the underlying physiochemical processes. Nanobioconjugates are commonly used to probe complex biomolecular and physiochemical

phenomenon such as protein binding<sup>15</sup> and protein conformational change.<sup>16, 17</sup> In this study, gold nanobioconjugates were subjected to *in situ* N-homocysteinylation and evaluated on the basis of plasmon resonance absorption, bioconjugate assembly growth, and susceptibility to thermally-induced protein conformational change.

## **5.2 Methods**

### **5.2.1 Materials**

L-homocysteine thiolactone hydrogen chloride, hydrogen tetrachloroaurate trihydrate, trisodium citrate, ethylenediamine tetra-acetic acid (EDTA), tris(2-carboxyethyl)phosphine (TCEP) hydrochloride and all other reagents used for the preparation of buffer and serum protein solutions were obtained from Sigma-Aldrich (St. Louis, MO) at the highest purity available and used as received. Ultra-pure water (18.2 MΩ) was obtained from an Elga model PURELAB Ultra water filtration system.

### **5.2.2 Synthesis of Nanobioconjugates**

Citrate-capped GNPs (ca.13 nm) were synthesized using the Turkevich-Frens method.<sup>18,</sup>  
<sup>19</sup> Hydrogen tetrachloroaurate trihydrate was dissolved in water and heated to reflux while stirring, followed immediately by the addition of a 40 M excess of trisodium citrate-water solution, which facilitates reduction of the gold salt. The reaction mixture was allowed to reflux for approximately 25 min until completion of the redox reaction and formation of GNPs, which was indicated by a change in solution color from pale yellow to dark-red. Excess citrate was not removed from solution in order to minimize nonspecific GNP aggregation during long term storage.<sup>19</sup> The concentration of the GNP solution was 1.0 mM, assuming complete reduction of the gold salt. The GNP solutions was purified using a 0.45 μm poly(tetrafluoroethene) syringe filter device and stored at room temperature in an amber glass bottle for no more than one month.



Nanoparticle size was confirmed with transmission electron microscopy (TEM). Protein-GNP bioconjugates (nanobioconjugates) were prepared by combining 4 mL of the GNP stock solution and 2 mL of 80 mg/mL cytochrome *c* (cyt *c*) or human serum albumin (HSA) dissolved in pH 7.4 phosphate buffer. The GNP-protein mixture was incubated at 37 °C for at least 12 h to allow for maximum protein adsorption and surface coverage. Unbound protein and excess buffer were removed from the nanobioconjugates using a Amicon Ultra 100 kDa molecular weight cut-off centrifugal (MWCO) filter devices (Millipore, Billerica, MA). The resultant solution was concentrated to 0.5 mL in the MWCO filter and subjected to 5 successive 1 mL washes with phosphate buffer. Lastly, the nanobioconjugates were reconstituted to the original volume with phosphate buffer and stored at 4 °C. Human serum nanobioconjugates were prepared as described above except 4 mL of the GNP stock solution was directly added to 2 mL of human serum (80 mg/mL protein) purchased from Sigma-Aldrich, St. Louis, MO.

### **5.2.3 *N*-homocysteinylation of Nanobioconjugates**

Post-translational *N*-homocysteinylation of nanobioconjugates was accomplished by incubation with HTL in 100 mM, sodium phosphate buffer containing 0.2 mM EDTA at room temperature for 3 h. Excess Hcy and unreacted HTL were removed from the modified nanobioconjugates by 4 successive 1 mL buffer washes in a 10 kDa MWCO filter. Purified nanobioconjugate solutions were reconstituted to the original volume with the desired buffer.

### **5.2.4 Instrumentation**

UV-Vis absorption spectra were acquired using a Shimadzu UV-3101PC UV-Vis-NIR equipped with thermoelectric temperature control. Dynamic light scattering (DLS) measurements were made with a Malvern Zetasizer Nano ZS dynamic light scattering spectrometer (Worcestershire, UK) equipped with thermoelectric temperature control.

Nanobioconjugates and reagents were purified using a 0.1  $\mu\text{m}$  syringe filter device prior to DLS analysis. The assembly behavior of nanobioconjugates ( $8.7 \times 10^{-2}$  mM) was monitored with DLS immediately after the additions of HTL ( $3.3 \times 10^{-3}$  mM). Each DLS data point is the composite of eleven consecutive 10 sec measurements. Circular dichroism (CD) spectroscopy measurements were made using an Aviv Model 62DS spectrometer equipped with a 1 mm path length quartz cell and temperature controlled cell holder. CD spectra were acquired in triplicate between 200 and 250 nm. CD response is reported as ellipticity and displayed in units of millidegree ( $\theta$ ). Protein standards and nanobioconjugate solutions were typically diluted to  $\sim 0.1$  mg/mL protein in pH 7.4, 10 mM phosphate buffer to obtain optimum CD signal. TEM imaging was performed using a JEOL model 100CX transmission electron microscope at 80 kV applied acceleration voltage. TEM specimens were prepared by depositing a thin layer of the nanobioconjugate solution onto carbon-coated copper grids followed by air-drying. SDS-PAGE separations were performed with a Mini-Protean 3 gel electrophoresis unit equipped with a 1000 V power supply (Bio-Rad Laboratories, Hercules, CA). Standard precast 4-20% Tris HCl polyacrylamide mini-gels were also purchased from Bio-Rad. When necessary, TCEP (50 mM) was added to the sample buffer prior to separation to achieve disulfide reduction. Gel separations were visualized by staining with coomassie blue for  $\sim 5$  h, followed by destaining with water for at least 5 h. Gel images were acquired using a Kodak Gel Logic 200 analyzer purchased from Eastman Kodak Co. (Rochester, NY).

## **5.3 Results and Discussion**

### **5.3.1 Characterization of Nanobioconjugates**

We have previously shown that GNPs behave as a concentration-dependent colorimetric sensor for *N*-homocysteinylnated serum protein.<sup>20</sup> The resulting colorimetric signal was found to

be long-lived and thermally stable. It is suspected that modification-directed GNP assembly and the subsequent colorimetric response are mediated by various protein and thiol binding interactions at the nanoparticle surface interface. Nanobioconjugates are an ideal molecular probe for biochemical processes. The protein component behaves as is an immobilized biomolecular ligand, while the GNP component serves as plasmon resonant biochemical indicator. The use of GNPs as biochemical and biomedical sensors has been reviewed the literature.<sup>11</sup> The principle for plasmon resonant GNP sensing is that dispersed nanocolloids having dimensions on the order of 10 nm typically exhibit intense localized surface plasmon resonance in the visible spectrum at ~520 nm, resulting in a red color solution. However, biochemically induced GNP self-assembly yields extended plasmon bands at ~620 nm, which causes a characteristic red-to-blue color change.<sup>21</sup>

Since human serum or plasma are usually the preferred biological media for clinical screening applications,<sup>10, 22</sup> albumin and human serum nanobioconjugates were studied initially. Representative visible absorption spectra of solutions containing nanobioconjugates prepared from HSA (HGNPs) and serum (SGNPs) are shown in Figure 5.1. Dispersed serum protein-GNP bioconjugates have an SPR absorption maximum centered at ~526 nm, which is slightly red-shifted from the absorption maximum of dispersed unconjugated GNPs (523 nm). This shift in SPR absorption maximum is generally indicative of successful bioconjugation.<sup>16, 23</sup> *N*-homocysteinylation of the nanobioconjugates was achieved by treatment with 2.5 mM HTL. Modification of the HGNP and SGNP nanobioconjugates resulted in the appearance of characteristic extended plasmon bands (EPBs) at  $\geq 620$  nm and a change in solution color from red to blue-violet. The spectral profiles of HGNPs and SGNPs are similar because albumin is the principal protein component in both systems. However, the relative change in colorimetric

signal detected at 620 nm for modified SGNPs was  $\sim 1.5$ -fold greater than what was observed for modified HGNPs. Based on these data, SGNPs appear to be more reactive toward *N*-homocysteinylation than HGNPs. One possible explanation is that serum contains additional protein constituents that are more reactive towards modification than albumin such as transferrin,  $\alpha_2$ -macroglobulin, and low density lipoprotein.<sup>24</sup>

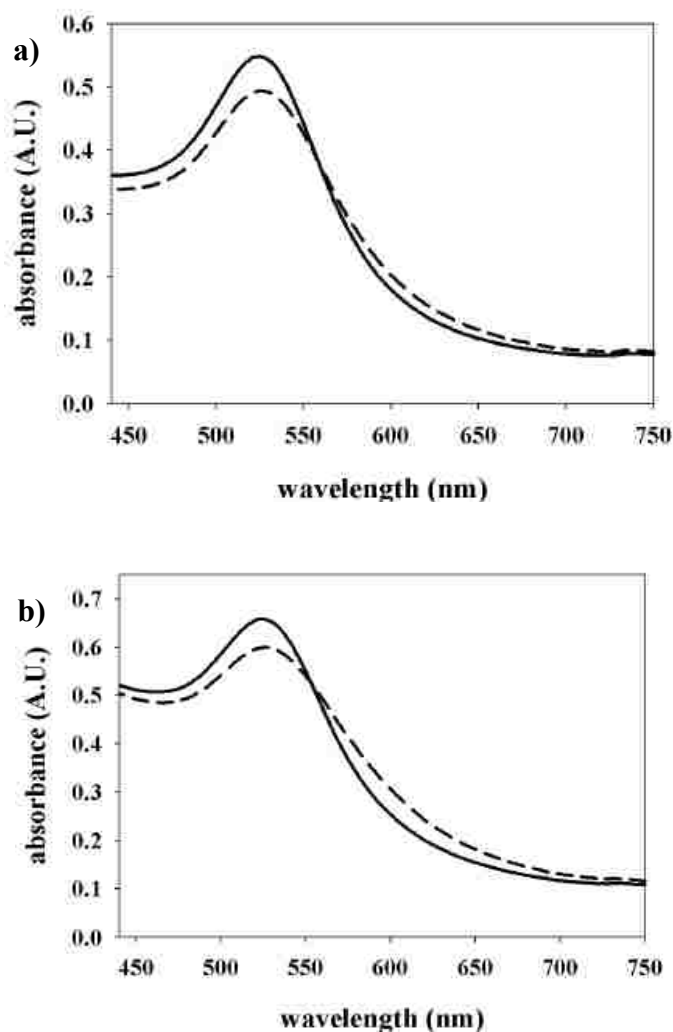


**Figure 5.1** Visible absorption spectra for unmodified (solid line) and 2.5 mM HTL-modified (dashed line), a) HGNP and b) SGNP nanobioconjugates.

Cyt *c*-GNP (CGNP) nanobioconjugates were also included in this study because cyt *c* provides an excellent model protein for studying *N*-homocysteinylation. For example, we

previously demonstrated that cyt *c* is highly susceptible to *N*-homocysteinylation and modification-induced protein oligomerization via disulfide cross-linking under physiological pH conditions.<sup>25</sup> This is because cyt *c* (12 kDa) is rich in lysine residues (~20% w/w),<sup>26</sup> the target site for post-translational protein modification by HTL.

The effect of *N*-homocysteinylation on CGNP nanobioconjugates is illustrated in Figure 5.2. Unmodified CNPs remained dispersed and appeared red ( $\lambda_{\text{max}} \sim 528 \text{ nm}$ ) in solution. In contrast, *N*-homocysteinylation caused a simultaneous decrease in SPR absorption at 528 nm and the emergence of broad extended plasmon bands appeared between 620-750 nm. Consequently, the color of the CGNP solution transitioned from red to dark blue-violet, thereby indicating the formation of relatively large nanobioconjugate assemblies. The dark blue-violet color typically persisted for ~1 h and gradually diminished due to precipitation of assembled nanobioconjugates. Complete precipitation occurred in 72 h, resulting in a near-colorless solution.

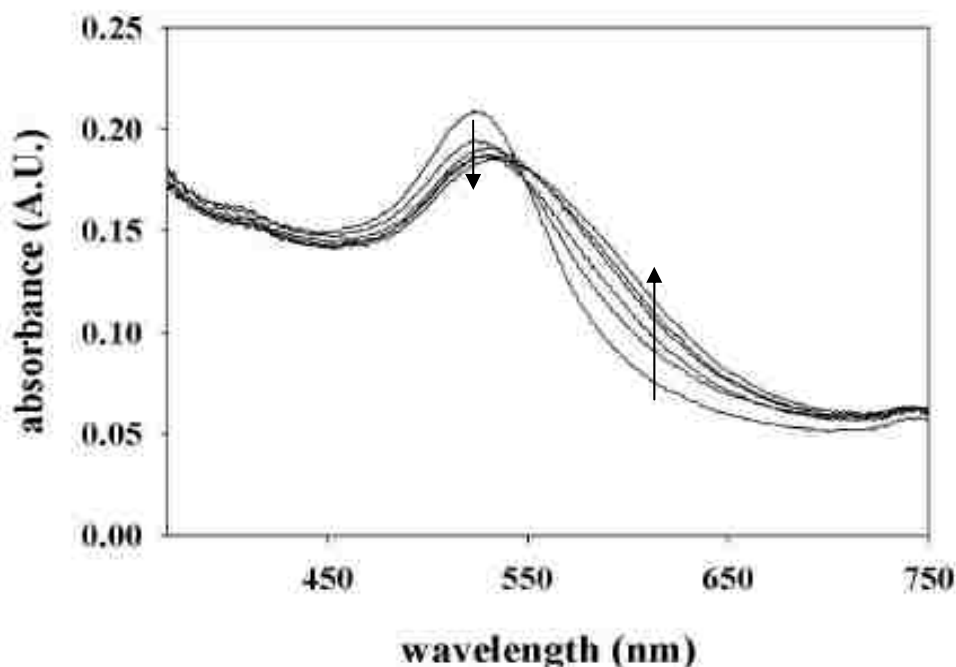


**Figure 5.2** Visible absorption spectra of CGNP bioconjugates (0.3 mM) modified with increasing concentrations of HTL (0-2.5 mM).

### 5.3.2 Monitoring Modification-Directed Nanobioconjugate Assembly

Since the colorimetric response produced by the *N*-homocysteinylation of nanobioconjugates is due to self-assembly, dynamic light scattering (DLS) spectroscopy was utilized to assess modification-directed GNP assembly. According to DLS measurements, the hydrodynamic diameter ( $D_h$ ) values for unmodified HGNP, SGNP, and CGNP nanobioconjugates were approximately 45, 91, and 22 nm, respectively, at 25 °C. As one would expect, the nanobioconjugates were significantly larger than unconjugated GNPs (~17 nm, measured by DLS) due to the adsorbed protein layer. The trend in  $D_h$  values for the protein-passivated GNPs was found to be generally consistent with the size of the proteins adsorbed on the surface of the GNPs.

Time-course DLS data acquired for HGNPs and SGNPs is shown in Figure 5.3. This study was conducted at 80 °C in order to allow the process to be satisfactorily monitored in a 30 min time period. The growth profiles for HGNP (Figure 5.3a) and SGNP (Figure 5.3b) bioconjugate assemblies were very similar. For instance, the profiles of both nanobioconjugate systems exhibit an initial sharp decrease in the  $D_h$  prior to the commencement of assembly growth. This feature is likely the result of temperature-induced desorption of loosely associated protein on the surface of the GNPs. Another explanation is that weak interparticle associations may be disrupted at 80 °C, thereby decreasing the mean  $D_h$  of bioconjugates. The size of these HGNP and SGNP bioconjugate assemblies grew to 70 and 135 nm, respectively.  $D_h$  values for unmodified HGNPs and SGNPs stabilized at ~33 and 72 nm, respectively. Conversely, CGNPs are much more responsive to modification by HTL. A 10-fold increase in nanobioconjugate assembly size was observed within the first 10 min of monitoring at 25 °C (Figure 5.3c). Nanobioconjugate assembly growth approached 300 nm and eventually produced insoluble

micron-sized superstructures, which began to precipitate from the blue-colored solution after ~1h. No appreciable nanoparticle assembly or change in solution color was detected in control solution containing unmodified CGNPs (Figure 5.3c). Corresponding time course visible absorption data are provided in Appendix C.

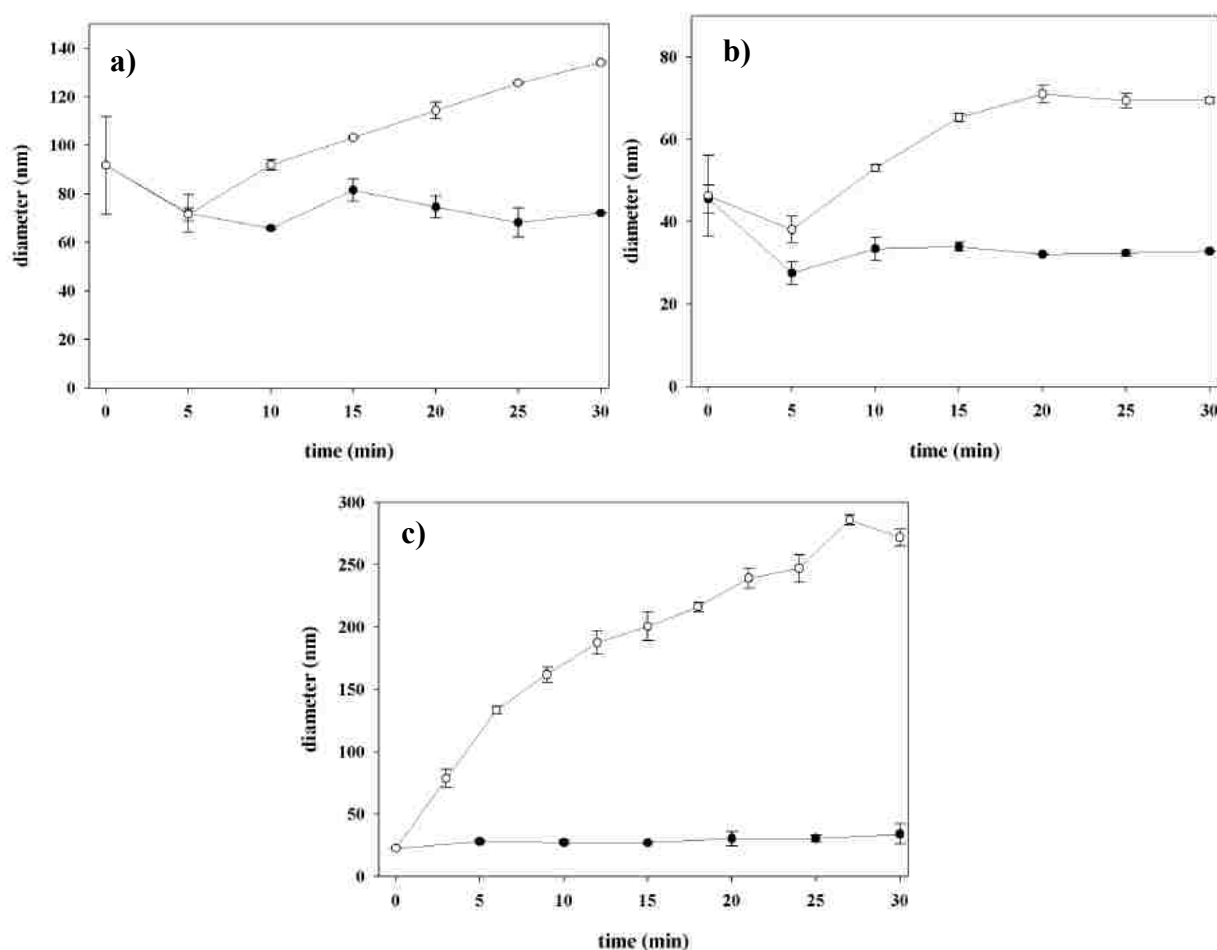


**Figure 5.3** Time course dynamic light scattering (DLS) plots illustrating nanostructure growth for unmodified (●) and *N*-homocysteinylylated (○) nanobioconjugates, a) HG NPs b) SG NPs, and c) CG NPs.

Visualization of nanostructures resulting from modification-directed bioconjugate assembly was achieved by use of TEM (Figure 5.4). Modification of HGNP (Figure 5.4a) and SGNP (Figure 5.4b) nanobioconjugates yielded relatively small structures that resemble the GNP clusters observed in previous studies.<sup>20</sup> Modified CGNPs stimulated prolific nanoparticle

assembly, which formed micron-sized superstructures (Figure 5.4c). Note that regions consisting of multiple layers of CGNPs appear darker in the TEM image. Unmodified nanobioconjugates remained well-dispersed (Figure C1 in Appendix C). Collectively, these data suggest that the degree of nanobioconjugate assembly is protein-dependent.

### 5.3.3 Assessing Modification-Induced Protein Conformational Change

The pathological effects of post-translational protein *N*-homocysteinylation are believed to have implications for vascular tissues and CVD. In particular, modification of protein by HTL is known to cause denaturation and loss of biological activity, which could induce vascular tissue damage and atherogenesis.<sup>27-30</sup> Jakubowski et al. recently used CD spectroscopy to study the effect of HTL-modification on cyt *c* protein structure.<sup>31</sup> Findings from this study indicate that modification did not significantly change the conformation of cyt *c*. To date, CD studies of *N*-homocysteinylation-induced conformational changes in nanobioconjugates have not been reported.

In this study, CD measurements were acquired for respective nanobioconjugate systems under identical protein and buffer concentration conditions in order to allow direct spectral comparison. The CD spectra shown in Figure 5.5 exhibit the typical ellipticity minima at ~208 and 222 nm, which are indicative of the  $\alpha$ -helical structural component of protein. In all cases, a small upward shift in CD spectral profile was observed post-modification, possibly indicating protein denaturation due to a loss of  $\alpha$ -helical structure.<sup>32</sup> Figures 5.5a and b illustrate the temperature-dependence of ellipticity resulting from unmodified and modified HG NPs, respectively. The difference in ellipticity for unmodified and modified HG NPs was significantly enhanced by heating the solutions for 10 min at 80 °C. Although SGNP bioconjugates exhibited less defined spectral minima (Figures 5.5c and d), the spectral behavior of SGNP



nanobioconjugate system before and after heating was essentially identical to the HGNP system. Modification of unmodified and modified CGNPs at 25 °C resulted in a much greater change in ellipticity but heating at 80 °C did not yield additional enhancements (Figures 5.5 e and f).

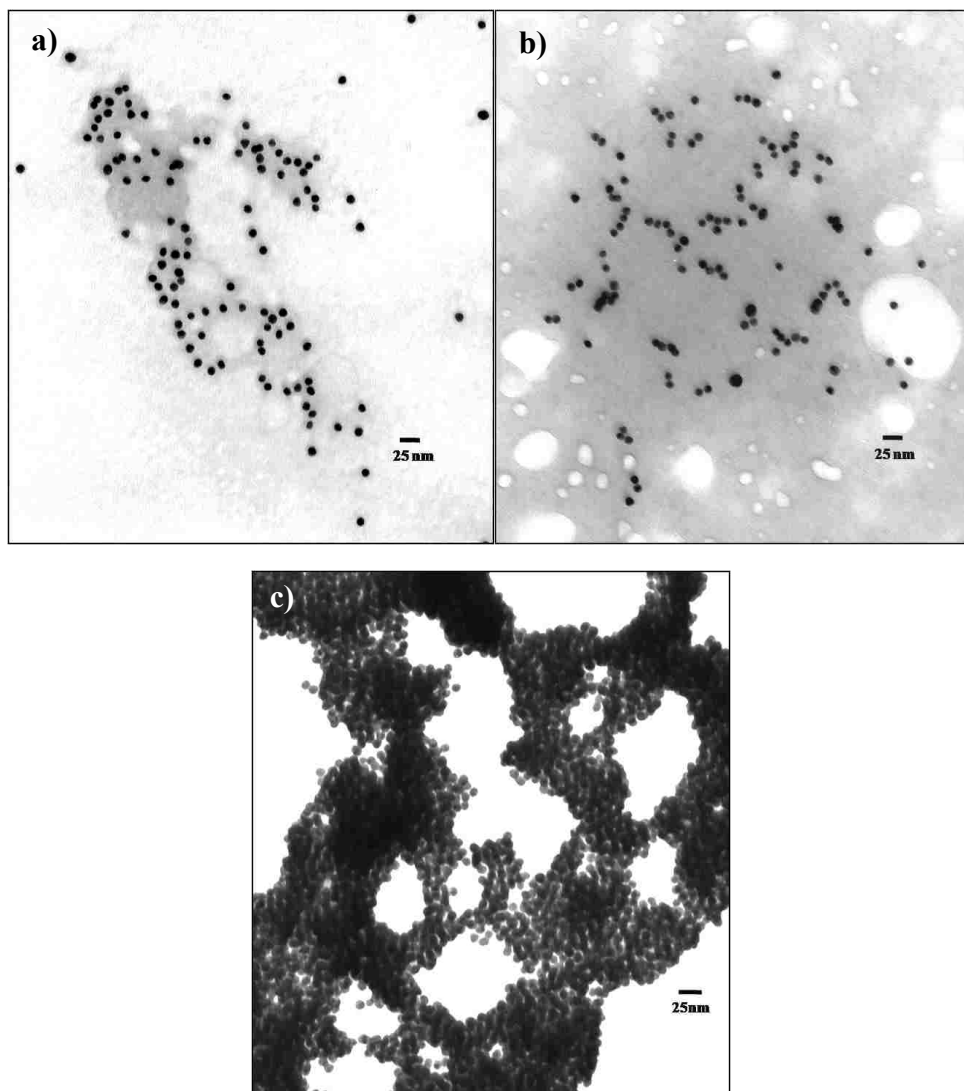


**Figure 5.4** TEM images of *N*-homocysteinylation a) HGNP, b) SGNP, and CGNP nanobioconjugates.

The observed thermal stability of CGNP bioconjugates is consistent with previously reported observations.<sup>33</sup> Based on these data, one might conclude that *N*-homocysteinylation of the bioconjugates does not induced gross protein denaturation at room temperature. However,

differences in ellipticity for modified HGNP and SGNP nanobioconjugates were more evident after heating, which may be indicative of protein denaturation and decreased colloidal stability in modified systems.

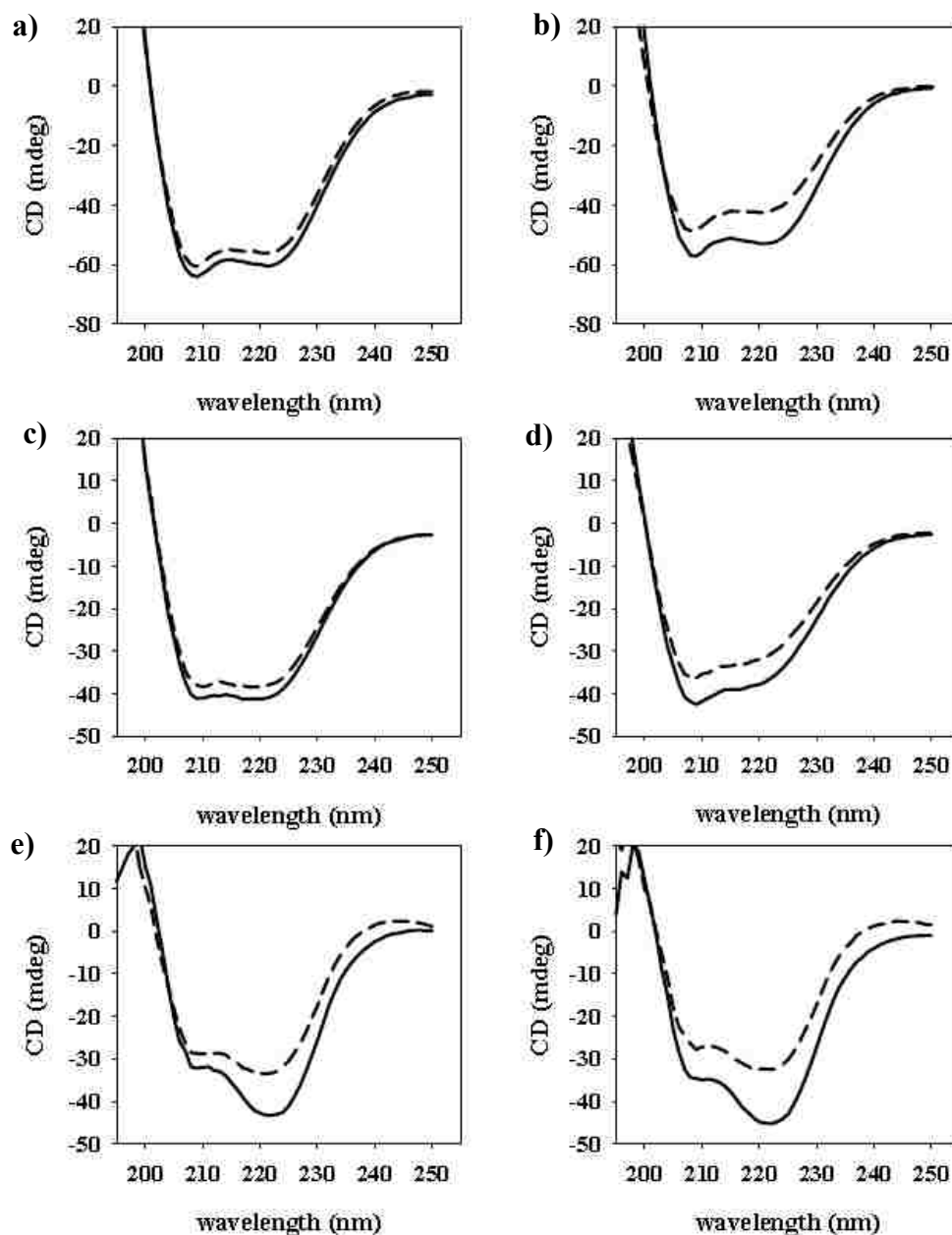


**Figure 5.5** CD spectra of unmodified (solid line) and modified (dashed line) nanobioconjugates a) HG NPs at 25 °C, b) HG NPs after 10 min incubation at 80 °C, c) SG NPs at 25 °C, d) SG NPs after 10 min incubation at 80 °C, e) CG NPs at 25 °C and f) CG NPs after 10 min incubation at 80°C.

### 5.3.4 Modification-Induced Changes in Redox Potential of Cyt *c* Nanobioconjugates

The use of cyt *c* as a spectrochemical redox indicator is well established in the literature.<sup>23, 33, 34</sup> Briefly, the heme moiety in cyt *c* can exist in an oxidized state ( $\text{Fe}^{3+}$ ), which is usually indicated by prominent Soret and Q-band peaks at ~408 and 530 nm, respectively. Reduction of the heme is indicated by a shift in the Soret band from 408 to ~416 and the appearance of new Q-bands at 520 and 550 nm.

CGNP nanobioconjugates were further studied with visible absorption spectroscopy in order to assess modification-induced changes in the redox potential. Initial attempts to observe the visible absorption of cyt *c* in the purified CGNP solutions were unsuccessful due to spectral overlap with SPR band of GNPs. For this reason, nanobioconjugate solutions were prepared in pH 7.4 phosphate buffer and spiked with additional cyt *c* 0.1 mg/mL in order to allow observation of spectral redox features. Representative absorption spectra from this study are shown in Figure 5.6. The unmodified mixture yielded peaks at 410 and 533 nm corresponding to the cyt *c* Soret and SPR absorption bands, respectively (dotted line). *N*-homocystenylation of the mixture resulted in the appearance of Q-bands at ~520 and 550 nm as well as extended SPR bands at  $\geq 620$  nm (solid line). This result indicates simultaneous reduction of cyt *c* and modification-directed nanobioconjugate assembly. Cyt *c* reduction was also further signified by a characteristic shift in the Soret band. The gradual disappearance of the extended SPR bands after 24 hr is indicative of precipitation of large-sized nanobiocojugate assemblies (dashed line). The remaining absorption peaks are due to reduced unconjugated cyt *c*. Given that the redox potential for denatured cyt *c* is less than that of the native protein,<sup>35</sup> the observed redox behavior is also consistent with modification-induced protein denaturation. Therefore, we infer that denaturation allows the heme group of cyt *c* to be exposed to solvent, where it undergoes redox.

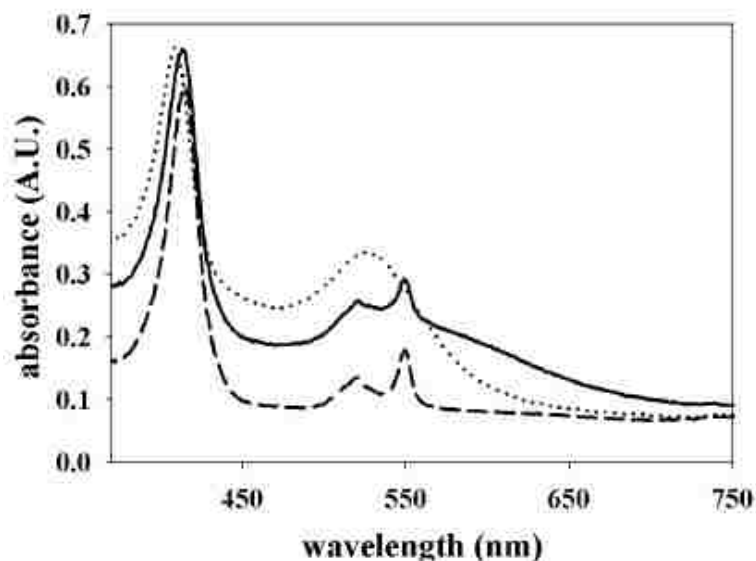


**Figure 5.6** UV-vis spectra of CGNP nanobioconjugate solution spiked with 0.1 mg/mL cyt *c* unmodified before (dotted line), immediately after *N*-homocysteinylation with 2.5 mM HTL (solid line), and 24 hr after modification (dashed line).

### 5.3.5 Effects of Disulfide Reduction on Nanobioconjugate Association

Interparticle association among *N*-homocysteinyllated nanobioconjugates is presumed to be the result of disulfide cross-linking. This hypothesis was tested by treating modification-derived nanobioconjugate assemblies with tris [2-carboxyethyl] phosphine (TCEP), a non-thiol containing disulfide reducing agent known to be thiol-probe compatible.<sup>36</sup> In this study, gel electrophoresis was used to evaluate nanobioconjugate associated based on the principle of size exclusion. SDS-PAGE separations of assembled nanobioconjugates performed on 4 - 20 % gradient polyacrylamide gels are shown in Figure 5.7. The rectangles in the image approximate the location of the stacking region of the gel, which contains pores large enough to accommodate assembled nanobioconjugates. The remainder of the gel, the resolving region, contains progressively smaller pores that are not large enough to accommodate assembled nanobioconjugates. Assembled HGNPs resulting modification with 10 and 20 mM HTL are

mostly retained in the stacking region of lanes a and b, respectively. Notably, more material is retained in the stacking region of lane b than lane a; because the degree of nanobioconjugate assembly is proportional to HTL concentration. Corresponding HGNP experiments conducted under reducing conditions, 50 mM TCEP, resulted in dissociation of assembled nanobioconjugates as was indicated by a significant decrease in the amount of material in the stacking region of lanes c and d. Consequently, more material permeated into the smaller pores of the resolving region of the gel. This outcome was mirrored in experiments performed with SGNP nanobioconjugates (lanes e-h). Neither unmodified nor modified CGNPs migrated into the gel matrix under normal or reversed polarity condition, presumably due to lack of sufficient binding between SDS and the CGNP nanobioconjugates. Nevertheless, these findings suggest that modification-derived nanobioconjugate assemblies are covalently stabilized by interparticle disulfide cross-linking.

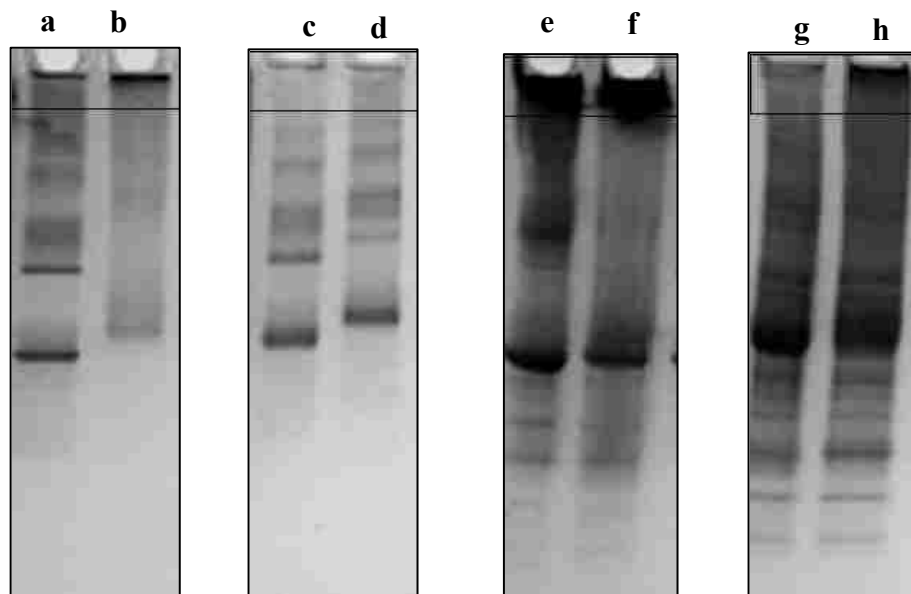


**Figure 5.7** SDS-PAGE separations of serum nanobioconjugate assemblies resulting from modification with 10 and 20 mM HTL) before (lanes a and b, respectively) and after treatment with TCEP (lanes c and d, respectively). Identical separations performed with SGNP bioconjugate assemblies are shown in lanes e-h. The stacking regions of the gels are indicated by rectangles.

## 5.4 Conclusions

In summary, we have reported a spectroscopic investigation of the physiochemical mechanisms of *N*-homocysteinylation-directed GNP assembly. Nanobioconjugates prepared from HSA, serum, and cyt *c* were examined in this study. UV-vis spectroscopy studies suggest that the red-to-blue color change observed post-modification is the result of nanobioconjugate assembly, which is indicated by the appearance of extended SPR bands at  $\geq 620$  nm. It was also found that modification of HG NPs and SG NPs yielded moderate colorimetric responses. Conversely, CG NPs were much more responsive to modification and produced extended SPR bands with greater intensity and more dramatic color changes. Time course DLS studies were conducted to characterize unmodified GNP bioconjugates and to monitor modification-directed bioconjugate assembly. Modified HG NPs and SG NPs exhibited similar assembly behavior, which resulted in moderate assembly growth, over a 30 min period at 80 °C. In contrast, modified CG NPs yielded a 10-fold increase in assembly size after 30 min at 25 °C. CD and visible spectroscopy data for nanobioconjugates indicate protein conformational change, which could signify modification-induced protein denaturation. In general, *N*-homocysteinylation nanobioconjugates were found to be less resistant to heat-induced protein conformational change. In addition, modification-induced nanobioconjugate association was shown to be the result of interparticle disulfide cross-linking.

## 5.5 Reference

- (1) Seshadri, S.; Beiser, A.; Selhub, J.; Jacques, P. F.; Rosenberg, I. H.; D'Agostino, R. B.; Wilson, P. W. F.; Wolf, P. A. *N. Engl. J. Med.* 2002, *346*, 476-483.
- (2) Clarke, R.; Daly, L.; Robinson, K.; Naughten, E.; Cahalane, S.; Fowler, B.; Graham, I. *N. Engl. J. Med.* 1991, *324*, 1149-1155.
- (3) Bonna, K. H.; Njolstad, I.; Ueland, P. M.; Schirmer, H.; Tverdal, A.; Steigen, T.; Wang, H.; Nordrehaug, J. E.; Arnesen, E.; Rasmussen, K. *N. Engl. J. Med.* 2006, *354*, 1578-1588.

- (4) Ducros, V.; Demuth, K.; Sauvant, M. P.; Quillard, M.; Causse, E.; Candito, M.; Read, M. H.; Drai, J.; Garcia, I.; Gerhardt, M. F. *J. Chromatogr. B* 2002, *781*, 207-226.
- (5) Wang, W. H.; Rusin, O.; Xiangyang, X.; Kwang, K.; Escobedo, J. O.; Fakayode, S. O.; Fletcher, K. A.; Lowry, M.; Schowalter, C. M.; Lawrence, C. M.; Fronczeck, F.; Warner, I. M.; Strongin, R. M. *JACS* 2005, *127*, 15949-15958.
- (6) Rusin, O.; St Luce, N. N.; Agbaria, R. A.; Escobedo, J. O.; Jiang, S.; Warner, I. M.; Dawan, F. B.; Lian, K.; Strongin, R. M. *JACS* 2004, *126*, 438-439.
- (7) Escobedo, J. O.; Wang, W.; Strongin, R. M. *Nat. Protocols* 2006, *1*, 2759-2762.
- (8) Wang, W. H.; Escobedo, J. O.; Lawrence, C. M.; Strongin, R. M. *J. Am. Chem. Soc.* 2004, *126*, 3400-3401.
- (9) Jakubowski, H. *J. Nutr.* 2000, *130*, 377S-381S.
- (10) Yang, X.; Gao, Y.; Zhou, J. *Clin. Chim. Acta* 2006, *364*, 230-234.
- (11) Liao, H. W.; Nehl, C. L.; Hafner, J. H. *Nanomedicine* 2006, *1*, 201-208.
- (12) Shimada, T.; OoKubo, K.; Komuro, N.; Shimizu, T.; Uehara, N. *Langmuir* 2007, *23*, 11225-11232.
- (13) Lim, I. I. S.; Ip, W.; Crew, E.; Njoki, P. N.; Mott, D.; Zhong, C. J.; Pan, Y.; Zhou, S. Q. *Langmuir* 2007, *23*, 826-833.
- (14) Zhang, F. X.; Han, L.; Israel, L. B.; Daras, J. G.; Maye, M. M.; Ly, N. K. *Analyst* 2002, *127*, 462-465.
- (15) Brewer, S. H.; Glomm, W. R.; Johnson, M. C.; Knag, M. K.; Franzen, S. *Langmuir* 2005, *21*, 9303-9307.
- (16) Chah, S.; Hammond, M. R.; Zare, R. N. *Chem. Biol.* 2005, *12*, 323-328.
- (17) Yokoyama, K.; Welchons, D. R. *Nanotechnology* 2007, *18*.
- (18) Kimling, J.; Maier, M.; Okenve, B.; Kotaidis, V.; Ballot, H.; Plech, A. *J. Phys. Chem. B* 2006, *110*, 15700-15707.
- (19) Frens, G. *Nat. Phys. Sci.* 1973, *241*, 20-22.
- (20) Gates, A. T.; Fakayode, S. O.; Lowry, M.; Ganea, G. M.; Murugesu, A.; Robinson, J. W.; Strongin, R. M.; Warner, I. M. *Langmuir* 2008, *24*, 4107-4113.
- (21) Grant, C. D.; Schwartzberg, A. M.; Norman, T. J.; Zhang, J. Z. *JACS* 2002, *125*, 549-553.

- (22) Uji, Y.; Motomiya, Y.; Hanyu, N.; Ukaji, F.; Okabe, H. *Clin. Chem.* 2002, *48*, 941-944.
- (23) Keating, C. D.; Kovaleski, K. M.; Natan, M. J. *J. Phys. Chem. B* 1998, *102*, 9404.
- (24) Jakubowski, H. *Faseb J.* 1999, *13*, 2277-2283.
- (25) Gates, A. T.; Lowry, M.; Fletcher, K. A.; Merugesu, A.; Rusin, O.; Robinson, J. W.; Strongin, R. M.; Warner, I. M. *Anal. Chem.* 2007, *79*, 8249-8256.
- (26) Nakashim, T.; Higa, H.; Matsubar, H.; Benson, A. M.; Yasunobu, K. T. *J. Bio. Chem.* 1966, *241*, 1166-&.
- (27) Jakubowski, H.; Zhang, L.; Bardeguet, A.; Aviv, A. *Circ. Res.* 2000, *87*, 45-51.
- (28) Jakubowski, H. *Biomed. Pharmacother.* 2001, *55*, 443-447.
- (29) Jakubowski, H.; Ambrosius, W. T.; Pratt, J. H. *FEBS Lett.* 2001, *491*, 35-39.
- (30) Jakubowski, H. *Clin. Chem. Lab. Med.* 2007, *45*, 1704-1716.
- (31) Perla-Kajan, J.; Marczak, L.; Kajan, K.; Pawel, S.; Twardowski, T.; Jakubowski, H. *Biochemistry* 2007, *46*, 6225-6231.
- (32) Shang, L.; Wang, Y.; Jiang, J.; Dong, S. *Langmuir* 2007, *23*, 2714-2721.
- (33) Jiang, X.; Shang, L.; Wang, Y.; Dong, S. *Biomacromolecules* 2005, *6*, 3030-3036.
- (34) Aubin-Tam, M.-E.; Hamad-Schifferli, K. *Langmuir* 2005, *21*, 12080-12084.
- (35) Bixler, J.; Bakker, G.; McLendon, G. *J. Am. Chem. Soc.* 1992, *114*, 6938-6939.
- (36) Mukai, Y.; Togawa, T.; Suzuki, T.; Ohata, K.; Tanabe, S. *J. Chromatogr. B* 2002, *767*, 263-268.



## CHAPTER 6

### IMMUNOAFFINITY EXTRACTION OF POLYCYCLIC AROMATIC HYDROCARBONS FROM ATHEROSCLEROTIC HEART TISSUES

#### 6.1 Introduction

Although there is currently no formal link between CVD and PAHs, exposure to tobacco smoke is both a CVD and a potential source for PAH exposure risk factor.<sup>1</sup> In fact, tobacco smoking releases over 4000 toxic chemical substances into the environment, including PAHs.<sup>2</sup> Table 6.1 lists some of the PAH compounds found in cigarette smoke. Since PAHs are ubiquitous in the environment, it is highly likely that some degree of bioaccumulation occurs in cardiovascular tissues. Various anthropogenic chemicals have been detected in heart plaque, but PAHs were not specifically identified.<sup>3</sup> Although PAHs are routinely analyzed with gas chromatography-mass spectrometry (GC-MS), atherosclerotic plaques and tissue presents a challenge due to the lack of selective extraction techniques for solid samples. For this reason, updated methodologies are needed to address this problem. We have proposed the use of a novel immunoaffinity-based method.

**Table 6.1 PAHs present in cigarette smoke.<sup>2</sup>**

<b>Anthracene</b>	<b>Chrysene</b>	<b>Indole</b>
<b>Benz[a]anthracene</b>	<b>Dibenz[a,h]anthracene</b>	<b>Methylamineethylchrysene</b>
<b>Benzo[a]pyrene</b>	<b>Dibenzo[a,l]pyrene</b>	<b>Naphthalene</b>
<b>Benzo[b]fluoranthene</b>	<b>Fluoranthene</b>	<b>Phenanthrene</b>

Organic liquid-solid (OLS) extraction is commonly used in the analysis of lipid-containing materials such as atherosclerotic plaques and tissues. While OLS extraction is capable of removing PAHs from solid fatty samples, it is poorly selective. In this work, OLS extraction and immunoaffinity extraction (IAE) are used in tandem to selectively isolate PAHs

from human atherosclerotic tissue samples harvested from the cadavers of two elderly male subjects. The tissue extracts were subsequently analyzed by use of GC-MS.

## **6.2 Methods**

### **6.2.1 Materials**

Atherosclerotic plaque samples were provided by Dr. R. E. Tracy of the Louisiana State University Medical School, New Orleans, LA. Neat anthracene, fluorene, naphthalene, phenanthrene, and pyrene were obtained at > 99% purity from AccuStandard, Inc. (New Haven, CT). UltraLink fritted 5 mL low-performance chromatography columns and azlatone-functionalized polyacrylamine beads, were obtained from Pierce Biotechnology, Inc. (Rockford, IL). Maxi-clean C<sub>18</sub> solid phase extraction cartridges with 600 mg bed volume were obtained from Alltech Associates Inc. Monoclonal anti-PAH antibodies (clone 2Z11) raised against phenanthrene were obtained from Strategic Biosolutions, Inc. (Newark, DE). Buffer salts and all other reagents used in this work were purchased from Sigma-Aldrich Chemical Co. (St. Louis, MO) in the highest available purity.

### **6.2.2 Preparation of Atherosclerotic Tissue Samples**

Human tissue samples were handled according to standard laboratory biohazard protocol. Protective eyewear, gloves, and a lab coat were worn at all times. Sample preparation steps involving biohazard materials were performed inside a disposable biohazard glove box purged with nitrogen. Atherosclerotic plaque-tissue samples were removed from aortas immediately upon arrival and stored in a cryogenic freezer at -77°C. Plaque samples were thawed to room temperature then carefully weighed prior to being homogenized in hexane. The organic solvent and sample mixtures were subsequently sonicated at 50°C for 4 hr. The organic layer was removed from each sample and stored in an amber glass vial. The aqueous layer was discarded after sterilization with a 10% sodium hypochlorite solution for 1 hr. Organic extracts with

significant adipose content were placed in an ice bath to precipitate the lipids, and carefully decanted from the lipid precipitate. The lipid precipitate was discarded after sterilization. Extracts were then concentrated to near dryness using a gentle stream of activated carbon filtered nitrogen. The samples were then reconstituted with 5 mL of HPLC grade 2-propanol. All glassware and laboratory utensils used in sample preparation were thoroughly disinfected with a 10% sodium hypochlorite solution then heat sterilized at 100 °C overnight. All solid and liquid waste derived from plaque or tissue samples were discarded in biohazard waste containers.

### **6.2.3 Immunoaffinity Extraction Protocol**

Phosphate buffered saline (PBS) was prepared by dissolving the appropriate amounts of sodium phosphate and sodium chloride in ultra-pure water (18 MΩ) followed by pH adjustment to 7.4 using either strong acid or base. Citrate-carbonate coupling buffer for the antibody immobilization reaction was prepared by dissolving the appropriate amounts of sodium carbonate and trisodium citrate in doubly deionized water to obtain 0.1 M sodium carbonate and 0.6 M sodium citrate at pH 9.0. Wash solutions for IAE column rinses were prepared by dissolving sodium chloride in water to obtain a 1.0 M solution. The IAE column elution buffer was prepared by dissolving sodium phosphate (monobasic and dibasic) in water followed by pH adjustment to 7.4.

### **6.2.4 Column Fabrication**

IAE columns used in this study were fabricated by covalently immobilizing anti-PAH antibodies to the chromatographic support according to manufacturer protocol. Briefly, monoclonal antibodies were dissolved in pH 9.0 citrate-carbonate coupling buffer then added to azlactone-activated polyacrylamide beads so that the antibody solution is 2-fold greater than the swell volume for the dry beads. The slurry mixture was allowed to react at room temperature for 1hr while mixing. Antibody immobilization occurred via nucleophilic attack at the azlactone

groups by the amino-terminus of the antibody, resulting in a covalent linkage. The immobilization reaction mixture was quenched for 3 hr with 3M ethanolamine. The resulting slurry was used to pack a low-performance “gravity-flow” chromatography column. The column was then filled with 20:80 (v/v) ethanol:phosphate buffer and stored at 4°C.

### **6.2.5 Extract Preparation**

Prior to IAE, organic extracts were diluted with pH 7.4 PBS to obtain a solution with no more than 5% organic solvent. The extract solutions were loaded onto the IAE column at 2 mL/min to allow for antibody binding. Next, weakly bound sample components were rinsed away with 10 column volumes of the wash solution. The target analyte was then removed from the column by rinsing with 5 column volumes of the elution buffer (pH 2.5 phosphate). The eluent was immediately reconcentrated and solvent exchanged with dichloromethane using C<sub>18</sub> solid phase extraction. The solvent exchange step is necessary because phosphate buffer is not compatible with GC-MS.

### **6.2.6 Instrumentation**

A Hewlett Packard 5971A gas chromatography-mass spectrometer (GC-MS) equipped with a DB-5 reversed phase column and electron impact ionization (EI) were used for the analysis of PAH extracts from atherosclerotic plaque samples. The temperature gradient was ramped at 10°C/min, from 40°C to a holding temperature of 280°C, for a total run time of 40 min. Mass spectra were collected in total ion chromatogram (TIC) mode. Peak identifications were further verified by visual comparison of EI fragment patterns with those in the Wiley7N.L database. Since humans possess the ability to degrade PAHs via cytochrome P-450 (naphthalene-1,2-dioxygenase) pathways,<sup>4, 5</sup> an effort was made to identify both parent compounds and PAH metabolites.

## 6.3 Results and Discussion

### 6.3.1 Gas Chromatography-Mass Spectrometry Analysis of Polycyclic Aromatic Hydrocarbons Standards

Figure 6.1 shows a representative GC-MS total ion chromatogram (TIC) for a PAH standard mixture containing fluorene, phenanthrene, anthracene, and pyrene. The peak identification software was unable to distinguish the structural isomers phenanthrene and anthracene, which have nearly identical EI fragmentation patterns. Thus, it was necessary to consider the relative chromatographic retention times in order to obtain positive identification. The total elapsed time for GC-MS analysis was less than 16 min.

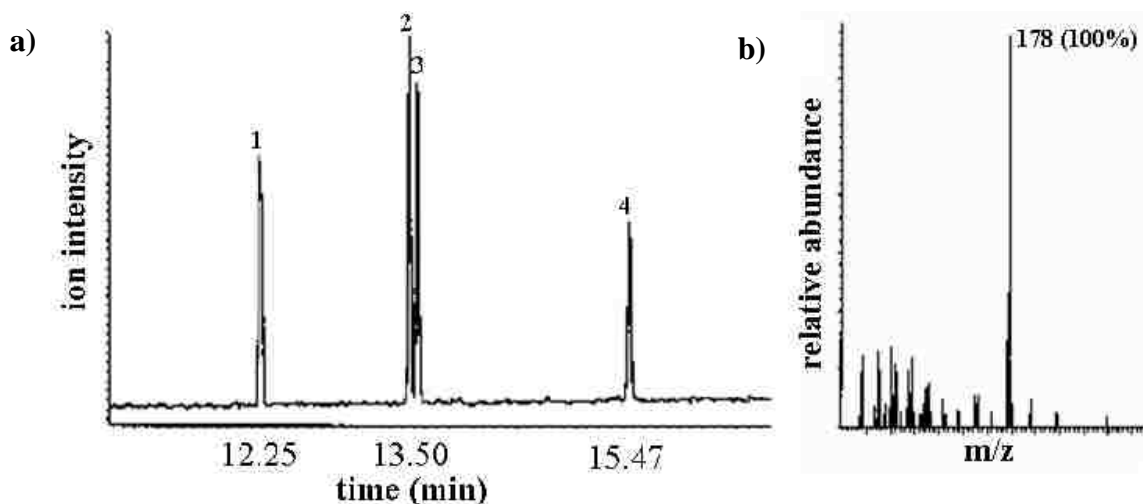


**Figure 6.1** Mass spectra (TICs) of a) mixture containing 10 ppm PAH standards: 1) fluorene, 2) phenanthrene, 3) anthracene, and 4) pyrene. b) mass spectra for phenanthrene and anthracene with molecular ion 178 at 100% abundance.

### 6.3.2 Analysis of Atherosclerotic Tissues Extracts

The atherosclerotic tissue samples used in this study were harvested from two elderly male subjects: 1) a 69 year old African American male, and 2) a 70 year old Caucasian male. No additional information about the subjects was provided. Two specimens (A and B) were provided for each sample. The sample masses recorded for 1A, 1B, 2A, and 2B were 12.14 g, 3.84 g, 5.73 g, and 2.41 g, respectively. The mass of sample 1A was larger than the other samples,

presumably due to high water content. It was noted that all samples contained a combination of fatty plaque, endothelial tissue, and aqueous material. Respective sample specimens were combined homogenized and extracted using the OLS-IAE method.

Internal standards were not used in these preliminary studies. Background GC-MS spectra were collected for column blanks and all organic solvents to confirm that baseline signal was minimal. Figure 6.2 shows typical total ion chromatographs (TICs) for atherosclerotic tissues extracted with hexane only versus the OLS-IAE and method, respectively.

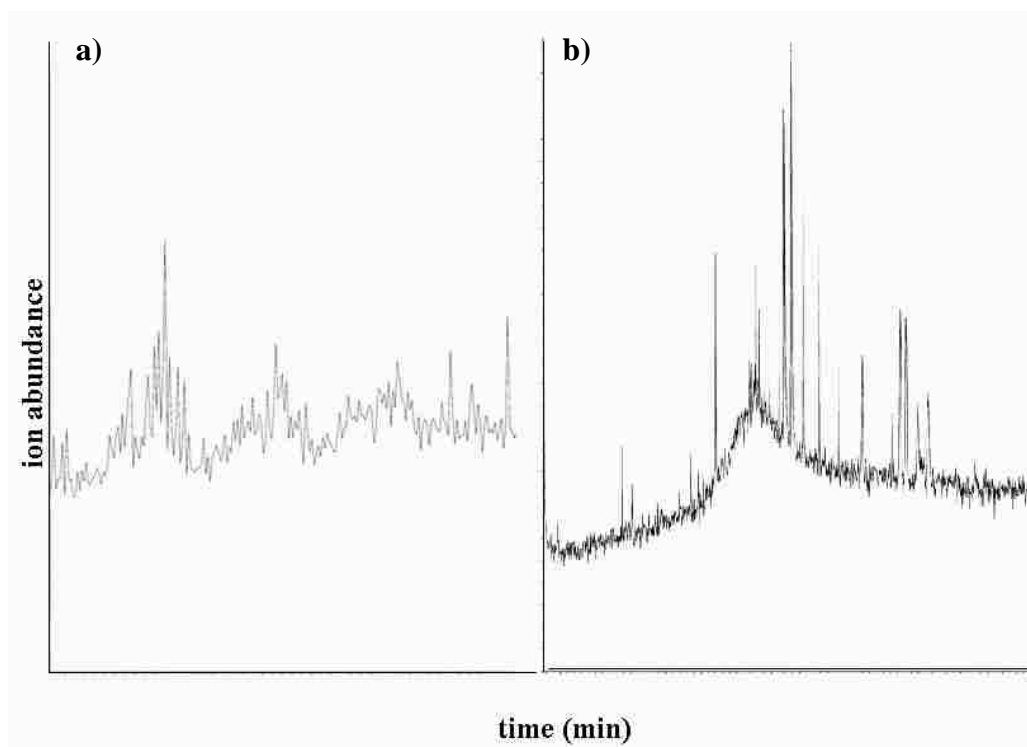


**Figure 6.2** Representative GC-MS TICs for atherosclerotic plaques extracted using: a) organic extract only and b) the OLS-IAE method.

Table 6.1 provides the structures and retention times for the compounds detected in sample 1 within a 5.83 min elution window. Interestingly, 2,4-Di-tert-butylphenol (11.38 min) and [1S-(1a,3ab,4a,8ab)]-decahydro-4,8,8'-trimethyl-9-methylene-1,4-methanoazulene (12.12 min) are structural isomers, both having molecular masses of 206. Chromatographic separation was not achieved for the next pair of structural isomers, naphthalene-1,6-dimethyl-4-(1-

methylethyl) and 1,4-dimethyl-7-isopropyl azulene (MW = 198), which coeluted at 12.83 min. However, confirmation was obtained by visual comparison of EI fragmentation patterns. The next compound eluted was 2,4-di (1-phenylethyl) phenol, which has a molecular mass of 302. The last compound eluted was 1,2-dihydro-3,5-dimethylbenz[J]aceanthrylene (MW = 284) at 17.21 min. In addition to the PAH metabolites, several long-chain alkane hydrocarbons ranging from C<sub>16</sub> to C<sub>35</sub> were also detected in Sample 1.

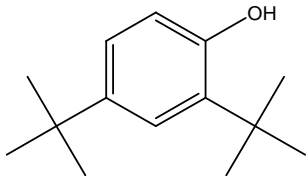
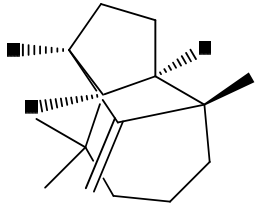
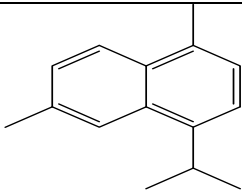
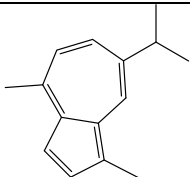
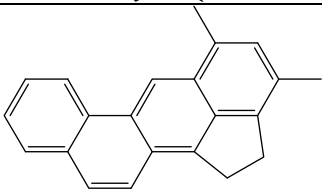
Only three compounds were detected in sample 2 within a 10.55 min elution window (Table 6.2). The first compound eluted was 4-Tert-butyl-1,2-benzenedithiol (198 Da) at 12.84 min. The second compound eluted was 1-Phenanthrene carboxylic acid at 16.72 min followed by benz[a]anthracenone at 16.80. 1-phenanthrene carboxylic acid and benz [a] anthracenone are singularly substations, making their structures very close to parent PAH compounds. Various long-chain alkanes were also detected in sample 2.

## 6.4 Conclusions

Studies were conducted with atherosclerotic tissue specimens from two elderly subjects to evaluate the feasibility of the proposed hybrid OLS-IAE method for the analysis of PAHs in atherosclerotic plaque and tissue samples. GC-MS analyses of OLS-IAE extracts indicate that PAH metabolites were present in both atherosclerotic plaque samples. A total of eight different compounds were identified. As expected, the reversed phase elution orders for the compounds in both samples were inversely proportional to the number of benzene rings contained in the compounds. However, sample 1 contained the structural isomers naphthalene-1,6-dimethyl-4-(1-methylethyl) and 1,4-dimethyl-7-isopropylazulene, which were not chromatographically resolved. The presence of the phenol derivative 2,4-di-tert-butylphenol may be indicative of *in vivo* cytochrome P-450 enzymatic metabolism. Likewise, sample 2 contained two singularly substituted metabolites, 1-phenanthrene carboxylic acid and benz[a]anthracenone, which may

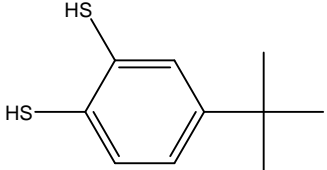
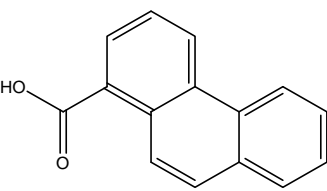
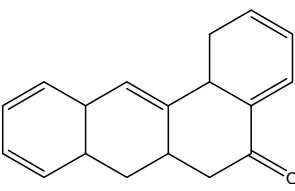
also be an indication of early stage cytochrome P-450 metabolism. Interestingly, sample 2 also contained 4-tert-butyl-1,2-benzenedithiol, a non-PAH compound. The presence of the long-chain hydrocarbons in both samples may be the result of thermal degradation of the reversed phase GC column. Alternatively, this signal could also be due to degradation of fatty acids and cholesterol esters in the atherosclerotic plaque.

**Table 6.2** Structures of PAH metabolites detected in sample 1 (69 year old African American male), molecular masses (MW) and retention times.

Compound Detected (molecular mass)	Structure	Retention Time (min)
2,4-di-tert-butylphenol (206)		11.38
[1-S-(1a,3ab,4a,8ab)]- decahydro-4,8,8'- trimethyl-9-methylene- 1,4-methanoazulene (206)		12.12
naphthalene, 1,6- dimethyl-4-(1- methylethyl) (198)		12.83
1,4-dimethyl-7- isopropylazulene (198)		12.83
1,2-dihydro-3,5- dimethylbenz[J] aceanthrylene (284)		17.21



**Table 6.3** Structures of PAH metabolites detected in sample 2 (70 year old Caucasian male), molecular masses (MW) and retention times.

Compound Detected (molecular mass)	Structure	Retention Time (min)
4-tert-butyl-1,2-benzenedithiol (198)		12.84
1-phenanthrene carboxylic acid (222)		16.72
benz[a]anthracenone (302)		16.80

These preliminary results suggest that proposed OLS-IAE method is viable. Future studies may address the inclusion of suitable internal standards for validation studies. The use of tandem MS (MS-MS) could further improve the method by allowing for greater certainty in PAH compound identification. The resultant method could be useful for studying the relationship between PAH bioaccumulation and CVD, which could shed light on the relationship between tobacco smoking and atherosclerosis.

## 6.5 References

- (1) Neufeld, E. J., Mietus-Snyder, M., Beiser, A.S., Barker, A.L. and New burger, J.W. *Circulation* 1997, 96, 1403-1407.
- (2) Centers for Disease Control and Prevention (CDC) and National Center for Chronic Disease Prevention and Health Promotion.
- (3) Ferrario, J. B.; Deleon, I. R.; Tracy, R. E. *Arch. Environ. Contamin. Tox.* 1985, 14, 529-534.

- (4) Jacob, J. *Pure & Appl. Chem.* 1996, 68, 301-308.
- (5) Enroth, C., Neujahr, H., Schneider, and G. Lindqvist, Y. *Structure* 1998, 6, 605-617.

## CHAPTER 7

### SUMMARY OF RESEARCH AND FUTURE STUDIES

This dissertation is a chronicle of recent work in our laboratory to develop novel bioanalytical methods for the analysis of Hcy and related CVD indicators. Throughout this work, emphasis was placed on gaining a better understanding of the physiochemical mechanisms critical to bioanalytical method development. In addition, updated nanotechnology-based research initiatives were implemented to address the lack of effective analytical methods for *N*-Hcy-protein. This chapter provides a summary of research and recommendations for future research.

The first chapter of this dissertation contains a review of the relevant literature and an introduction of the objectives and scope of research. Chapter 2 is a report of fundamental spectrochemical studies pertaining to *in vitro* PT formation. Pyridoxal-5-phosphate was exhibited chemical reactivity toward Hcy under physiological pH conditions. Benesi-Hildebrand analysis of the fluorescence data suggested 1:2 [pyridoxal:Hcy] binding stoichiometry. One Hcy molecule is covalently bound to the aldehyde group of pyridoxal. The other Hcy molecule is weakly associated with the pyridoxal phosphate group via ionic interactions. The preliminary findings support the feasibility of the PT-Hcy sequestration-clearance hypothesis. In Chapter 3, we discuss using electrophoretic separation as a means of examining the effect of pyridoxal on *in vitro* protein *N*-homocysteinylation. CE separations were performed with cationic polymer-coated capillaries, which allowed highly efficient separations without significant non-specific protein binding. The short-end injection format was utilized to obtain more rapid separations and shorter analysis times, usually less than 2 min. The optimized method was subsequently used to further investigate the validity of PT-Hcy sequestration-clearance hypothesis. It was shown that PT formation competes with the *N*-homocysteinylation protein reaction, thereby

inhibiting *in vitro* post-translational modification. This finding provides additional empirical support for pyridoxal-mediated Hcy clearance.

Plasmon resonant GNP sensing of *N*-Hcy-protein was introduced in Chapter 4. GNPs were proven to be a viable alternative to conventional bioanalytical methods such as HPLC and ELISA for selective detection. Direct colorimetric sensing of *in vitro*-synthesized *N*-Hcy-serum protein was accomplished via modification-directed nanoparticle assembly, which caused a shift in GNP plasmon resonance. The resultant GNP assemblies appeared to exhibit irreversible association characteristics even at elevated temperatures. In fact, the colorimetric response was enhanced by heating the sensor-protein solutions at 80 °C. Further investigations of the physiochemical mechanisms involved in GNP sensing of *N*-Hcy-protein were discussed in Chapter 5. GNP-protein bioconjugates prepared from albumin, cyt *c*, and serum, respectively, were subjected to *in vitro* *N*-homocysteinylation and monitored with various spectroscopic methods in order to assess nanoparticle assembly size and modification-induced protein conformational changes. Nanobioconjugate self-assembly was found to be dependent on protein susceptibility toward *N*-homocysteinylation. Consequently, cyt *c* nanobioconjugates yielded the highest degree of self-assembly and the largest shift in plasmon resonance. CD experiments revealed that modification-induced changes in protein conformation were most detectable after heating at 80 °C, thereby indicating the possibility of protein denaturation. Assembled nanobioconjugates were also subjected to SDS-PAGE separation under reducing conditions in order to probe the mechanism of association. Gel separations indicated that interparticle association is the result of disulfide cross-linking among *N*-homocysteinyllated nanobioconjugates.

In Chapter 6, the poor of quality of GC-MS analysis of PAHs in atherosclerotic plaques was addressed. The proposed solution was a hybrid organic solvent-immunoaffinity technique

that provided selective PAH extraction. First, liquid-solid extraction was performed on the plaque samples. Aqueous solvent exchange was subsequently performed on the organic extract to give a phosphate buffered sample. The resultant solution was further extracted with an IAE column. Unlike normal organic extraction, the hybrid method allowed for detection of several PAH metabolites in two different atherosclerotic plaque samples. These preliminary results demonstrated the potential utility of the hybrid extraction method for GC-MS plaque characterizations.

Perhaps the most promising aspect of this dissertation is the demonstrated use of plasmon resonant GNP sensors for detection of *N*-Hcy-protein screening. The ultimate goal of this project is to development a reliable clinical screening method. Realization of this goal will likely involve three phases; 1) further optimization of the current method, 2) incorporation of an immunoaffinity component, and 3) clinical evaluations. Efforts to optimize the current sensing method are ongoing. Experimental parameters such as and GNP size, protein concentration, and buffering conditions have been identified for further study. The next logical step is to immobilize an immunoaffinity ligand to the GNPs in order to attain enhanced selectivity. Both antibodies and aptamers should be considered. Antibodies for *N*-Hcy-protein are not commercially available; however, it may be possible to obtain them from other researchers or custom antibody producers. Alternatively, aptamers could be employed as the immunoaffinity component. Aptamers are oligonucleotide sequences that can be engineered with specificity to *N*-Hcy-protein. Departmental resources and expertise are currently available to assist in the development of aptamers. An effort should also be made to demonstrate the use of the sensor in a 96-well format, which would dramatically increase sample throughput. GNP plasmon resonance absorption and fluorescent labeled immunoaffinity ligands are potential detection options. Having already established a working relationship with the Pennington Biomedical

Research Center, the optimized high throughput immunoaffinity sensing scheme could be tested and validated with a large number of clinical serum samples. The finalized method could help establish the usefulness of *N*-Hcy-protein as a CVD biomarker.

## APPENDIX A: CHARACTERIZATIONS OF PROTEIN AND PYRIDOXAL REACTIONS

### Table of Content

**Figure A.1:** MALDI-TOF mass spectrum for the protein reaction mixture.

**Figure A.2:** Black and white photograph of SDS-PAGE separation of protein reaction mixtures treated with pyridoxal-5-phosphate.

**Figure A.3:** UV-Vis Spectrophotometric study of in situ pyridoxal tetrahydrothiazine formation in protein reaction mixtures treated with pyridoxal-5-phosphate.

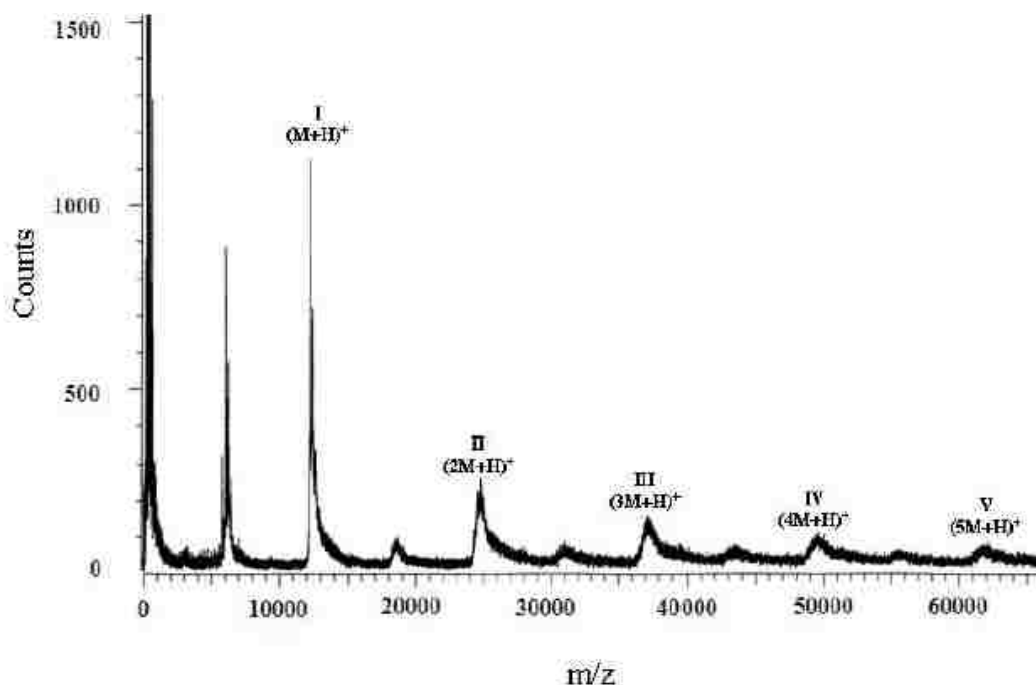


**Figure A.1** MALDI-TOF mass spectrum for the protein reaction mixture (10 mg/mL bovine cyt *c* + 2.5 mM homocysteine thiolactone) acquired after 24 hrs. The molecular ion ( $M+H$ )<sup>+</sup> for monomeric bovine cyt *c* was detected at approximately 12.3 kDa, which is consistent with the literature. The roman numerals indicate molecular ion species corresponding to monomeric (I), dimeric (II), trimeric (III), tetrameric (IV), and pentameric (V) bovine cyt *c*. The peak preceding the monomer molecular ion is due to the doubly protonated monomeric species. The minor peaks preceding the aggregate molecular ion peaks are due to various trace higher order aggregate species.

Mass spectrometry experiments were performed using a Bruker ProFLEX III™ matrix assisted laser desorption ionization time of flight- mass spectrometer (MALDI TOF-MS) in linear mode with a sinapinic acid (SA) matrix. The matrix was prepared by dissolving SA in a 2:3 acetonitrile/0.1% TFA mixture to obtain a 10 mg/mL SA solution. Protein reaction mixture samples and SA were mixed to obtain a 1:1 protein/matrix solution.

The resultant solution was deposited drop-wise onto a MALDI target and allowed to dry and crystallize. Mass spectra were acquired using 100 shots with a 0 ns delay. Relevant instrumental parameters: linear mode, 100 shots, 0 ns delay, and sinapinic acid matrix.

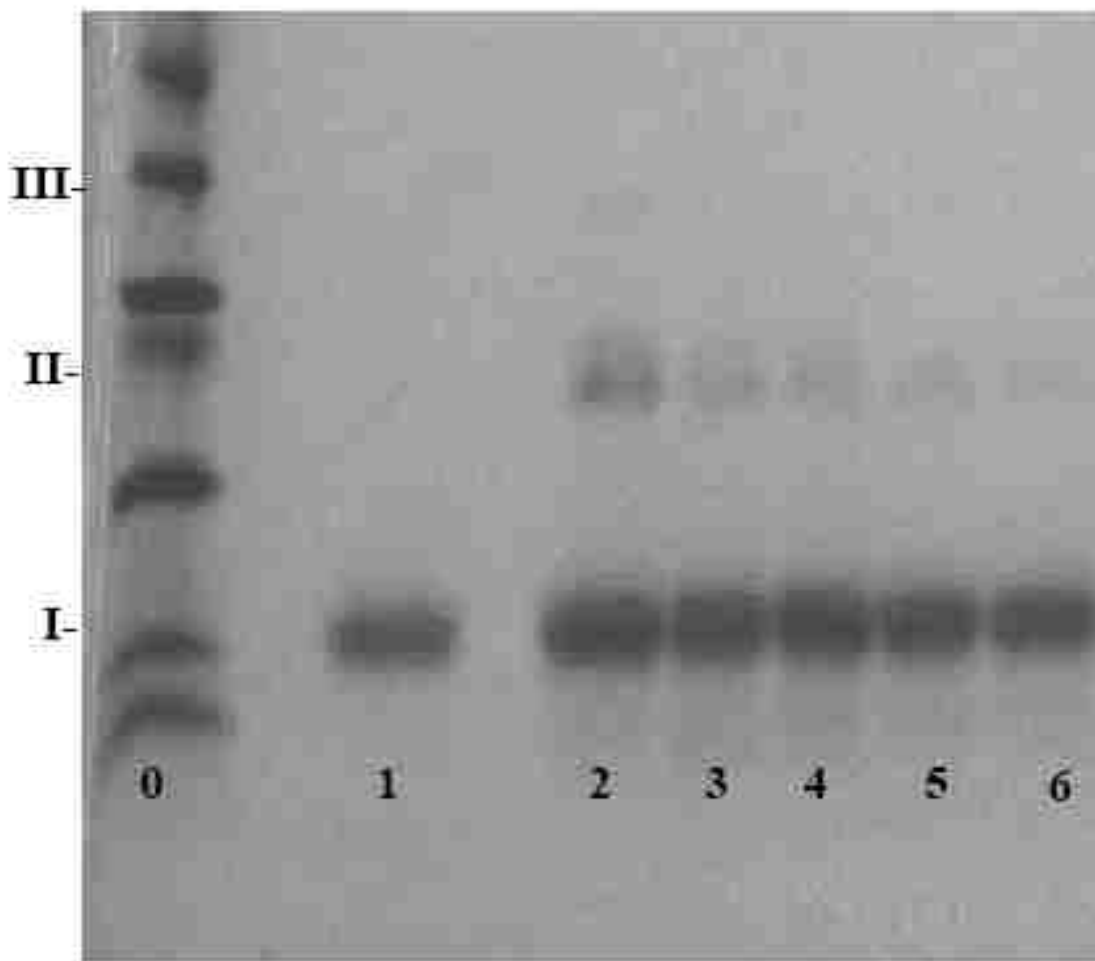


**Figure A.2** Bovine cyt *c* and hcy thiolactone (10 mg/mL and 2.5 mM, respectively) were reacted with pyridoxal-5-phosphate (PLP) for 24 h at room temperature. The resultant samples were denatured by heating at 95°C for 5 min in the presence of SDS and separated using SDS-PAGE on 4–20% gels at approximately pH 9. A representative gel is shown above. Unmodified cyt *c* migrated as a single band (lane 1). Lanes 2–6 show 1:0, 1:0.25, 1:0.5, 1:0.75, and 1:1 hcy thiolactone:PLP, respectively. Cyt *c* monomers, dimers, and trimers are denoted as I, II, and II, respectively as determined by comparison with protein mass standards (lane 0). Note the decrease in aggregate band intensities as the concentration of PLP increases, eventually resulting in the disappearance of the trimeric species as well as an appreciable reduction in the dimeric species.



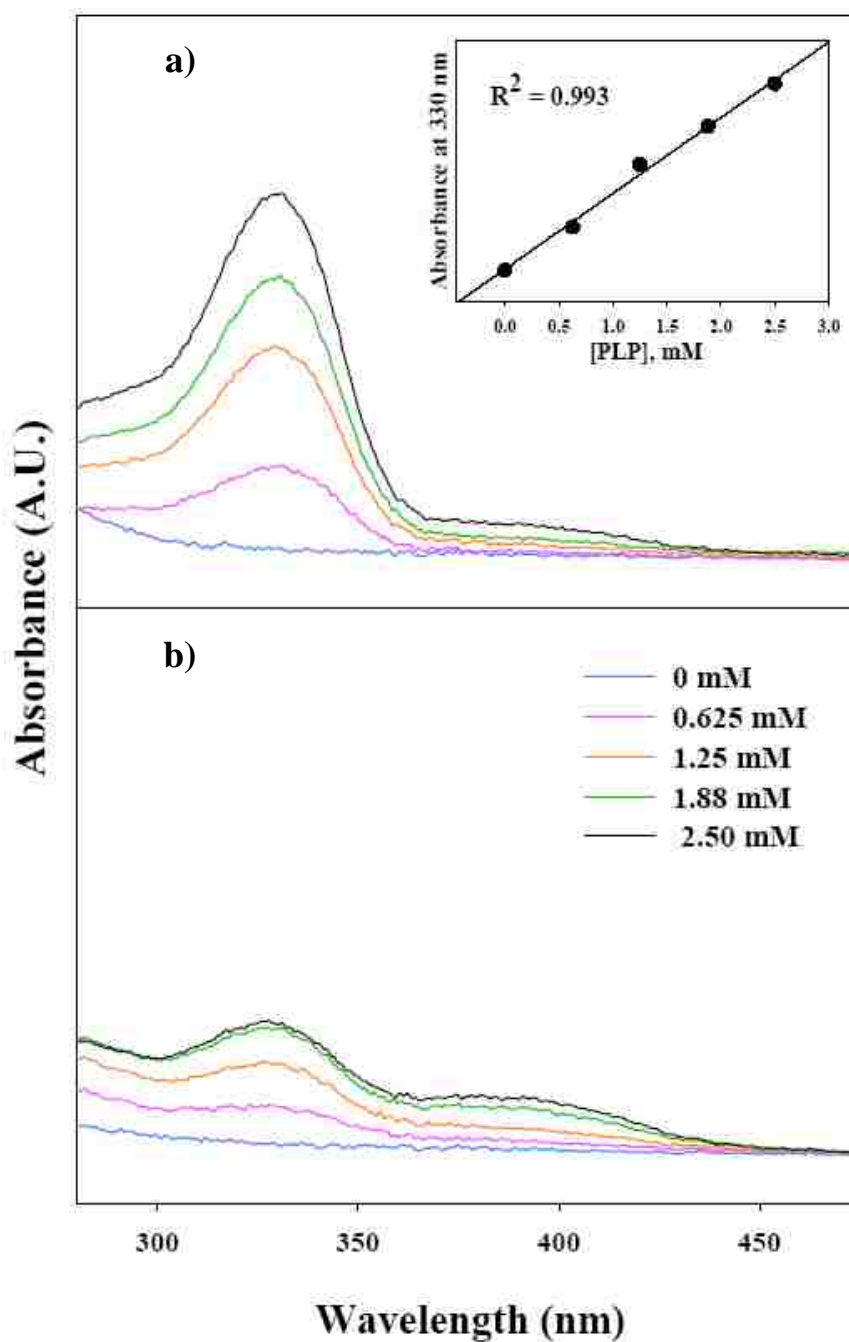


**Figure A.3** Spectrophotometric detection of in situ pyridoxal tetrahydrothiazine formation after 12 h in a) control reaction mixtures containing 2.5 mM Hcy thiolactone and PLP in the indicated concentrations (inset: pyridoxal tetrahydrothiazine production monitored at 330 nm), and b) protein reaction mixtures containing 10 mg/mL bovine cyt c, 2.5 mM Hcy thiolactone, and PLP in the indicated concentrations after 12 h. All samples were diluted 10-fold with pH 7.4, 100 mM sodium phosphate, 0.2 mM EDTA buffer prior to analysis. UV-Vis spectra acquired in triplicate at 25°C using a Shimadzu model UV-3101PC spectrophotometer equipped with a 1 cm quartz cell.

## APPENDIX B: GOLD NANOSENSOR CHARACTERIZATIONS AND CALIBRATION DATA

### Contents

**Figure B1:** MS data for unmodified and HTL-modified albumin

**Figure B2:** Calibration curve for GNP sensor response

**Figure B3:** TEM images of regions within oligomeric protein network containing GNP clusters

**Figure B4:** Dilution stability study for the GNP sensor

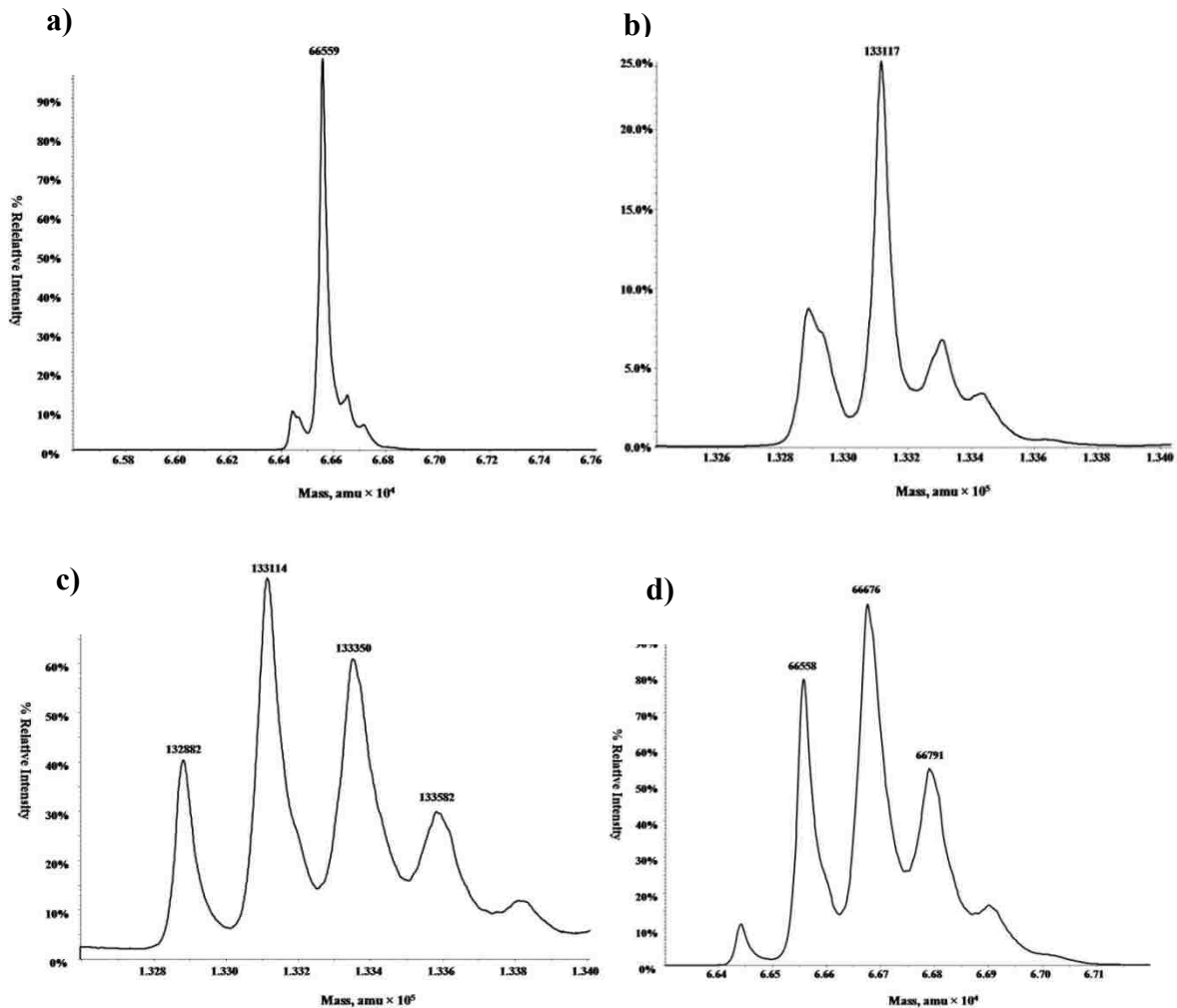


**Figure B1.** Mass spectra for a) the monomeric, b) the dimeric mass regions, respectively, of an unmodified HSA (control sample). Mass spectra for c) the monomeric and d) dimeric mass regions, respectively, of an HTL-modified HSA sample illustrate the extent of modification produced in the protein reaction mixture.

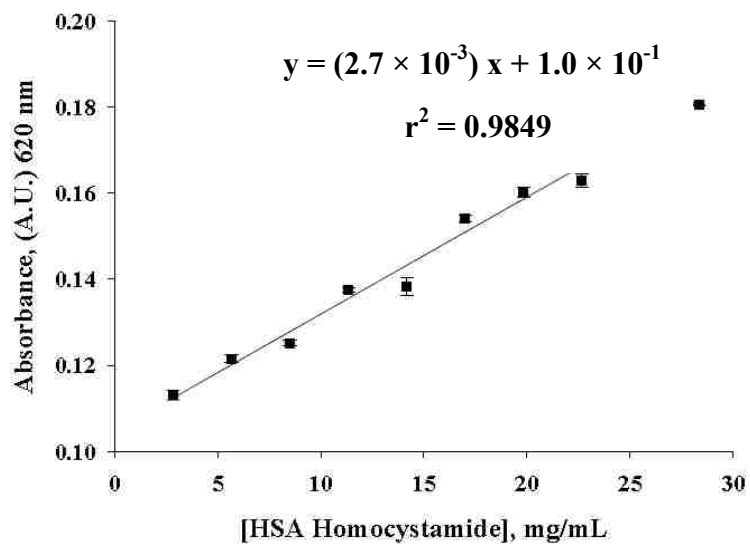


**Figure B2.** GNP sensor response at 620 nm to HSA-homocystamide (2.8 – 28 mg/mL), assuming complete modification. Each data point is the average of triplicate measurements.

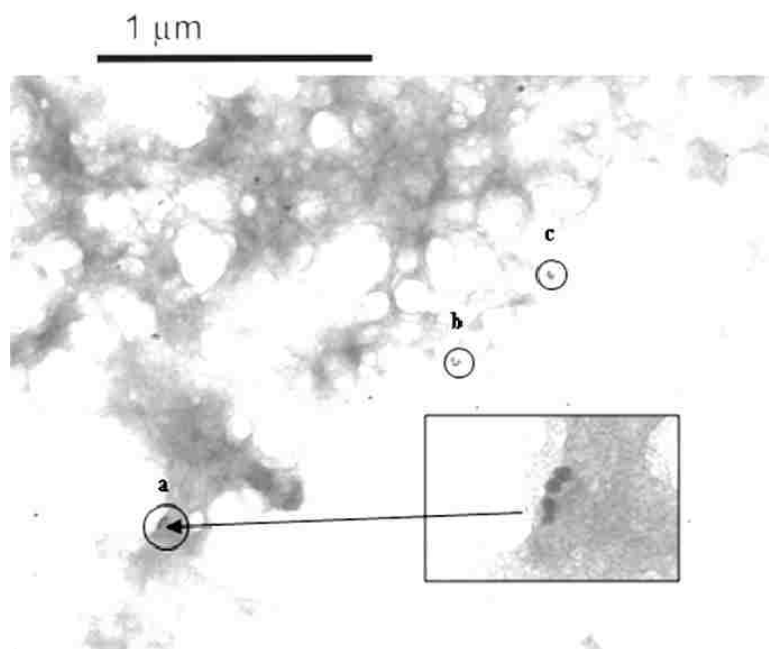


**Figure B3.** Transmission electron micrograph (TEM) images of the GNP sensor in the presence of HSA-homocystamide. The circled regions a) and b) highlight regions within the oligomeric protein network containing 4-GNP clusters at 33,000 × magnification. The inset shows a) at 100,000 × magnification. Region c) contains a 2-GNP cluster (33,000 × magnification).

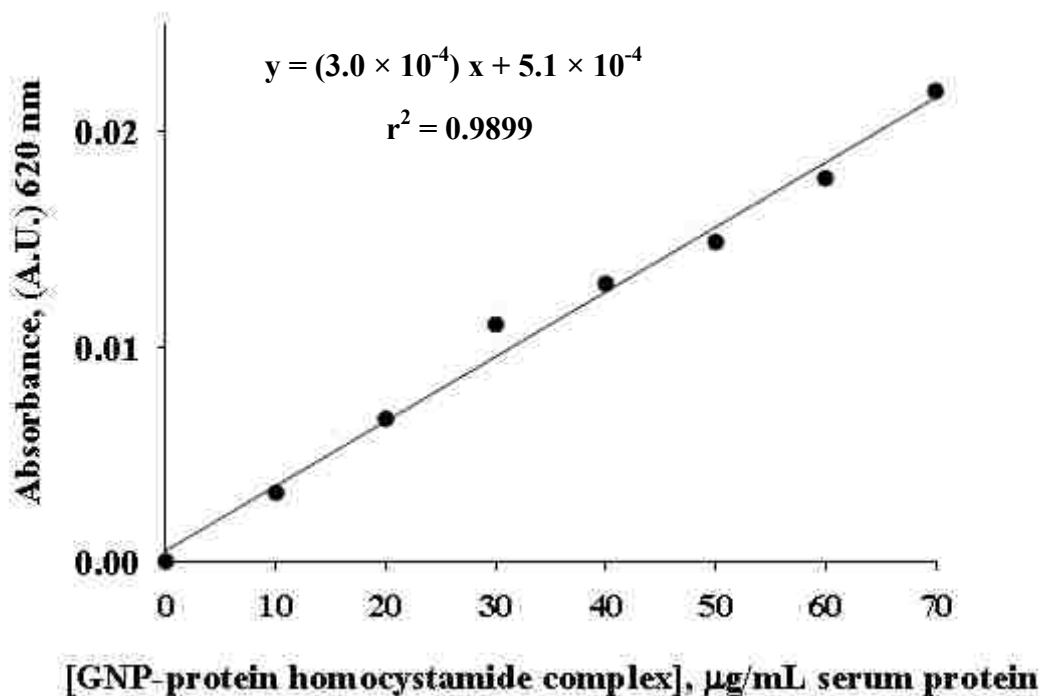


**Figure B4.** The dilutional stability of the sensor-protein homocystamide complex was evaluated by serial dilution of a sensor solution containing the GNP-protein complex (2.3 mg/mL sera homocystamide and 0.7 mM GNP). The concentration of the sensor complex is reported in unit of  $\mu\text{g/mL}$  serum protein, assuming complete modification. Deviation from linearity is indicative of a weakly bound complex; while linearity is indicative of a tightly bound complex. The calibration sensitivity is  $0.30 \text{ AU} \cdot (\text{ng/mL})^{-1}$ . This data suggest that the colorimetric complex resulting from modification-induced nanoparticle assembly is irreversible under the conditions used in this study. Each data point is the average of 5 measurements.

#### Brief Discussion of MS data (Figure B.1)

ESI-MS was employed to verify HTPM and assess the extent of modification obtained for the protein modification protocol used in study. Fresh protein reaction mixtures were prepared and diluted with water to obtain a 1 mg/mL solution. The resultant solution was further diluted 2-fold with a 1:1 (acetonitrile:water) prior to injection onto an LC-MS column. The total elapsed time from the initiation of the modification reaction to MS analysis was 6 hr. Note that the predominant species in the control sample is monomeric HSA (66559 amu). A small signal

corresponding to naturally occurring dimeric HSA, ~25% relative intensity, was also detected in the control sample. In contrast, the signal due to the unmodified HSA species (66558 amu) is greatly diminished in the modified sample. The differences in amu between consecutive species in the monomeric region of the mass spectra for the modified sample are ~117 amu, which is consistent with the formation protein homocystamide formation via dipeptide bond formation, which results in the loss of H<sub>2</sub>O (18 amu). Substantial signals from singularly and doubly modified HSA species are detected at 66676 and 66791 amu, respectively. A smaller signal corresponding to triply modified HSA is also observed. Additionally, there is a substantial increase in the signals corresponding to dimeric HSA species in the protein reaction mixture due to modification-induced oligomerization.

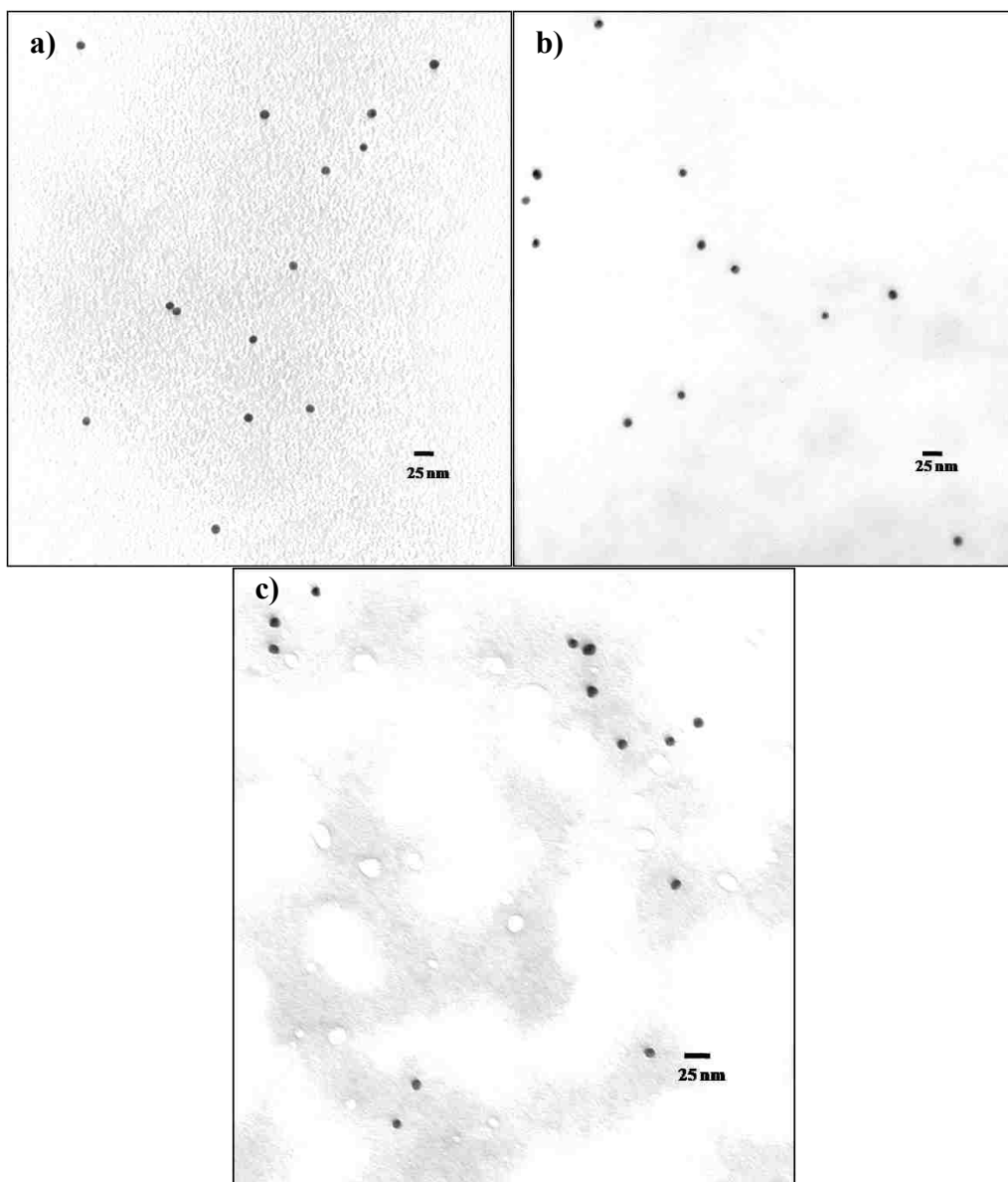
## APPENDIX C: NANOBIOCONJUGATE CHARACTERIZATIONS

### Contents

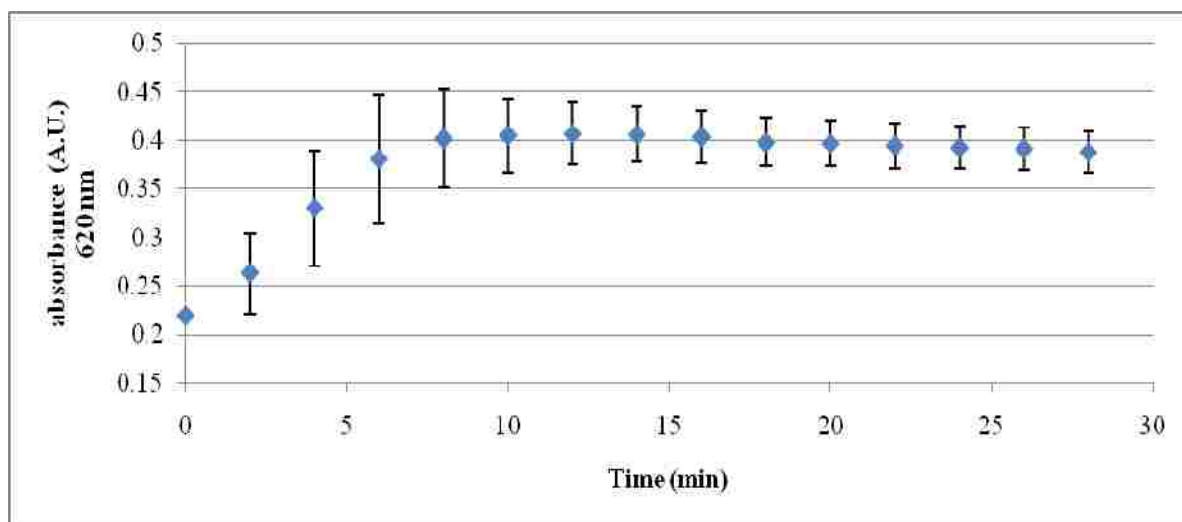
**Figure C1:** TEM images of unmodified protein nanobioconjugates

**Figure C2:** UV-vis absorption study for *N*-homocysteinylation of CGNP nanobioconjugates

**Figure C3:** UV-vis absorption study for *N*-homocysteinylation of AGNP and SGNP nanobioconjugates

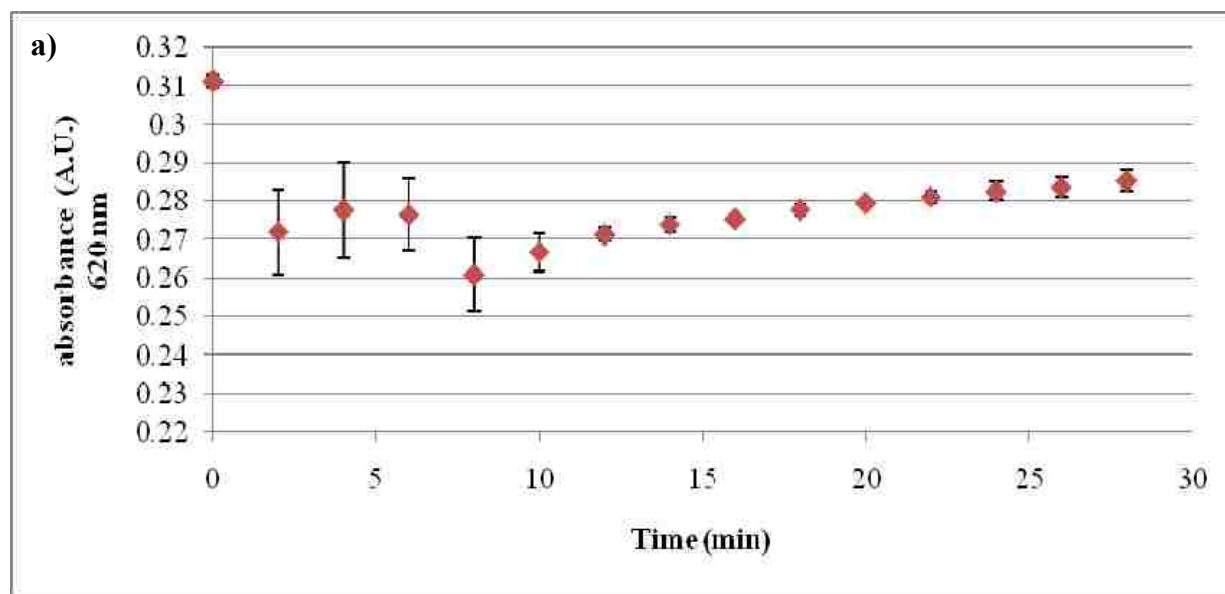


**Figure C1.** TEM images of unmodified nanobioconjugates. a) CGNPs, b) (AGNPs, and c) SGNPs. Note that some of the GNPs are irregularly shaped due to the dried protein coating.



**Figure C2.** UV-vis absorption spectra acquired at 620 nm (25 °C) over a 28 minute time period for *N*-homocysteinylation of a) CGNPs. Each data point represents the average of triplicate measurements.

UV-vis spectroscopy used to monitor the effect of *N*-homocysteinylation on the plasmon resonance behavior of the CGNP systems at 25 °C. Self-assembly resulting from *N*-homocysteinylation of CGNPs was monitored at at 620 nm for 28 min. Extended plasmon resonance absorption intensity for modified CGNPs increased over a period of approximately 10 min, which indicates the formation of nanobioconjugate assemblies.



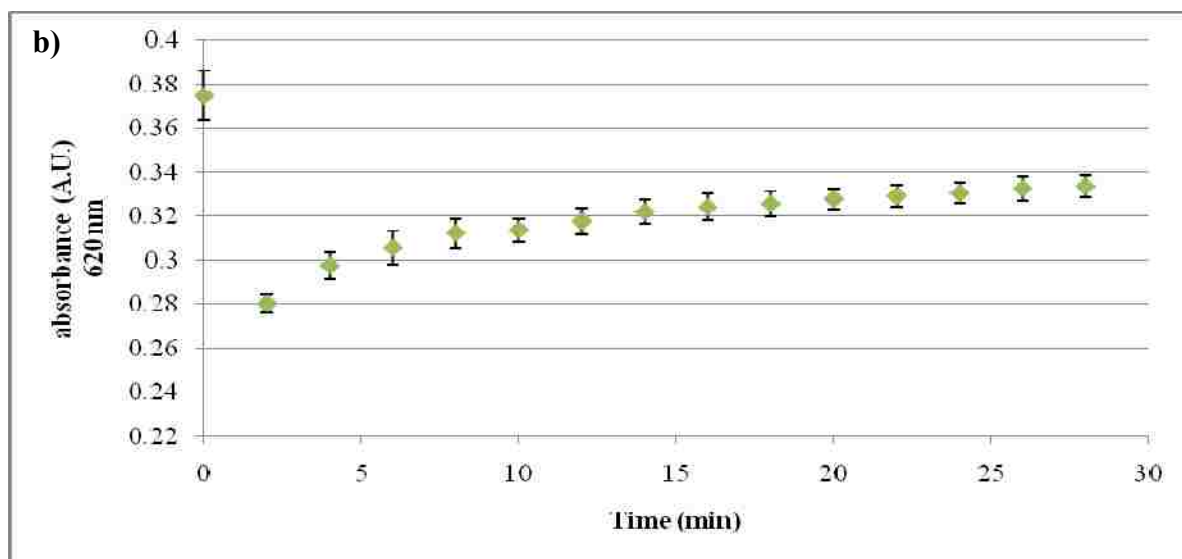


**Figure C3.** UV-vis absorption data acquired at 620nm (60°C) over a 28 minute time period for *N*-homocysteinylation of a) AGNPs and b) HG NPs illustrate the growth of nanoparticle assemblies. Each data point represents the average of triplicate measurements.

UV-vis spectroscopy was also employed to monitor the effect of *N*-homocysteinylation on the plasmon resonance behaviors of AGNPs and SGNPs. Absorption spectra were acquired at 620 nm over a period of 28 minutes at 60 °C, highest temperature attainable for the instrumentation. An initial decrease in absorbance at 620 nm was observed upon *N*-homocysteinylation of AGNPs (Figure C3a). Subsequently, there was a steady increase in absorption, which indicates the formation of nanobioconjugate assemblies. The SGNP system behaved nearly identical to the AGNP system (Figure C3b). Collectively, these data correspond to the DLS trends discussed in the text (Figure 5.2).



## **APPENDIX D: LETTERS OF PERMISSION**

**Karen Buehler**

---

**From:** Arther Gates [agates1@lsu.edu]  
**Sent:** Wednesday, August 27, 2008 9:45 PM  
**To:** Copyright  
**Subject:** Permission to Reproduce Published Work in Dissertation

To whom it may concern:

I hereby request permission to reproduce text and/or figures from the journal articles listed below in my doctoral dissertation. Note that I am the first author for both articles. Per university protocol, the dissertation will be archived in the Louisiana State University electronic thesis database. ~~SEE ATTACHED LETTER~~

1) Capillary Electrophoretic Screening for the Inhibition of Homocysteine Thiolactone-induced Protein Oligomerization, ANALYTICAL CHEMISTRY, 2007, 79 (21), 8249-8256.

2) Gold Nanoparticle Sensor for Homocysteine Thiolactone-induced Protein Modification, LANGMUIR, 2008, 24 (8), 4107-4113.

Please fax your decision to my attention at 225-578-3971.

Thank you very much for your consideration.

Regards,

Arther T. Gates  
Ph.D. Candidate,  
Louisiana State University  
Department of Chemistry  
336 Choppin Hall  
Baton Rouge, LA 70802  
phone 225-578-7453



# American Chemical Society

Publications Division  
Copyright Office

1155 Sixteenth Street, NW  
Washington, DC 20036  
Phone: (1) 202-872-4368 or -4367  
Fax: (1) 202-776-8112 E-mail: [copyright@acs.org](mailto:copyright@acs.org)

VIA FAX: 225-578-3971      DATE: September 25, 2008

TO: Arther T. Gates, Department of Chemistry, Louisiana State University  
336 Choppin Hall, Baton Rouge, LA 70802

FROM: C. Arleen Courtney, Copyright Associate *C. Arleen Courtney*

Thank you for your request for permission to include **your** paper(s) or portions of text from **your** paper(s) in your thesis. Permission is now automatically granted; please pay special attention to the implications paragraph below. The Copyright Subcommittee of the Joint Board/Council Committees on Publications approved the following:

Copyright permission for published and submitted material from theses and dissertations

ACS extends blanket permission to students to include in their theses and dissertations their own articles, or portions thereof, that have been published in ACS journals or submitted to ACS journals for publication, provided that the ACS copyright credit line is noted on the appropriate page(s).

Publishing implications of electronic publication of theses and dissertation material

Students and their mentors should be aware that posting of theses and dissertation material on the Web prior to submission of material from that thesis or dissertation to an ACS journal may affect publication in that journal. Whether Web posting is considered prior publication may be evaluated on a case-by-case basis by the journal's editor. If an ACS journal editor considers Web posting to be "prior publication", the paper will not be accepted for publication in that journal. If you intend to submit your unpublished paper to ACS for publication, check with the appropriate editor prior to posting your manuscript electronically.

If your paper has not yet been published by ACS, we have no objection to your including the text or portions of the text in your thesis/dissertation in **print and microfilm formats**; please note, however, that electronic distribution or Web posting of the unpublished paper as part of your thesis in electronic formats might jeopardize publication of your paper by ACS. Please print the following credit line on the first page of your article: "Reproduced (or 'Reproduced in part') with permission from [JOURNAL NAME], in press (or 'submitted for publication'). Unpublished work copyright [CURRENT YEAR] American Chemical Society." Include appropriate information.

If your paper has already been published by ACS and you want to include the text or portions of the text in your thesis/dissertation in **print or microfilm formats**, please print the ACS copyright credit line on the first page of your article: "Reproduced (or 'Reproduced in part') with permission from [FULL REFERENCE CITATION.] Copyright [YEAR] American Chemical Society." Include appropriate information.

**Submission to a Dissertation Distributor:** If you plan to submit your thesis to UMI or to another dissertation distributor, you should not include the unpublished ACS paper in your thesis if the thesis will be disseminated electronically, until ACS has published your paper. After publication of the paper by ACS, you may release the entire thesis (**not the individual ACS article by itself**) for electronic dissemination through the distributor; ACS's copyright credit line should be printed on the first page of the ACS paper.

\* **Use on an Intranet:** The inclusion of your ACS unpublished or published manuscript is permitted in your thesis in print and microfilm formats. If ACS has published your paper you may include the manuscript in your thesis on an intranet that is not publicly available. Your ACS article cannot be posted electronically on a publicly available medium (i.e. one that is not password protected), such as but not limited to, electronic archives, Internet, library server, etc. The only material from your paper that can be posted on a public electronic medium is the article abstract, figures, and tables, and you may link to the article's DOI or post the article's author-directed URL link provided by ACS. This paragraph does not pertain to the dissertation distributor paragraph above.

## VITA

Arther Terrell Gates was born to Arther Lee and Delliah Gates of Marks, MS. He attended George H. Oliver Elementary School, W. A. Higgins Jr. High School, and Clarksdale High School. He regularly participated in science and engineering competitions throughout high school and received several awards for his efforts to develop environmentally-friendly building materials from chemically treated post-consumer cardboard fibers. Arther was inducted into the Clarksdale High School Hall of Fame and graduated at the top of his senior class in 1995. He later received a Bachelor of Science (*Cum Laude*) in chemistry from Alcorn State University (May 2000). As an undergraduate, Arther participated in prestigious research internships sponsored by the Naval Research Laboratory (J.C. Stennis Space Center, MS), Grand Gulf Nuclear Station (Port Gibson, MS), and the University of Nebraska-Lincoln (UNL). His undergraduate achievements include the Pan-Hellenic Council Academic Award, Walter Washington Fellowship, and Kappa Alpha Psi Academic Award. Arther matriculated to graduate school at UNL in January of 2000, where he studied analytical chemistry and earned a Master of Science in August of 2002. Immediately thereafter, Arther began doctoral studies in analytical chemistry at Louisiana State University under the tutelage of Dr. Isiah M. Warner. Arther was awarded several honors during his tenure at LSU including fellowships from *Procter & Gamble Company*, *the National Science Foundation*, *Dow Chemical Company*, *Graduate Alliance for Education in Louisiana (GAELA)*, and *the National Organization for Advancement of Black Chemist and Chemical Engineers*. He was also awarded two of the highest honors conferred by the department of chemistry, the *James W. Robinson Outstanding Analytical Research Award* and the *Outstanding Graduate Research Seminar Award*. Arther graduated with the degree of Doctor of Philosophy in chemistry from Louisiana State University in December 2008. His scholarly publications and conference presentations include:

Nanoparticle-based Sensor for Protein Homocystamide; **Arther Gates**<sup>1</sup>, Mark Lowry<sup>1</sup>, James Robinson<sup>1</sup>, Robert Strongin<sup>1</sup>, Isiah Warner<sup>1</sup>; <sup>1</sup>Louisiana State University, Gordon Research Conference on Bioanalytical Sensors: Bryant University, Smithfield, RI June 29-July 4, 2008

**Gates, Arther**; Fakayode, Sayo; Lowry, Mark; Ganea, Gabriela; Robinson, Murugesu, Abitha, James W.; Strongin, Robert M.\* and Warner Isiah M.\* Gold Nanoparticle Sensor for Homocysteine Thiolactone-Induced Protein Modification, *Langmuir*, 2008; 24(8); 4107-4113.

Investigation of Homocysteine Thiolactone-induced Protein Modification; **Arther Gates**<sup>1</sup>, Mark Lowry<sup>1</sup>, Kristin Fletcher<sup>1</sup>, Abitha Merugesu<sup>1</sup>, Oleksandr Rusin<sup>1</sup>, James Robinson<sup>1</sup>, Robert Strongin<sup>1</sup>, Isiah Warner<sup>1</sup>; <sup>1</sup>Louisiana State University, The 34th FACSS Conference: Memphis, TN October 15-17, 2007

**Gates, Arther**; Merugesu, Abitha; Robinson, James W.; Lowry, Mark; Fletcher, Kristin A.; Rusin, Oleksandr; Strongin, Robert M.\* and Warner Isiah M.\* Capillary Electrophoretic Screen for the Inhibition of Homocysteine Thiolactone-Induced Protein Oligomerization. *Analytical Chemistry* (2007), 79(21); 8249-8256.

Nelson, Mary Anne; **Gates, Arther**; Dodlinger, Maud; Hage, David S. Development of a Portable Immunoextraction-Reversed-Phase Liquid Chromatography System for Field Studies of Herbicide Residues. *Analytical Chemistry* (2004), 76(3), 805-813.